The first schedule protects against compressor stall, and the second protects against turbine overtemperature. Both functions are scheduled as functions of corrected core speed. The digital control memory incorporates logic to select the lower of the acceleration fuel limits which are computed from the two functions. Figure 87 depicts the OTW engine acceleration fuel schedule. The corrected core speed function is calculated from measured core speed, fan speed, and fan inlet temperature. The corrected acceleration fuel limit is a function of fuel flow, compressor discharge pressure, fan speed, and fan inlet temperature. The digital control logic compares the scheduled acceleration fuel limit with the real-time calculated level of the acceleration fuel function and multiplies the difference by compressor discharge pressure to establish the actual engine-fuel-flow limit. This calculation process is repeated approximately 80 times per second.

The OTW control also incorporates limits for engine protection.

3.8.9 OTW Transient Thrust Response

As noted earlier the QCSEE was required to have rapid thrust-response capability. The UTW and OTW requirements were the same. Figure 88 shows the results of a thrust-response study using a transient model of the OTW engine. The thrust-response requirement is noted on the figure. The dashed line on the figure shows the predicted response of a conventional turbofan in which fan speed and core speed are both varied with changes in engine fuel flow. With a conventional system, the required response could not be achieved due to the acceleration fuel schedule - which is designed to prevent compressor stall and turbine overtemperature.

Since the required response could not be achieved using conventional methods, a study was conducted to determine if the thrust-response time could be improved by more effective use of the core stators. It was determined that, by setting the stators closed from the nominal schedule, the thrust-response rate could be increased. When the core stators are closed, the core speed increases to maintain sufficient power to hold the fan speed and maintain the thrust setting. Therefore, with closed core stators the core engine was not required to accelerate to achieve thrust response. The core stator closure was implemented by biasing the base stator schedule with the power-demand signal and by an operating-mode signal. With a step increase in the power-demand signal, the core stators would open rapidly to provide the power for fan acceleration to takeoff speed. The solid line on Figure 88 shows the predicted thrust response of the OTW engine with the core stator reset function.

3.8.10 Failure Indication and Corrective Action

One propulsion-control-technology objective in the QCSEE program was to reduce the impact of control-system sensor failures. This concept was implemented by using the inherent capability of a digital computer to rapidly compare and act on a large amount of data.

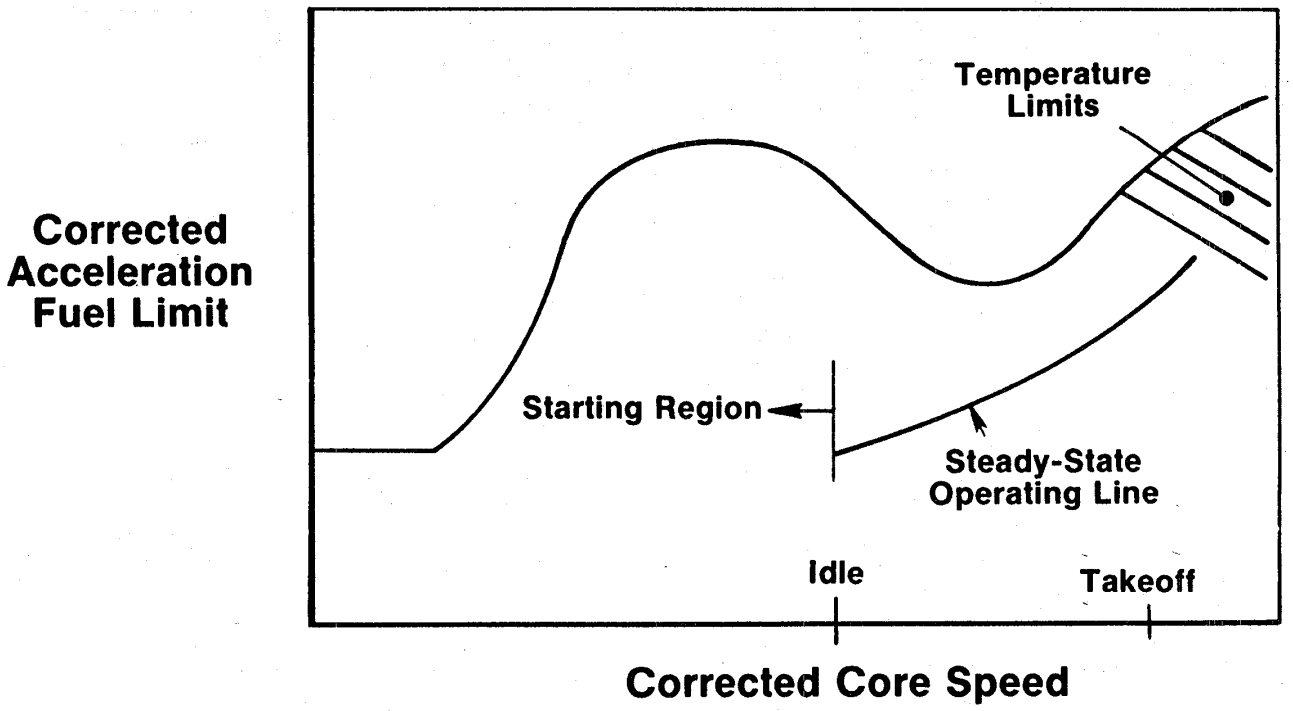

Figure 87. OTW Acceleration Fuel Schedule.

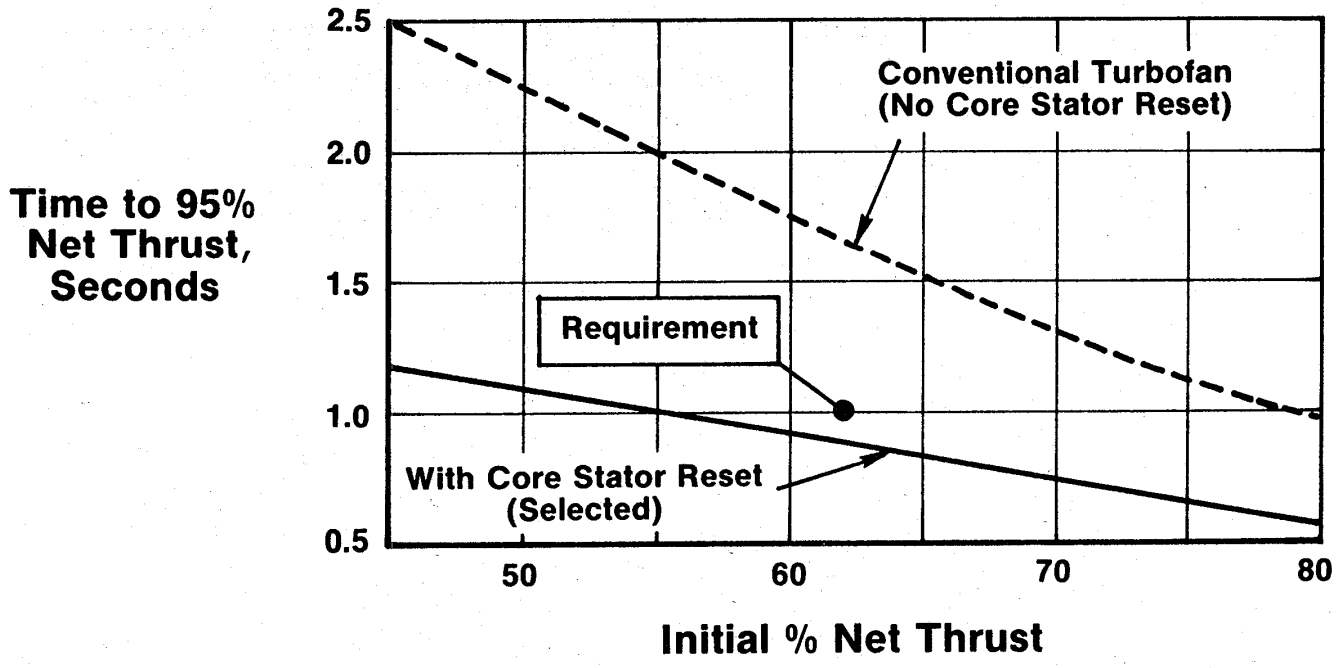

Figure 88. OTW Predicted Transient Response.

The digital control memory incorporated a nonlinear model of the OTW engine cycle. This model was combined with a logic-update scheme to form an extended Kalman-Bucy filter which provided a calculated estimate of the engine sensor outputs. These calculated sensor values were compared with the measured sensor values. If the difference was small, the engine model was updated to calculate new estimated sensor outputs. If an engine sensor fails excessive error is detected, the engine sensor is automatically disconnected, and the engine continues to operate using the calculated value of the sensed output. The calculated value of a given sensor is based on the fact that sensed variables are interrelated through the engine model. Figure 89 is a schematic of the sensor failure indication and corrective action (FICA) concept. Figure 90 shows the results of dynamic-simulator study on the OTW engine with the FICA concept incorporated. The data on the far left show normal system operation with all sensors operating during a power chop and a power burst. The center set of data shows engine operation with a compressor-discharge sensor failure. The data on the right show operation with a fan-speed sensor failure. Even with the failed sensors, the dynamic simulation indicates that the engine should perform satisfactorily.

3.9 LOW-EMISSIONS COMBUSTOR

In July 1973, the U.S. Environmental Protection Agency (EPA) issued standards to regulate and minimize the quantities of carbon monoxide (CO), hydrocarbons (HC), oxides of nitrogen (NO_x), and smoke emissions that may be discharged by aircraft operating within or near airports. These standards were defined for several different categories and types of fixed-wing, commercial-aircraft engines and are presented in terms of a calculated parameter called the EPA Parameter (EPAP). This parameter is based on an EPA-defined, landing/takeoff cycle consisting of specific operating times at engine power settings for ground idle, takeoff, climbout, and approach. The CO and HC emissions are mostly generated at the low-power ground idle conditions while the NO_x emissions are generated at the higher power settings including takeoff, climbout, and approach.

3.9.1 Design Requirements

The requirements for the QCSEE combustor were predicated on meeting the very stringent EPA standards for certified Class T2 subsonic engines. These standards, shown below, are presently scheduled to become effective in 1979:

• CO	4.3	lbm/1000 lbf/hr
• HC	0.8	lbm/1000 lbf/hr
• NO_x	3.0	lbm/1000 lbf/hr
• Smoke	22	SAE-SN

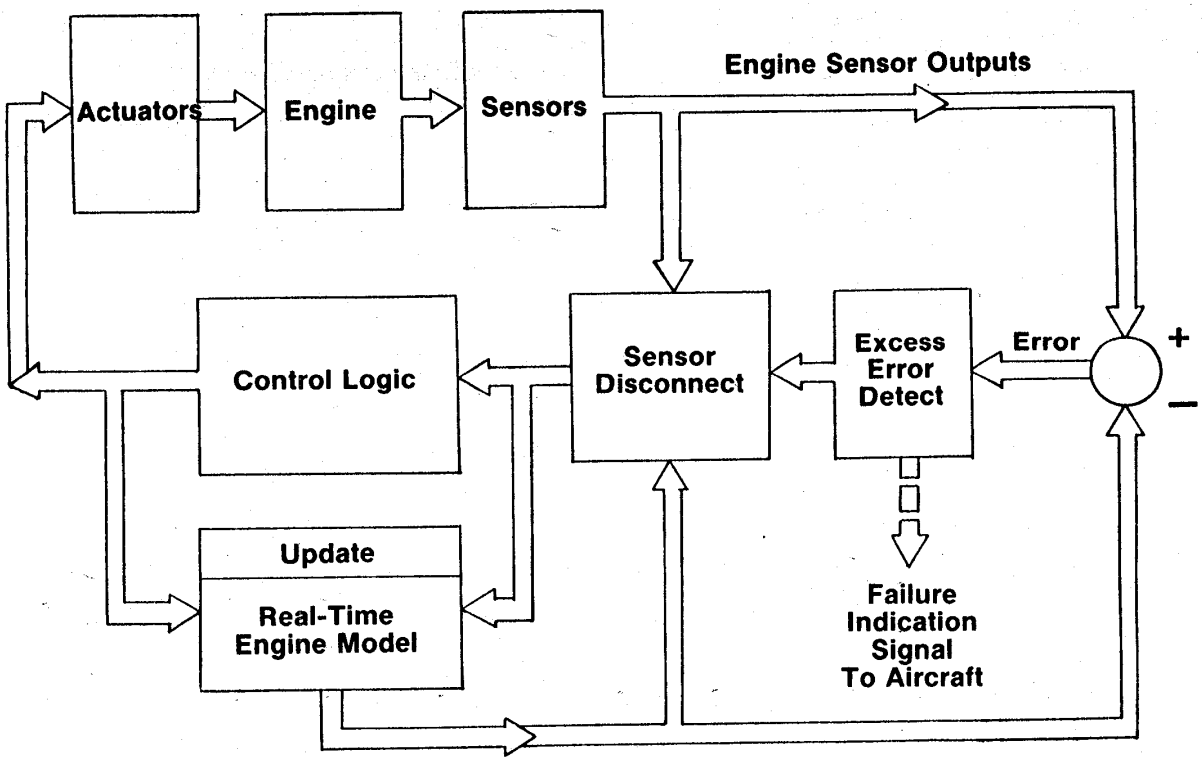

Figure 89. OTW Failure Indication and Corrective Action.

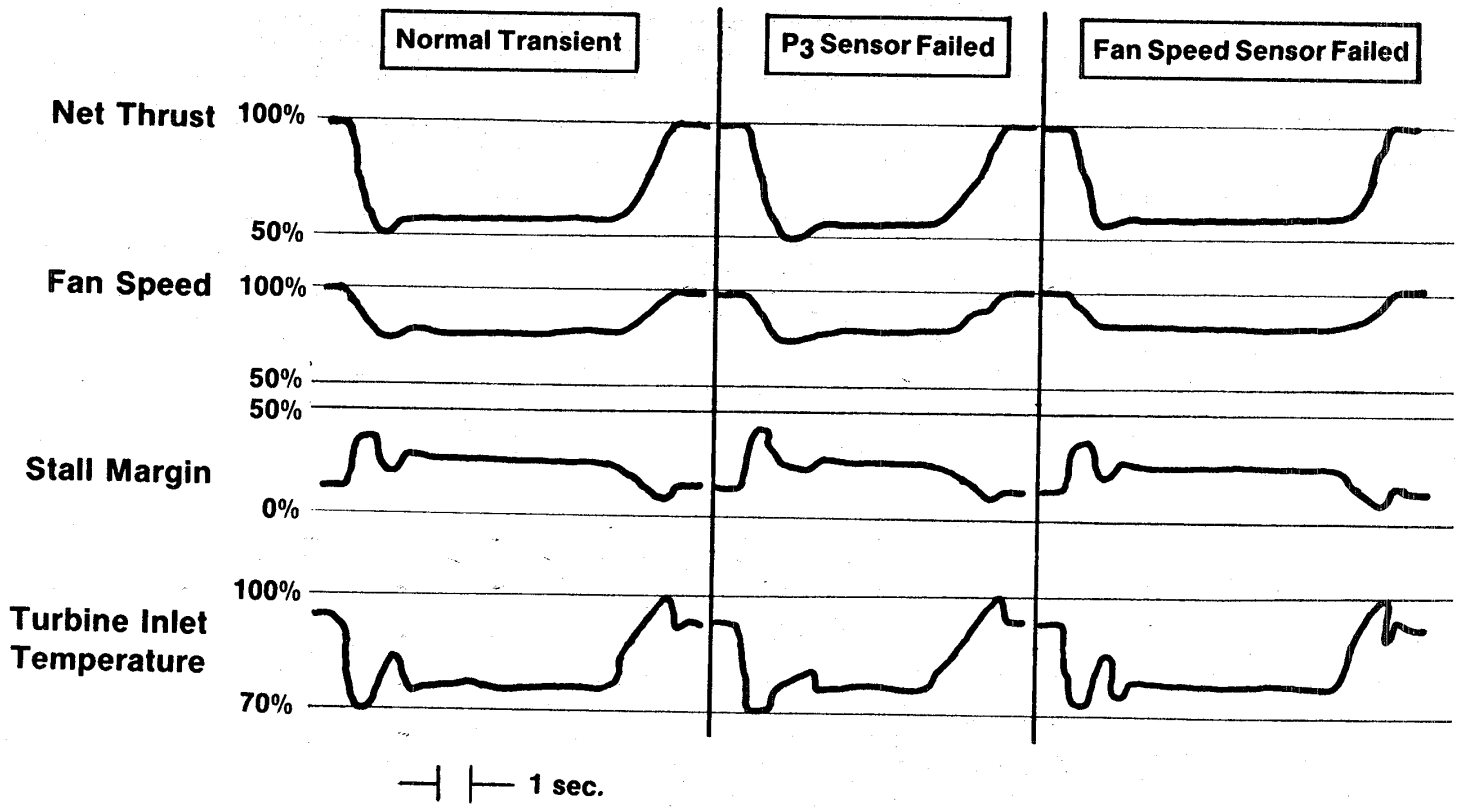

Figure 90. FICA Dynamic Simulation Results; Power Chop to 60% and Power Burst to 100%.

Proposed amendments to these standards are currently being reviewed by the EPA. Revised standards could possibly result in relaxation of the requirements and the effectivity dates for Class T2 engines.

In addition to the combustor-emissions requirements, the combustor must be sized to fit within the dimensional envelope of the existing core engine and meet performance requirements such as combustion efficiency, exhaust-temperature distribution, and altitude ignition typically required for any advanced, high-bypass engine.

As shown in Table XX, meeting the CO and HC emissions requirements in the QCSEE applications is particularly challenging because of severe combustor-inlet operating conditions at ground idle compared to those of a current state-of-the-art engine such as the CF6-50. The CO and HC emissions of the QCSEE are strongly and adversely affected by these lower combustor-inlet temperatures and pressures. In addition, the requirements must be met with a combustor sized to fit within the confines of the very short, compact envelope of the F101 combustor casing. Figure 91 shows the most recent version of a single-annular combustor configuration sized to fit the QCSEE and designed specifically for low emissions.

The QCSEE UTW and OTW configurations both use the F101 core, resulting in low-pressure-ratio cycle designs. With the low combustor-inlet temperatures and pressures associated with this low cycle pressure ratio, the NO_x emissions would not be expected to be a problem. Since the technology being developed was intended for higher-pressure-ratio engines, the development was carried out in a test rig using the higher-pressure-ratio cycle conditions listed in Table XXI. The use of this "emissions program" cycle did result in improved combustor inlet conditions at the QCSEE ground idle power setting of 4.5% of sea level takeoff thrust. In addition, the higher combustor inlet temperatures and pressures associated with this higher-pressure-ratio cycle result in higher NO_x emission levels than would be expected with the original QCSEE cycles, making the EPA NO_x emissions standard more challenging.

Table XXII shows the CO, HC, and NO_x emission levels of the single-annular combustor in terms of the EPA parameter compared to the program goals. As is shown in the table, the combustor did not meet the program goals for CO or NO_x emissions with the high-pressure-ratio cycle. Therefore, to meet the emissions goals in the short, compact, combustor envelope, a more advanced combustor concept was required.

3.9.2 Approach

The primary approach was to design and develop a double-annular dome combustor, as shown in Figure 92, based on technology developed previously in the NASA/GE Experimental Clean Combustor Program (ECCP). Figure 93 shows the much smaller size of QCSEE double-annular combustor compared to the CF6-50 size double-annular combustor developed in the ECCP. The QCSEE double-annular dome combustor uses many of the features of the CF6-50 double-annular combustor,

Table XX. QCSEE Combustor Design Challenges.

- **Meet 1979 CO/HC Emissions Standards with Low Ground Idle Combustor Inlet Operating Conditions**

	QCSEE	CF6-50
Combustor Inlet Temperature	415K (287 F)	429K (313 F)
Combustor Inlet Pressure	2.4 Atm. (36 psia)	2.9 Atm. (43 psia)
Engine Thrust at Idle (% Takeoff)	4.0	3.4

- **Meet Very Stringent NOX Emissions Goals**

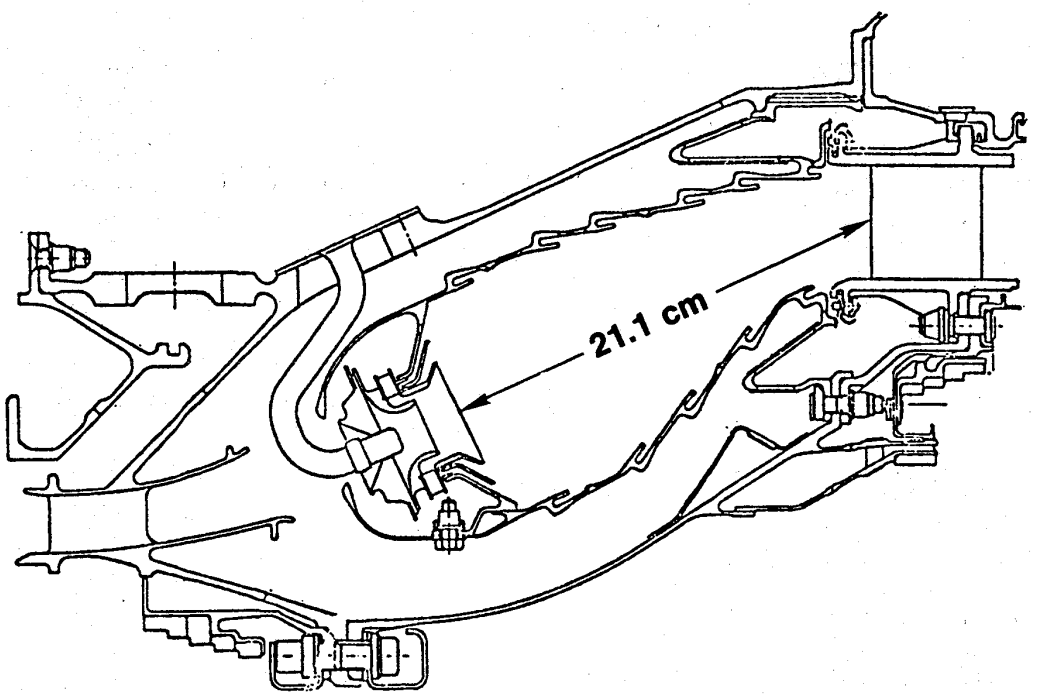

Figure 91. QCSEE Single-Annular, Low-Emissions Combustor.

Table XXI. Emissions Program Cycle Selection.

	UTW Engine	OTW Engine	Emissions Program
Pressure Ratio	14	17	25
Pressure, N/cm² (psi)	143 (208)	172 (250)	245 (356)
Temperature, K(°R)	684 (1231)	726 (1307)	789 (1416)

Table XXII. QCSEE Single-Annular Combustor.

- With 4% Ground Idle Thrust
- With Sectorized Burning at Idle
- High P/P QCSEE Cycle
- Jet A Fuel

		Emissions Status	Goals
CO	Pounds Per 1000 Pounds Thrust Per Hour Per Cycle	7.2	4.3
HC		.6	.8
NOX		3.8	3.0

Conclusion:

Advanced Combustor Concept Required to Meet Emissions Goals

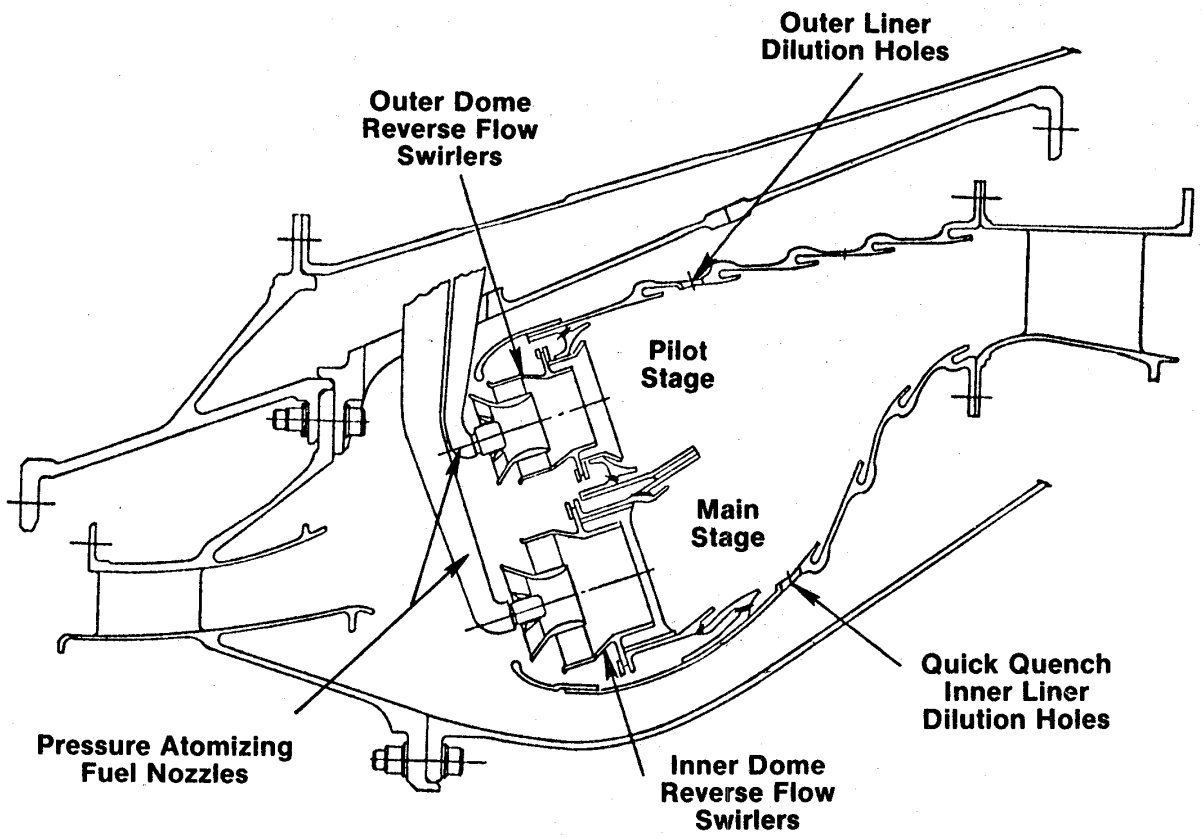

Figure 92. QCSEE Double-Annular Dome Combustor.

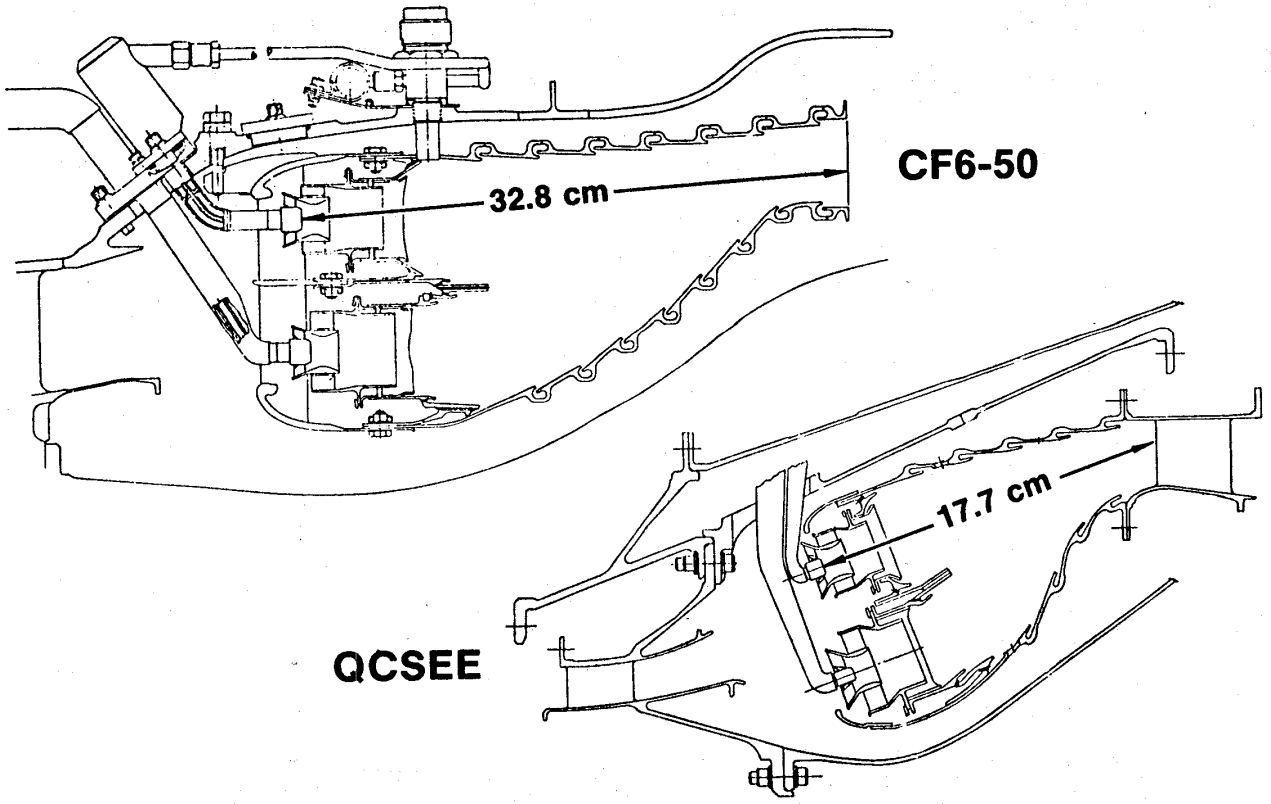

Figure 93. NASA QCSEE Double-Annular Combustor.

such as independently staged domes, counterrotating air-blast swirl cups, and pressure-atomizing fuel nozzles. However, a substantial scale-down was needed, particularly in length and dome heights, compared to the ECCP design. The staged combustor concept permits operation of only the pilot-stage dome, which is designed specifically to obtain low CO and HC emissions levels, at the low-power operating conditions. At the high-power operating condition both domes are operated with fuel staging selected to obtain low NO_x emission levels.

3.9.3 Development Program

The development program was conducted using a sector combustor, shown in Figure 94. A disassembled view of this five-swirl-cup, 90° sector combustor is shown in Figure 95. The tests were conducted in a rig designed to accept the sector combustor and duplicate exactly the flowpath of the F101 engine. Figure 96 shows a photograph of the test rig with the sector combustor installed. Although the major effort was focused on developing low CO and HC emissions at idle, the NO_x emissions levels of the QCSEE double-annular combustor were also evaluated at simulated high-power conditions; however, it was necessary to derate the pressure at higher power conditions and to adjust the measured NO_x emissions for the pressure difference.

3.9.4 Test Results

The number and types of combustor development tests conducted in the sector combustor program and the total number of test conditions at which data were acquired for each test category are shown below.

	Number of Test Configurations	Data Points
Emissions Development	32	310
Ignition Development	2	26
Combustor Performance	1	8
Fuel Spray Development	6	18

Figure 97 shows the four major categories of combustor configurations tested and the key design features of each. As shown in Figure 98, the baseline configuration exceeded the emissions goals by a large margin. Significant improvements were obtained with modified geometry by increasing the pilot-zone length in conjunction with cooling- and dilution-airflow modifications. Even further improvements in CO emissions were obtained by reducing the cup spacing in the pilot dome. Reduced cup spacing was obtained by relocating the pilot stage to the inner annulus. This configuration produced lower CO and HC emission levels than any of the previous configurations. The lower CO and HC emissions are believed to result from a reduction or elimination of the quenching regions between swirl cups. However, the very low CO and HC emission levels occurred at a fuel/air ratio below the QCSEE ground

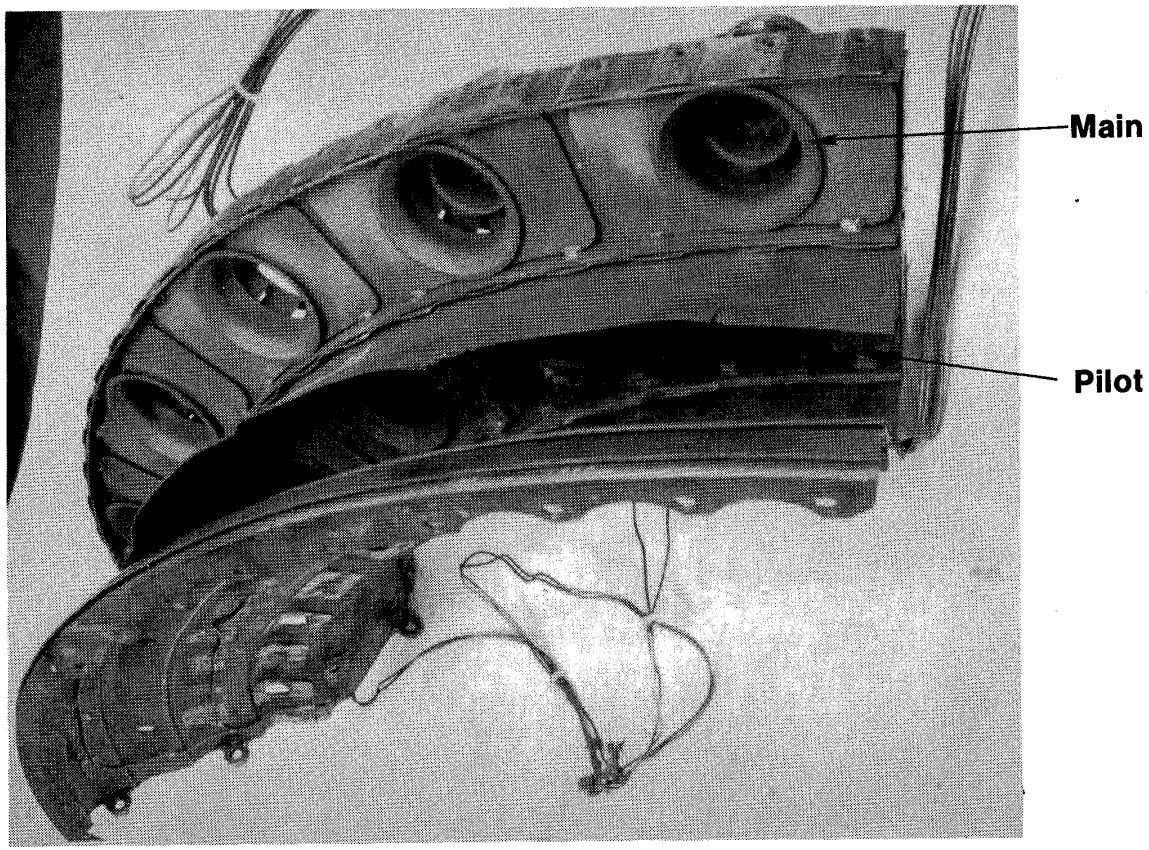

Figure 94. Double-Annular Test Sector.

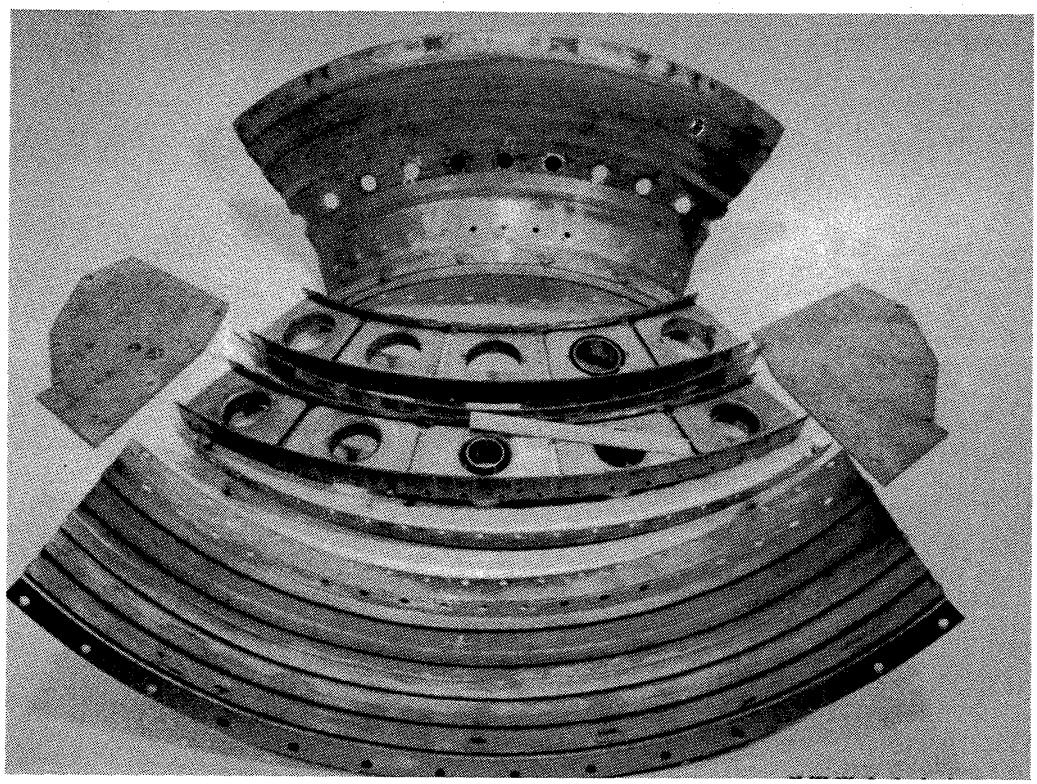

Figure 95. Double-Annular Sector Prior to Assembly.

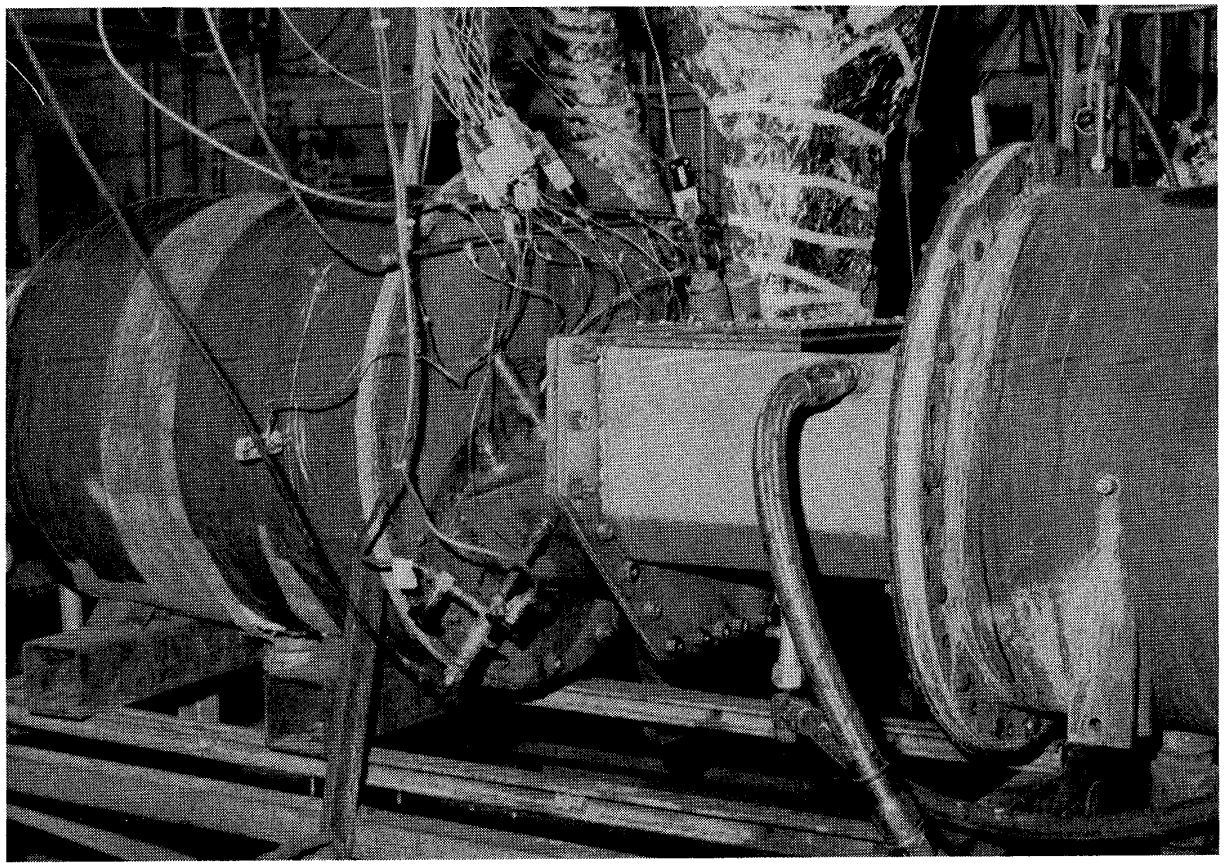

Figure 96. Double-Annular Combustor Test Rig.

Combustor Configurations

- Baseline
- Modified Geometry
  (Increased Combustion
  Zone Length)

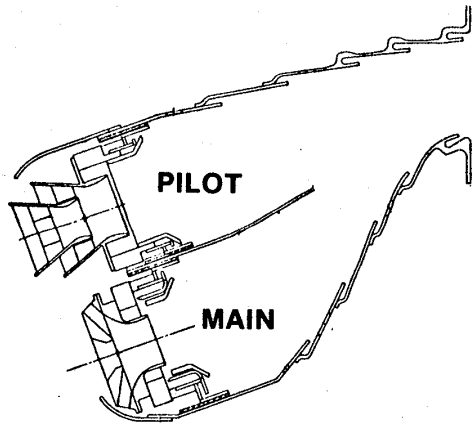

- Inner Annular Pilot Dome
- Selected Final Design
  (Radial Axial Air Blast Swirlers)

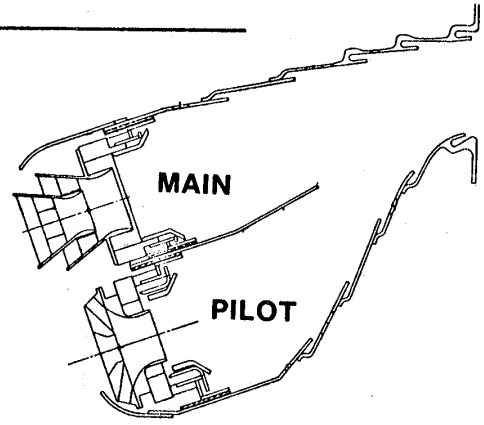

Figure 97. Key Development-Test Results.

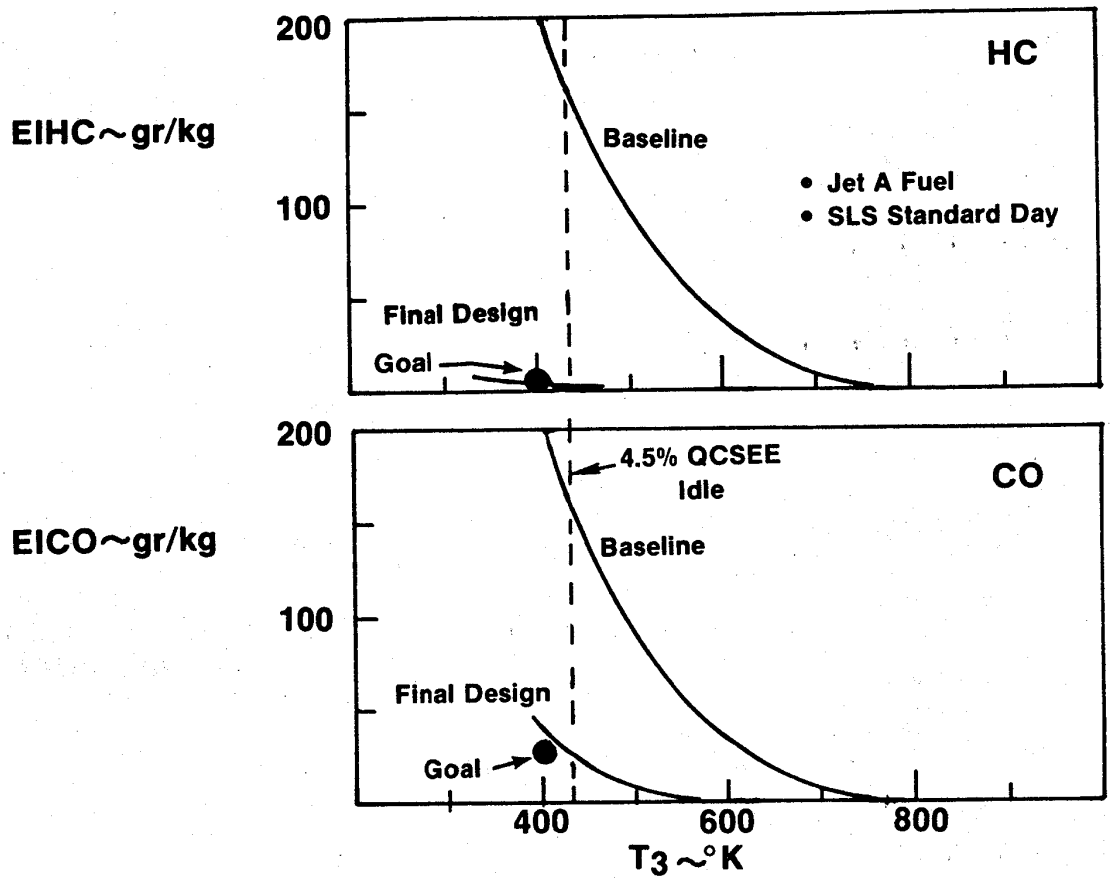

Figure 98. Key Emissions-Test Results.

idle design fuel/air ratio. Therefore, to further reduce the CO emission levels at the QCSEE ground idle fuel/air ratio, an improved pilot-stage swirl-cup design with higher airflow capacity and improved atomization was developed as the final design.

Figure 99 shows the improved pilot swirl-cup design and a similar design developed for the main stage. These design-improvement features were incorporated with the previously developed design features to obtain the final configuration. Figure 100 shows the preferred sector combustor configuration and the key dimensions.

Table XXIII shows the emissions levels for the final double-annular combustor configuration compared to those expected with the best single-annular combustor. Compliance with the program emissions goals, with a ground idle thrust of 4.5% takeoff thrust, is projected with this selected configuration.

The final configuration was also tested to investigate other important combustor-performance characteristics. Figure 101 shows the altitude ignition results obtained with the final double-annular combustor configuration. These tests were conducted with the sector combustor subjected to combustor-inlet conditions based on the altitude windmilling characteristics expected with QCSEE. The Jet A fuel temperatures were maintained at 244 K to simulate in-flight conditions. As shown, excellent altitude-relight results were obtained with successful ignition obtained in all regions tested within the flight envelope.

Although sector combustors are not generally conducive to accurate measurement of exhaust gas temperature-pattern factors, due to their limited circumferential size, data were acquired to examine trends. Because of the limited combustor airflow available for profile control and the very short length of this combustor design, it is expected that additional tailoring of the combustor profile would be required before introduction into a production engine.

In conclusion, it was demonstrated in a prototype sector combustor test that a double-annular dome combustor suitable for the QCSEE application can be developed which will satisfy the emissions goals of the program at a ground idle thrust of 4.5%. Furthermore, the selected final configuration demonstrated excellent altitude-relight performance for a combustor at this early stage of development. Other performance characteristics of this double-annular design will require further development before engine testing.

3.10 ACOUSTIC DESIGN

A schematic showing the QCSEE noise objectives is presented in Figure 102. These objectives are for a four-engine aircraft operating in the powered-lift mode from a 610-m (2000-ft) runway. The noise levels are those that would be heard by an observer on a 152-m (500-ft) sideline parallel to the runway centerline. At takeoff, the noise goal was 95 EPNdB with the engines at 100% thrust and on a 12.5° flight path. Under approach conditions, with the engines

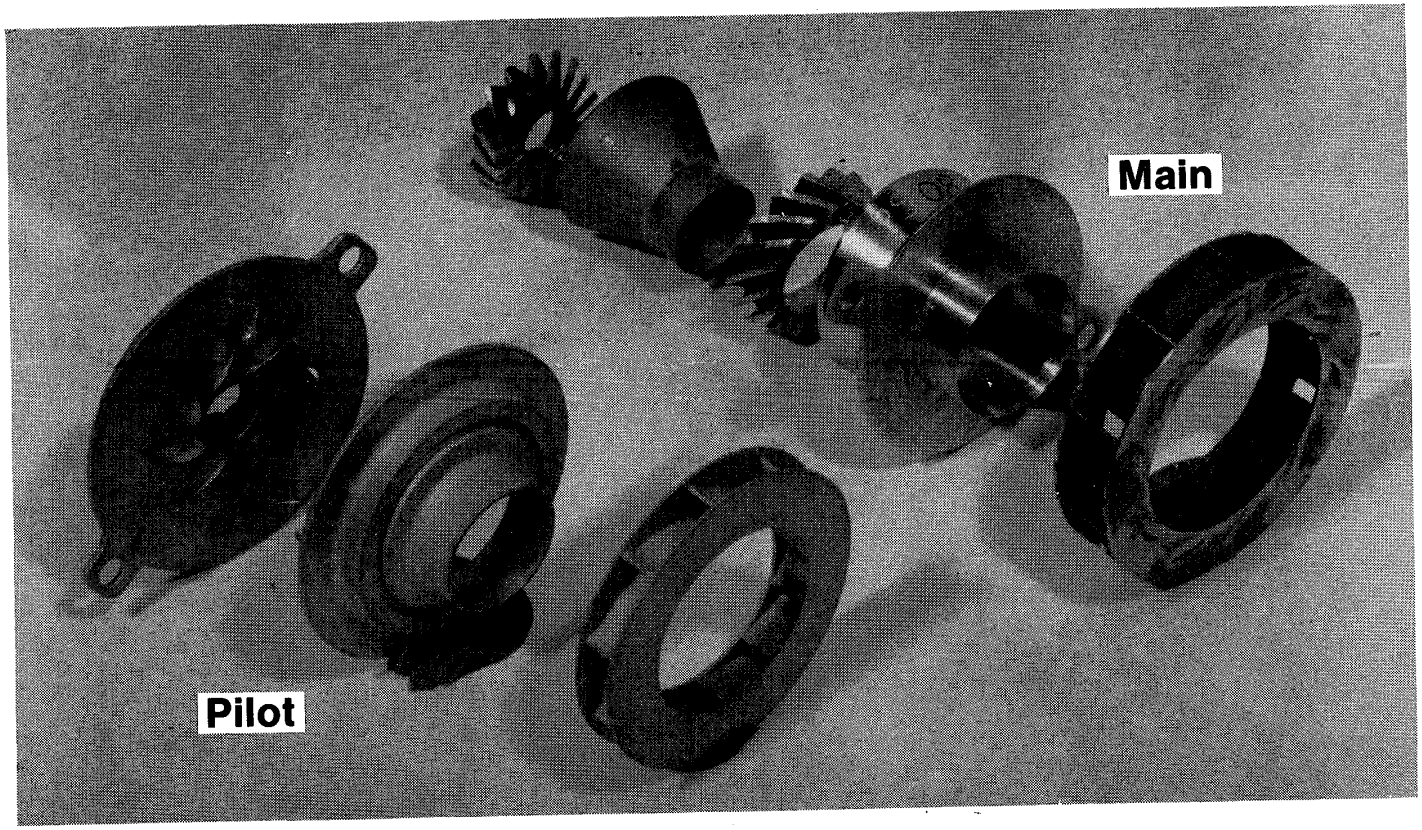

Figure 99. Swirl Cups.

Figure 100. Final Configuration.

Table XXIII. Emission Results for QCSEE Double-Annular Combustor.

High P/P QCSEE Cycle

	Double Annular		Best Single Annular with Sector Burn at Idle		Goals	
Idle Thrust	4.0%	4.5%	4.0%	4.5%		
CO	5.6	4.3	7.2	6.7	4.3	lb/1000 lb Thrust Per Hour-Cycle
HC	.32	.13	.57	.43	.8	
NOX	3.0*	3.0*	3.8	3.8	3.0	

* Estimated Based on Sector Combustor Results at Simulated High Power Conditions

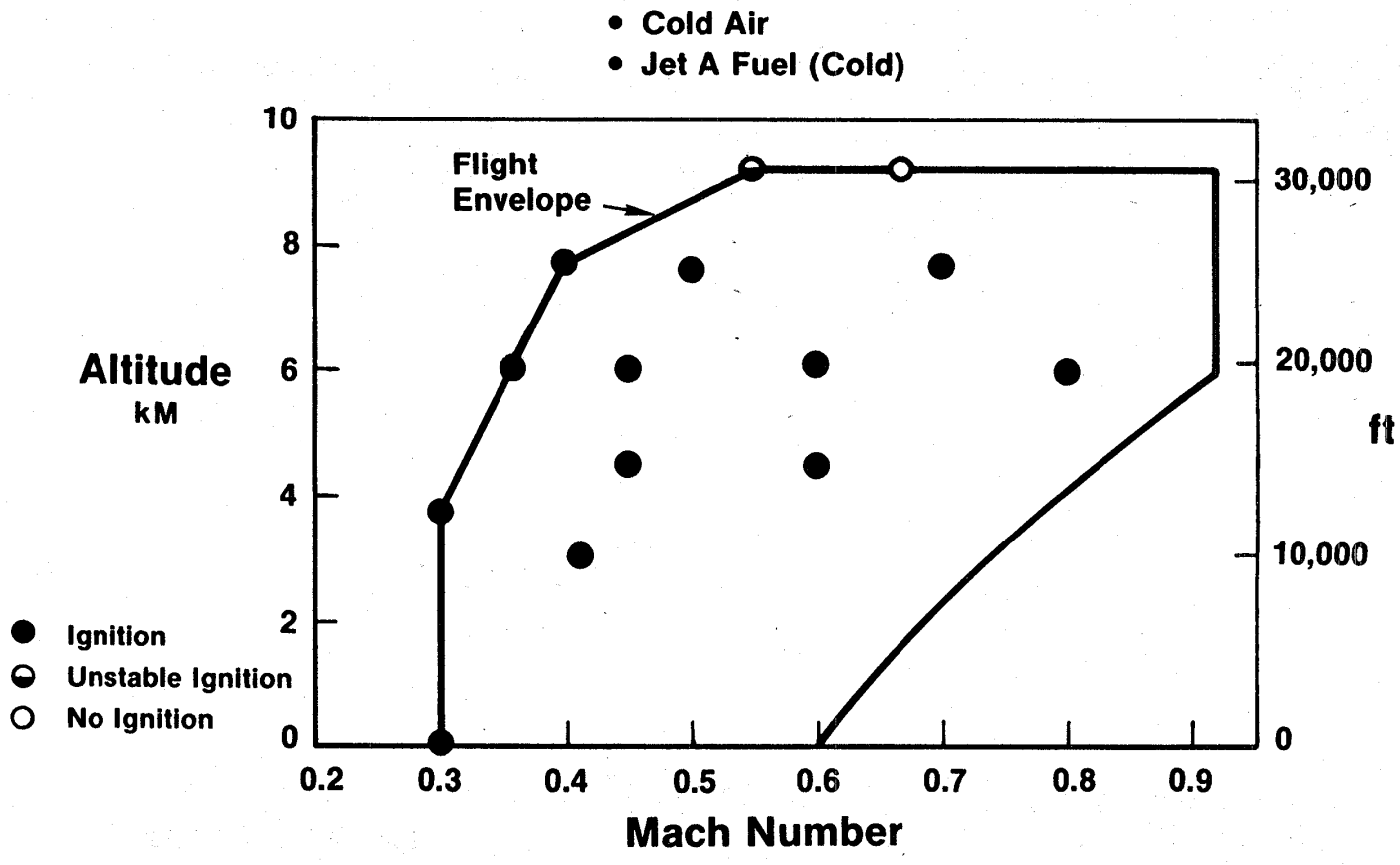

Figure 101. Altitude Ignition Results.

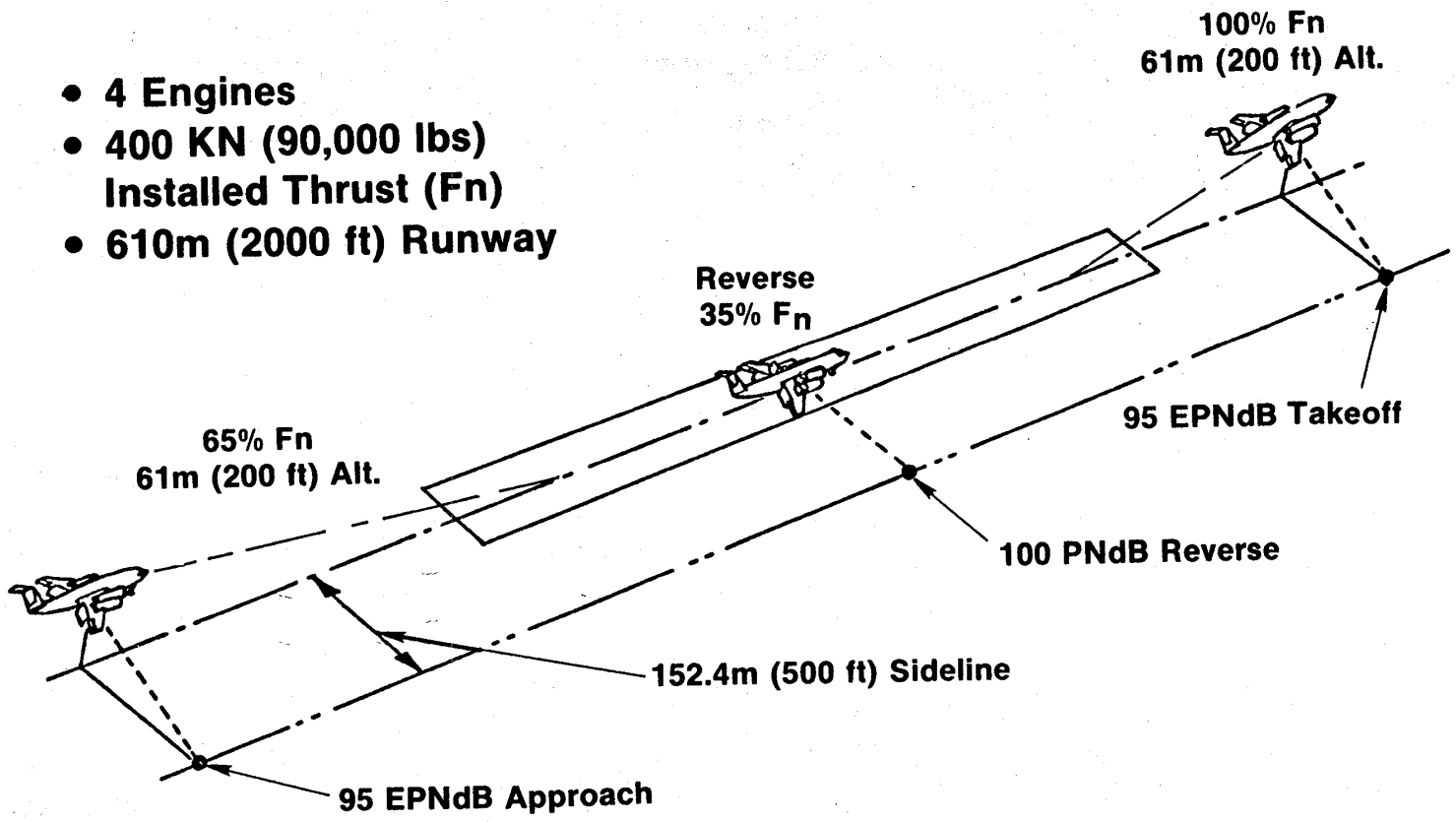

Figure 102. QCSEE Acoustic Objectives.

developing 65% of takeoff thrust and the aircraft on a 6° glide path, the goal was also 95 EPNdB. After touchdown on the 610-m (2000-ft) runway, with the engines developing reverse thrust at 35% of takeoff thrust, the noise goal was 100 PNdB on the 152-m (500-ft) sideline. These noise objectives were very challenging; this can be seen more clearly by examination of Figure 103. The figure shows the relative decrease in EPNL over the years for the older narrow-body aircraft, current widebody, next-generation widebody, and finally an Energy Efficient Engine (E^3) powered aircraft. QCSEE powered aircraft that meet the 95 EPNdB goal are about 10 EPNdB below the next-generation aircraft.

These stringent noise goals meant that any noise source on the engine which had the potential for contributing to the far field had to be evaluated. The sources which were considered are listed below:

- Fan-inlet-radiated noise
- Fan-exhaust-radiated noise
- Turbine noise
- Combustor noise
- Jet/flap noise
- Compressor noise
- Gear noise
- Treatment regenerated flow noise
- Strut noise
- Splitter trailing-edge noise

The design procedure for each noise constituent was to estimate the level by scaling existing test data from similar fan and core engines or by using the latest analytical techniques available. These estimated levels were then extrapolated to a simulated-flight condition of 61-m (200-ft) altitude, 152-m (500-ft) sideline. Precontract studies had indicated that maximum noise levels would occur with the aircraft at 61-m (200-ft) altitude during either takeoff or approach. As an example the predicted, unsuppressed, fan-exhaust-radiated noise spectrum for the UTW engine at takeoff is shown in Figure 104. This spectrum was then noy-weighted to determine the frequencies at which suppression or source-noise reduction techniques should be applied for maximum acoustic benefit. It can be seen that the second-harmonic tone required more reduction than the blade-passing frequency and that, after noy-weighting, treatment should be tuned to 2500 to 3150 Hz to provide the best broadband suppression.

A similar procedure was followed for each potential noise source for each of the three operating conditions. After several iterations, the levels of suppression which were required to meet the noise goals were established. Test and component programs were then conducted to verify that the required levels of suppression could be achieved and that the basic source noise (unsuppressed) levels were correct. System noise levels were updated and revised continuously as new data became available.

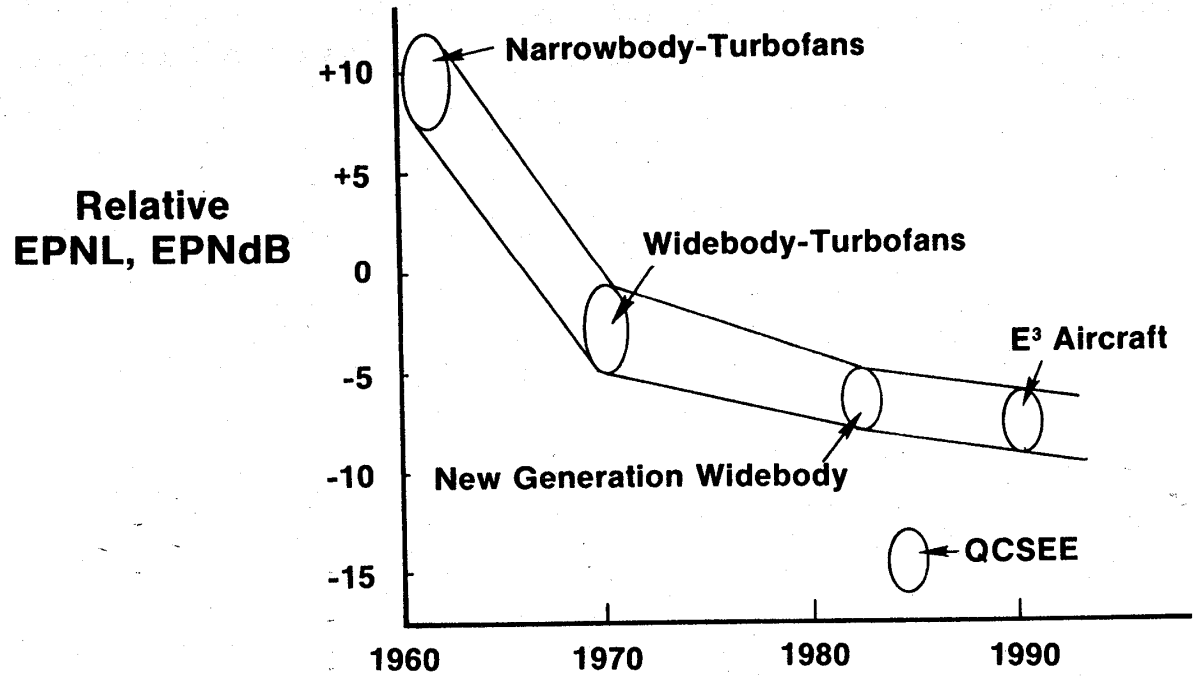

Figure 103. Aircraft Noise Trends.

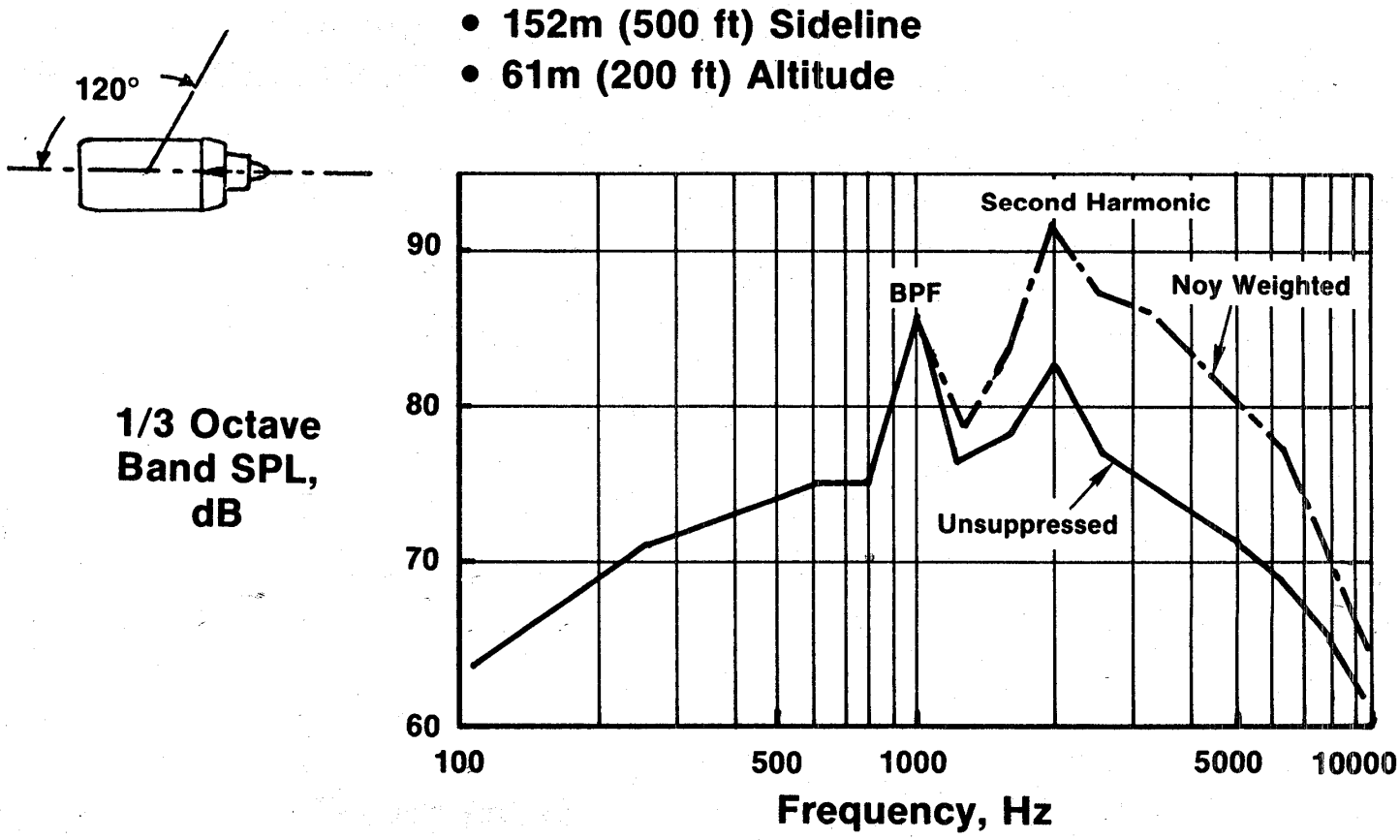

Figure 104. Unsuppressed Fan Exhaust Spectra.

3.10.1 Engine Acoustic Features

Before discussing the component tests which led to the treatment designs, the basic acoustic features on each engine will be reviewed. These acoustic features can be divided into two main categories: those dealing with reduction of the source itself and those dealing with the reduction of noise after it has been generated.

UTW features are shown in Figure 105. A low-pressure-ratio fan was selected primarily to keep jet/flap interaction noise as low as possible by reducing the fan-bypass exit velocity. This low pressure ratio also aided in keeping exhaust-radiated fan noise low. The fan had a subsonic tip speed of 290 m/sec (950 ft/sec) at takeoff which eliminated high noise levels from multiple pure tones associated with supersonic tip-speed fans. A wide rotor/stator spacing of 1.5 rotor tip chords was selected to lower rotor/stator interaction noise. Additional reduction could have been achieved with wider spacing; however, an acoustic splitter could achieve the reduction with less weight penalty than that associated with a fan frame weight increase due to wider spacing. The vane/blade ratio of 1.83 was selected based upon analysis to minimize propagation of the UTW fan second-harmonic tone - which makes a major contribution to the noy-weighted spectrum.

A high throat Mach number (0.79) inlet was used to suppress inlet-radiated fan noise at takeoff; wall treatment having a length equal to 0.74 fan diameters was added to provide suppression at approach and in reverse thrust.

Fan exhaust suppression utilized inner- and outer-wall suppression with variable-depth, variable-porosity treatment sections to provide wide suppression bandwidth. Preliminary design studies indicated that wall treatment alone would not achieve sufficient suppression in the length allowable; therefore, a 1.02-m (40-in.) acoustic splitter was added to provide the required exhaust suppression. Mach number in the fan exhaust duct was limited to 0.47 to minimize strut noise, treatment regenerated noise, and splitter trailing-edge noise. Treatment was added to the core inlet to suppress high-frequency compressor tones. Fan frame treatment consisted of wall treatment to suppress fan blade-passing-frequency tones and treatment on the pressure surface of the outlet guide vanes (OGV's) to attenuate high-frequency, broadband, fan noise.

The single-degree-of-freedom (SDOF) treatment that was specified on the UTW was an integral part of the support and load-carrying structure of the composite nacelle.

The engine utilized a "stacked" treatment core suppressor which was designed to attenuate both low-frequency combustor noise and high-frequency turbine noise.

In order to maintain commonality, the OTW engine shown in Figure 106 utilized essentially the same composite fan frame design as the UTW. With the 33 vanes and 28 fan blades, the OTW vane/blade ratio is a low 1.18. This low vane/blade ratio was a departure from the usual design practice of

- p/p = 1.27
- Tip Speed = 290m/sec (950 ft/sec)

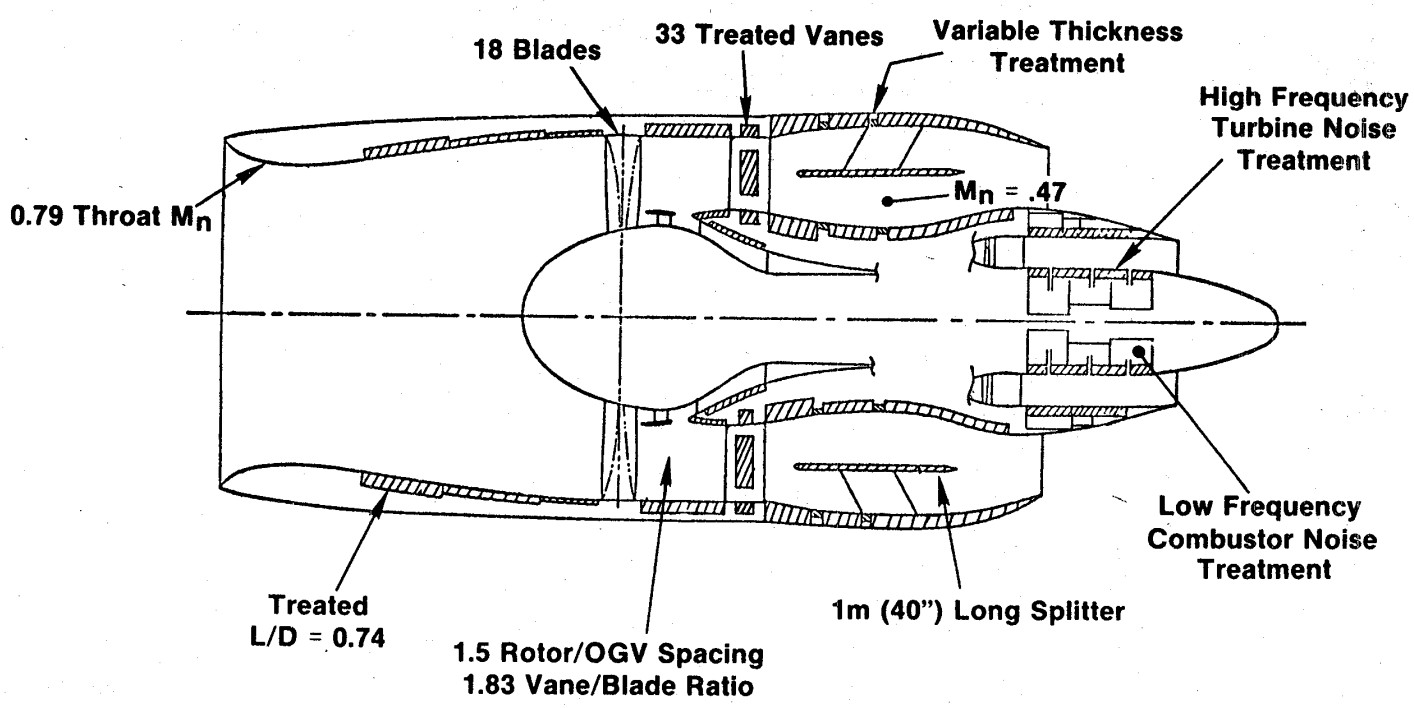

Figure 105. UTW Engine Acoustic Features.

- p/p = 1.34
- Tip Speed = 350m/sec (1150 ft/sec)

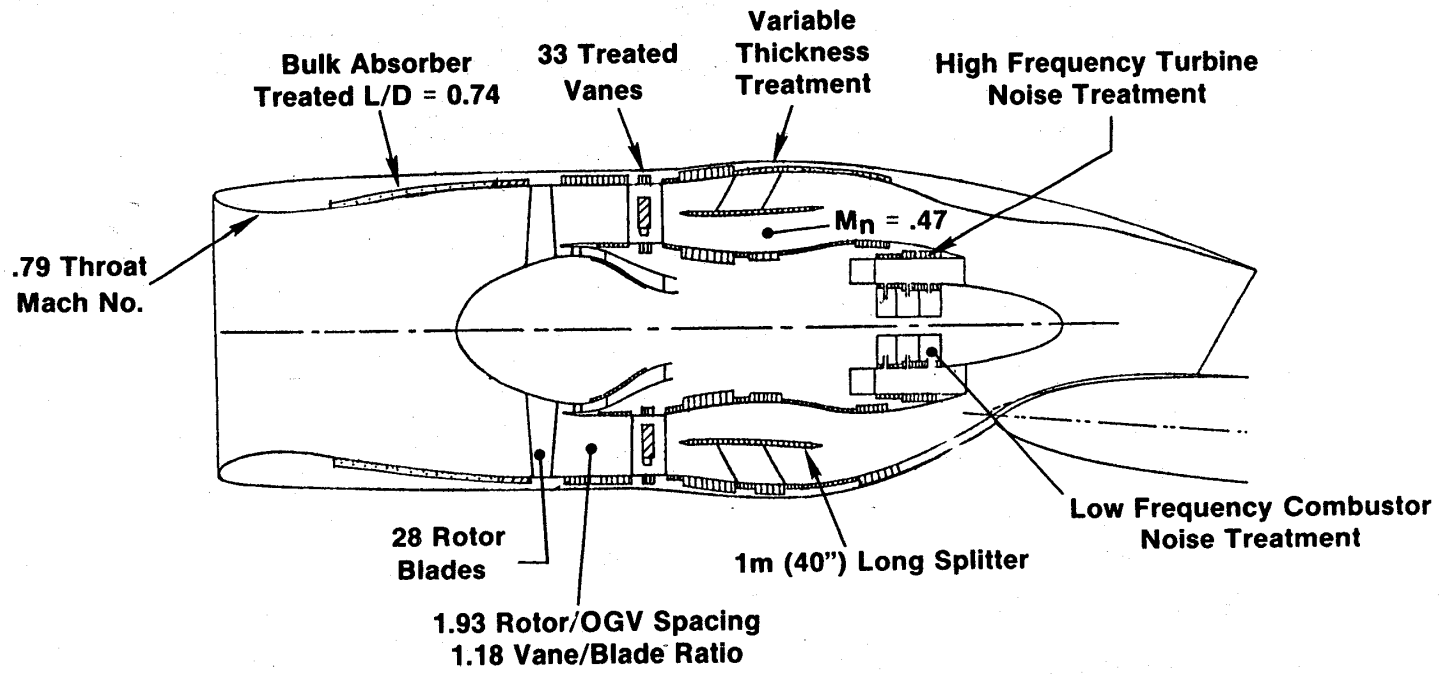

Figure 106. OTW Engine Acoustic Features.

having a vane/blade ratio value near 2 to cut-off rotor/stator interaction noise. It was felt that the wide spacing of 1.93 rotor tip chords for the OGV/fan rotor would reduce rotor/stator interaction noise to the point where it would not be a major contributor; thus, there was no need for "overkill" by selecting a high vane/blade ratio.

Other acoustic features of the OTW are very similar to the UTW including the treated vanes, "stacked" core treatment, variable-depth and variable-porosity fan exhaust wall treatment, 1.02-m (40-in.) acoustic splitter, and high throat Mach number inlet. At approach and reverse thrust, the OTW inlet provides suppression with bulk absorber wall treatment.

3.10.2 Fan Inlet Design

Preliminary system studies conducted on both engines indicated that achieving a balanced design would require the following levels of inlet PNL suppression:

	UTW (PNdB)	OTW (PNdB)
Takeoff	12.8	13.5
Approach	6.3	10.4
Reverse Thrust	4.5	11.5

These high levels of required suppression could be achieved with a conventional inlet; however, with wall treatment only the treated-length-to-diameter ratio would be much greater than 1.0 and/or inlet splitters would be required. Previous experience has shown that large levels of inlet suppression can be achieved from high throat Mach number inlets. As shown in Figure 107, which compares inlet-noise-reduction concepts, takeoff suppression can be achieved with a treated high throat Mach number inlet. At approach and reverse thrust, suppression is achieved with the wall treatment only since the inlet Mach number is much lower.

In order to demonstrate that the high levels of inlet suppression can be achieved, a scale-model test program was conducted in the General Electric anechoic chamber shown in Figure 108. The anechoic chamber can handle models for inlet-radiated-noise studies or for exhaust-radiated noise as will be discussed later. The models are powered by a 1.86-MW (2500-hp) drive system. Physical dimensions of the chamber are approximately 10.7 m (35 ft) long by 7.6 m (25 ft) wide by 3 m (10 ft) high with microphones located at model-centerline height on a 5.2-m (17-ft) arc.

An exact scale model of the UTW fan was used for these studies. It was 5.8 cm (20 in.) in diameter and could be manually adjusted for various blade angles including those required to demonstrate reverse thrust. Test objectives are summarized below:

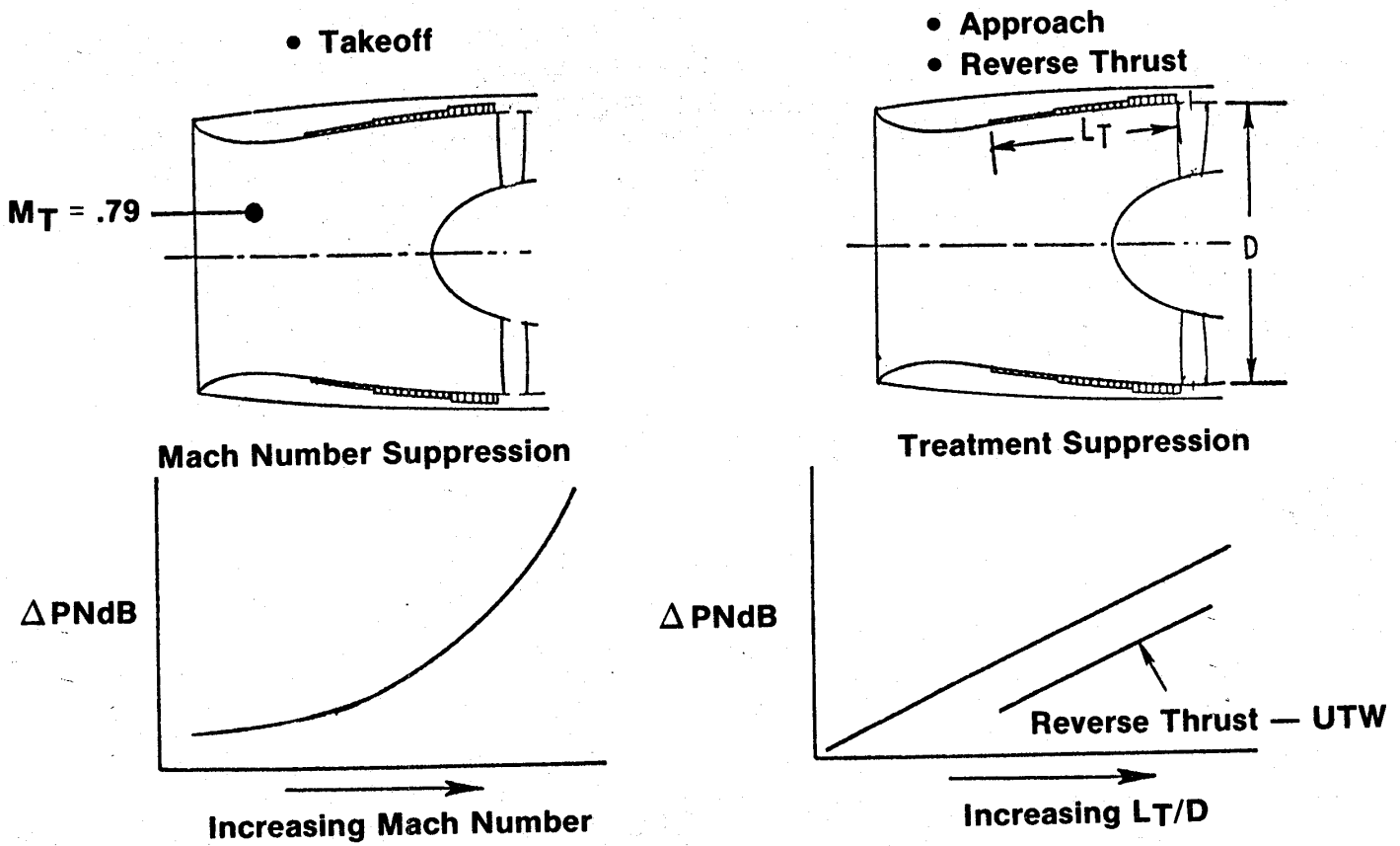

Figure 107. QCSEE Inlet-Noise-Reduction Concepts.

Figure 108. UTW QCSEE in Anechoic Chamber.

Forward Thrust

- Define unsuppressed spectrum and level
- Define suppression due to high throat Mach number
- Define suppression due to treated wall

Reverse Thrust

- Define unsuppressed spectrum and level
- Define suppression due to treated wall

Figure 109 presents the variation in inlet noise with throat Mach number and the PNL suppression that was achieved. These results indicate that the UTW takeoff suppression requirement of 12.8 PNdB could be met at an average throat Mach number of 0.79. The suppression due to high Mach number alone was about 10 PNdB with the wall treatment adding almost 3 PNdB.

In reverse thrust, the model tests indicated (as shown in Figure 110) that the objective level of suppression could be achieved; however, the unsuppressed levels were higher than expected. As will be shown later, this fact resulted in the UTW system-noise estimate in reverse thrust being revised to be above the goal of 100 PNdB.

Both inlets, as finally designed, are shown schematically in Figure 111. Both are high throat Mach number inlets designed to achieve takeoff suppression at a 0.79 throat Mach number. The treated-length-to-diameter ratio was 0.74 for both inlets. Wall treatment utilized on the inlets is shown schematically in Figure 112. The UTW utilized single-degree-of-freedom resonator treatment with a faceplate porosity of 10% and cavity depths ranging from 1.2 cm (0.5 in.) to 3.9 cm (1.5 in.). A bulk absorber type treatment was incorporated into the OTW inlet to provide wider bandwidth suppression. The bulk absorber consisted of seven compressed layers of a Kevlar material. It was a constant depth of 2.54 cm (1 in.) with porosity of 14% over the first half and 22% over the latter half. Although a scale model of the OTW fan was not tested, the inlet design was based upon General Electric experience from previous tests and consideration of the results of UTW model tests.

3.10.3 Fan Exhaust Design

As pointed out earlier in Figures 105 and 106, the engine designs incorporated both source-noise-reduction techniques and significant amounts of acoustic treatment to reduce exhaust-radiated noise. Source-noise-reduction techniques and treatment configurations were evaluated on the basis of past experience and the results of testing a low-pressure-ratio, variable-pitch, model fan (NASA Rotor 55) in the General Electric anechoic chamber. A photograph of the model as installed in the exhaust mode is shown in Figure 113. Testing evaluated such source-noise-reduction concepts as optimizing vane/blade ratio to minimize second-harmonic-tone propagation, rotor/stator spacing, and rotor/OGV treatment.

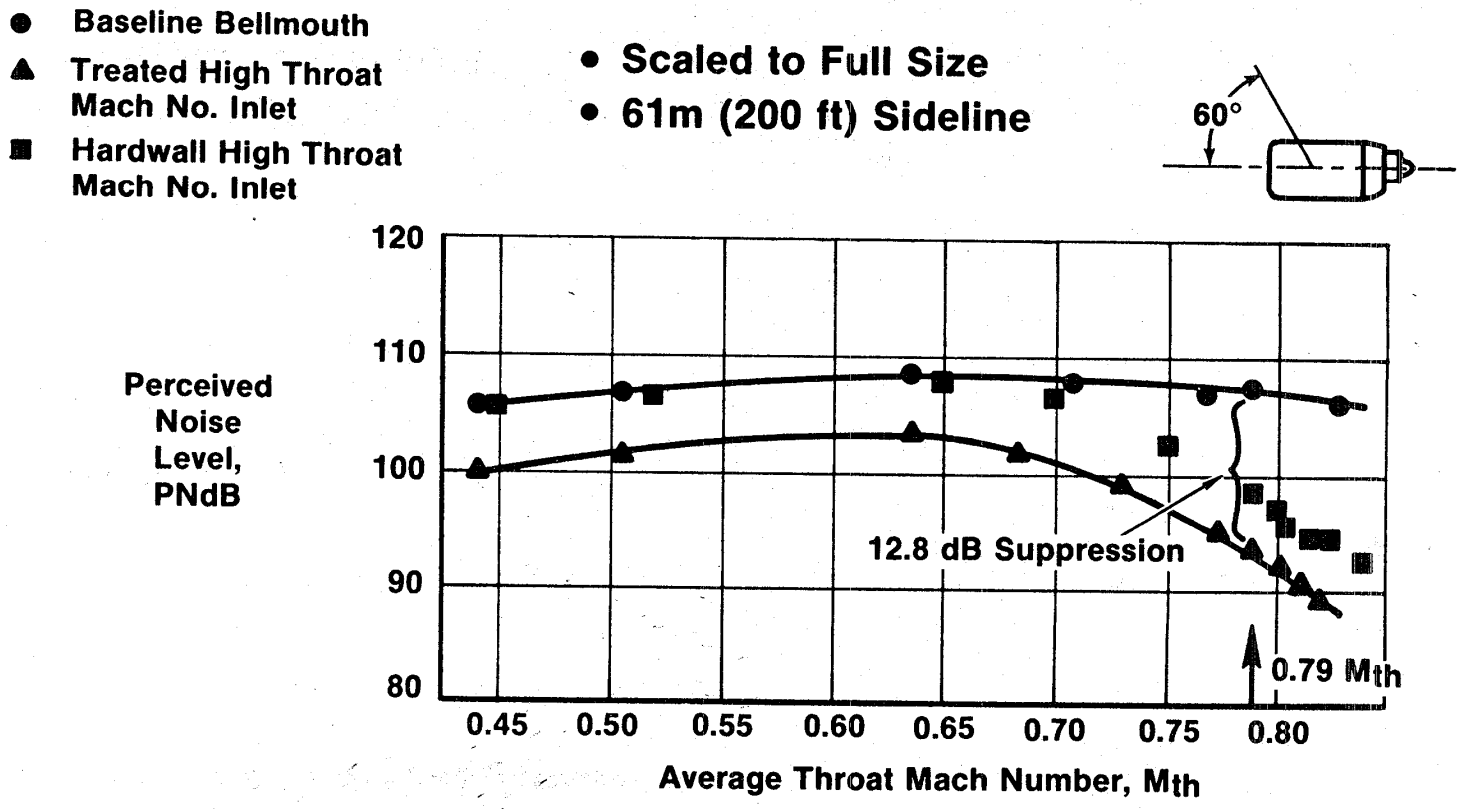

Figure 109. High Throat Mach No. Inlet Suppression, 50.8 cm (20 in.) Simulator Test.

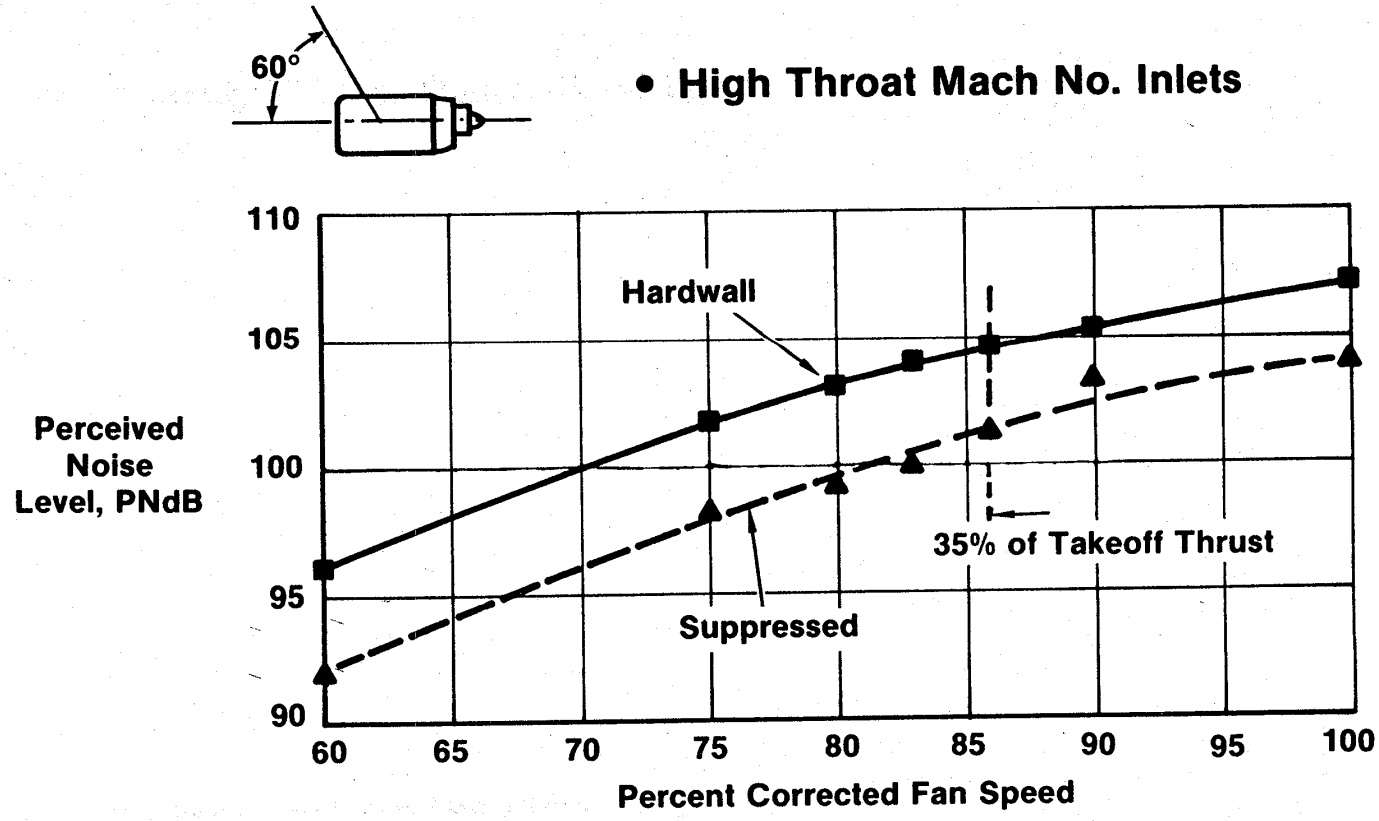

Figure 110. Reverse-Thrust Suppression, 50.8 cm (20 in.) Simulator Test.

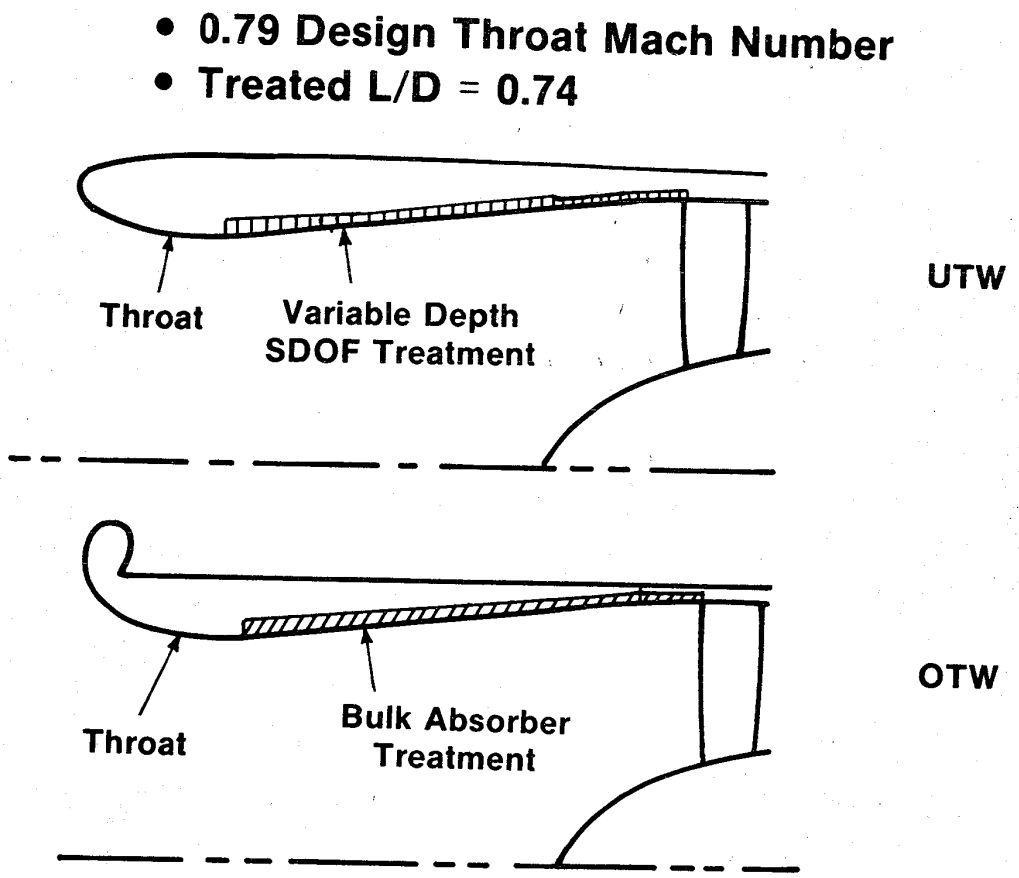

Figure 111. Inlet Acoustic Configurations.

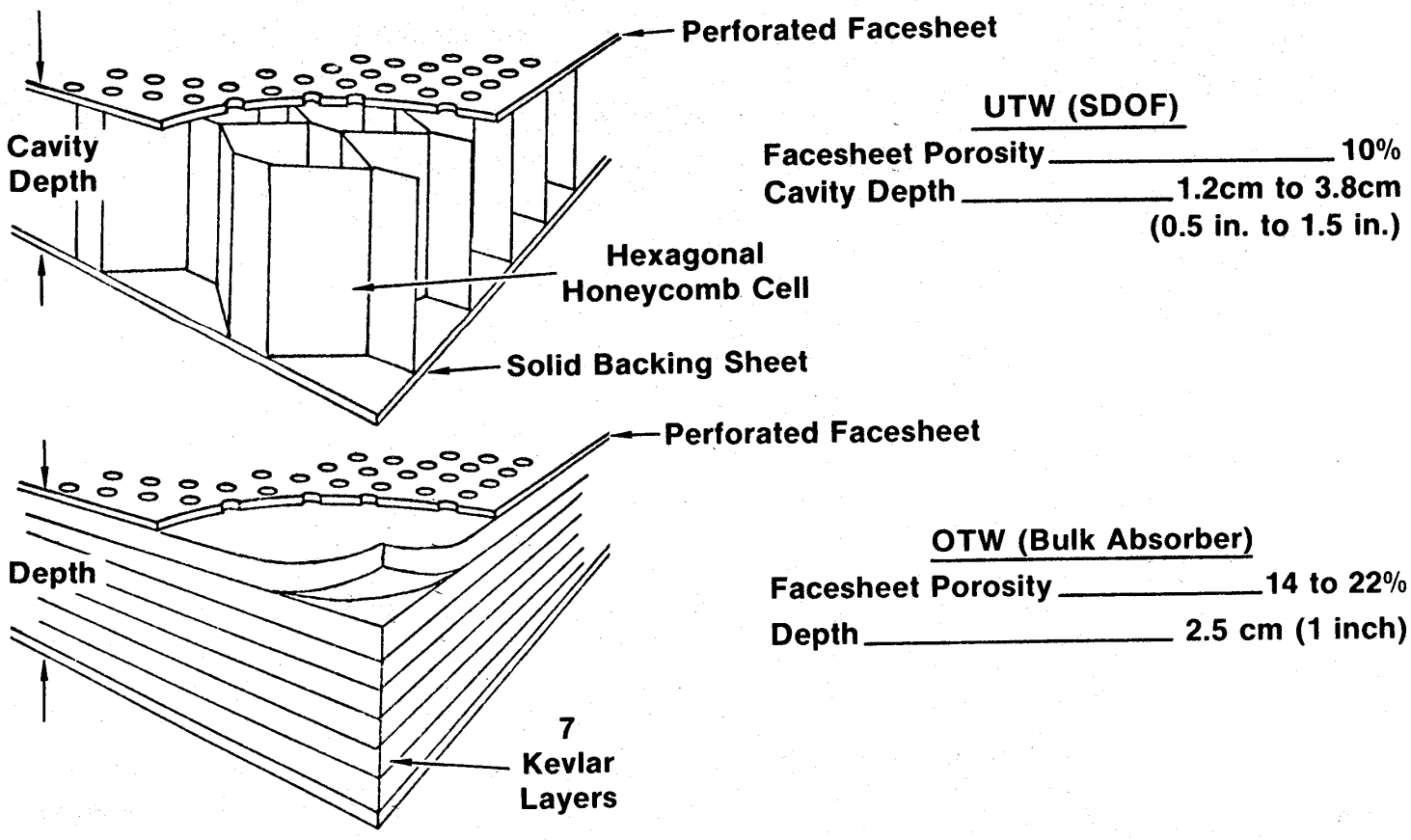

Figure 112. Inlet Acoustic Treatment.

Figure 113. Exhaust-Radiated-Noise Model.

The vane/blade ratio study was conducted at two different rotor/stator spacings. As shown in Figure 114, the data at 0.5 chord spacing indicates a second-harmonic SPL minimum at a vane/blade ratio of 1.88. At the wider spacing of 1.5 chords, the data do not show this because the rotor/stator interaction noise is masked by rotor noise caused by turbulence generated upstream of the rotor. At the close spacing, rotor/stator noise is dominant, allowing us to see the second-harmonic minimum.

A series of spacing tests from 0.5 chords to 2.0 chords was conducted. Figure 115 is a comparison between the measured levels and the sum of predicted rotor/stator interaction noise and rotor/turbulence noise at each spacing. This was done at the optimum vane/blade ratio. Excellent agreement between predicted and measured data is evident.

Tests of treatment between the rotor and OGV indicated that 4 to 5 dB suppression could be achieved at the blade-passing frequency. Accordingly, the fan frame was designed to incorporate rotor/OGV treatment.

The model fan had the capability to test up to four axial sections of treatment in the exhaust mode. Various combinations of faceplate porosity, treatment depths, and axial deployment were evaluated. Suppression results from one of those configurations are represented in Figure 116. Note the axial variation in treatment depth and faceplate porosity. The results indicate that such an orientation achieves higher suppression above the peak tuning frequency than one would predict from summing the suppressions of the individual panels. On the basis of these results, design curves for the engines were changed to account for this higher level of suppression with variable-depth, variable-porosity treatment.

A schematic of the exhaust treatment design for the UTW is presented in Figure 117. OTW engine exhaust treatment was very similar. All the suppression material was the single-degree-of-freedom resonator type shown in Figure 118. Fan frame treatment between the rotor and OGV was tuned to the blade-passing frequency of each engine and had a faceplate porosity of 10%. Fan-bypass wall treatment depths varied from 1.9 cm (0.75 in.) to 5.1 cm (2.0 in.) and porosities from 15 to 22%. Splitter length of 1.02 m (40 in.) included single-degree-of-freedom treatment of 1.27 cm (0.5 in.) with a porosity of 11.5%. Although a scale-model test with treated vanes was not conducted, design studies indicated a potential for reducing high-frequency, broadband noise; thus, the pressure surface of the OGV's was treated on the full-scale engines. The resulting suppression spectrum for the UTW aft-radiated fan noise, utilizing the treatment of Figure 117, is shown in Figure 119. Such a suppression spectrum would achieve 13.4 PNdB of aft-fan-noise suppression at takeoff on the UTW.

3.10.4 Core Suppressor Design

The QCSEE core exhaust provides a rather severe problem in acoustic-suppression design. The unsuppressed source-noise spectrum has both high-frequency, broadband noise from the turbine and low-frequency, broadband noise

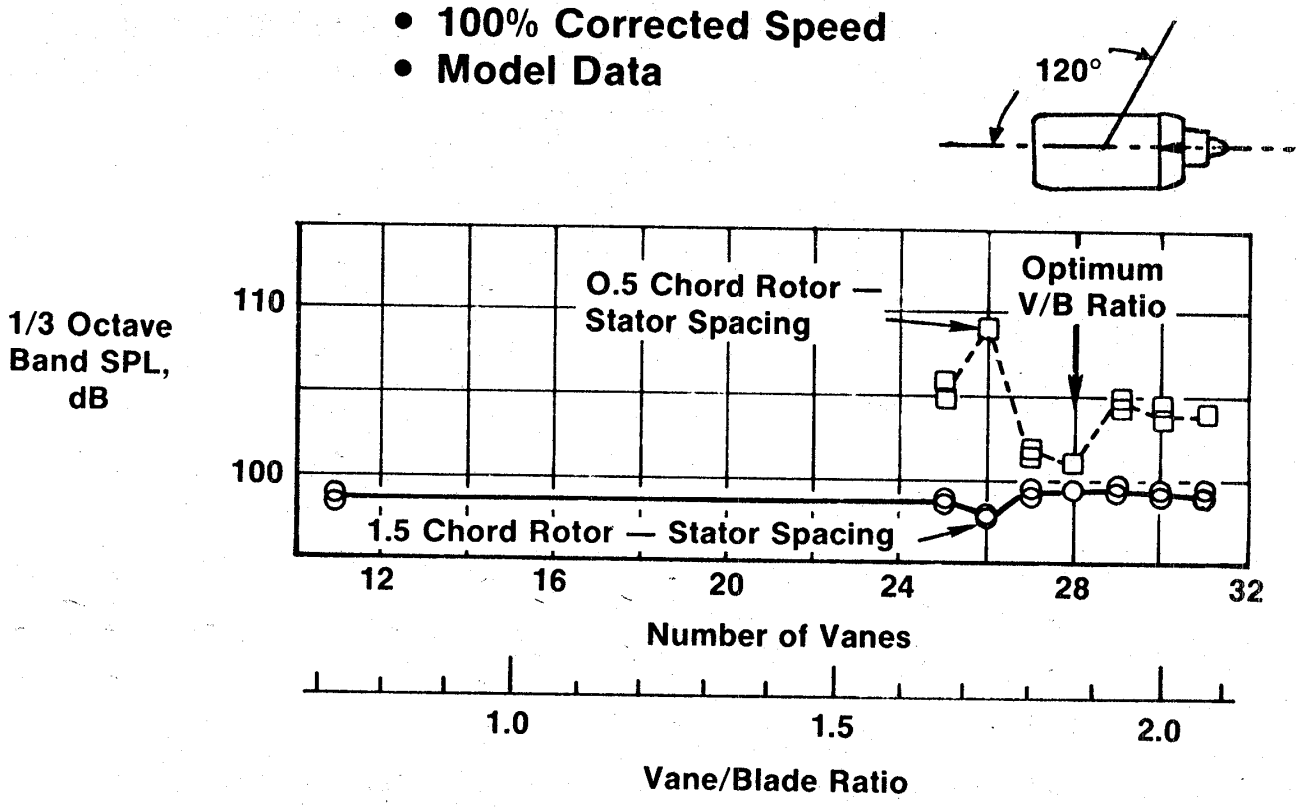

Figure 114. Effect of Vane Number on Second-Harmonic SPL.

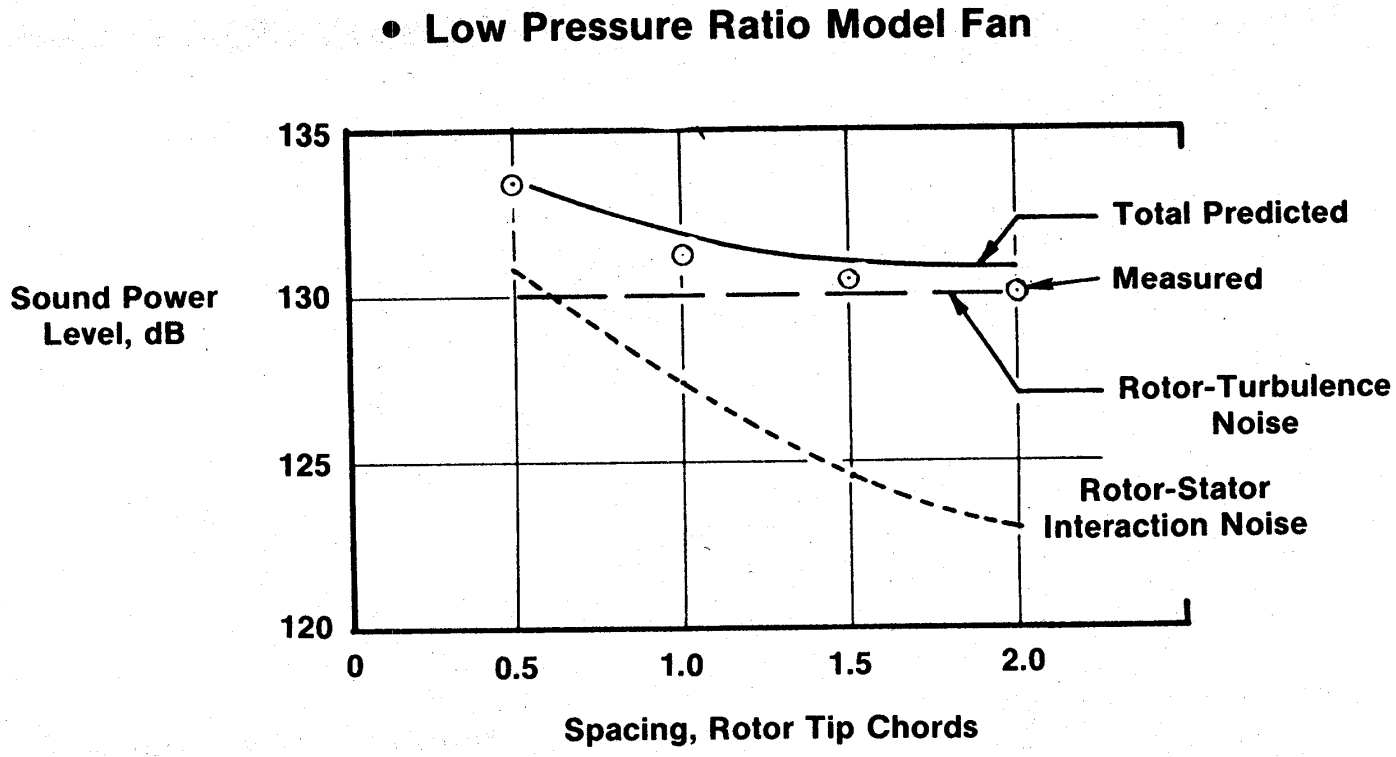

Figure 115. Summation of Rotor-Turbulence and Rotor/Stator Noise.

- Low Pressure Ratio Fan (NASA Rotor 55)
- 100% N/$\sqrt{\theta}$
- Variable Depth, Variable Porosity

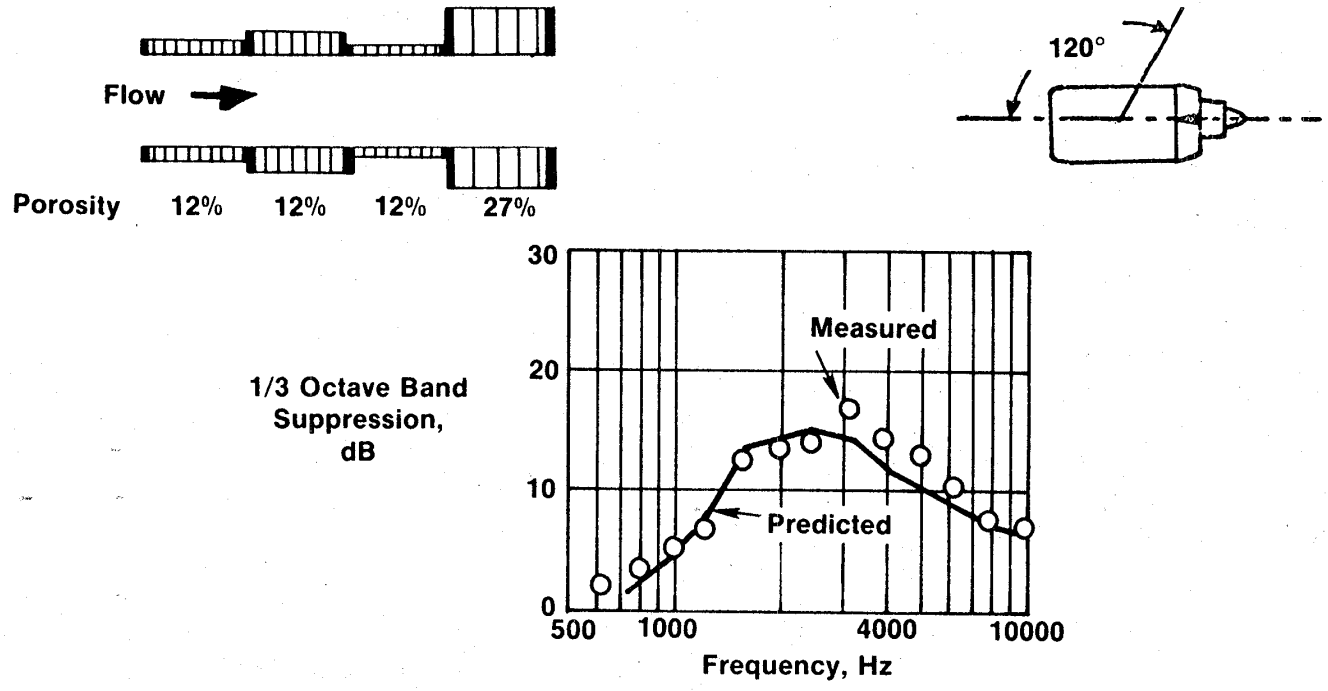

Figure 116. Scale-Model Suppression Test Results.

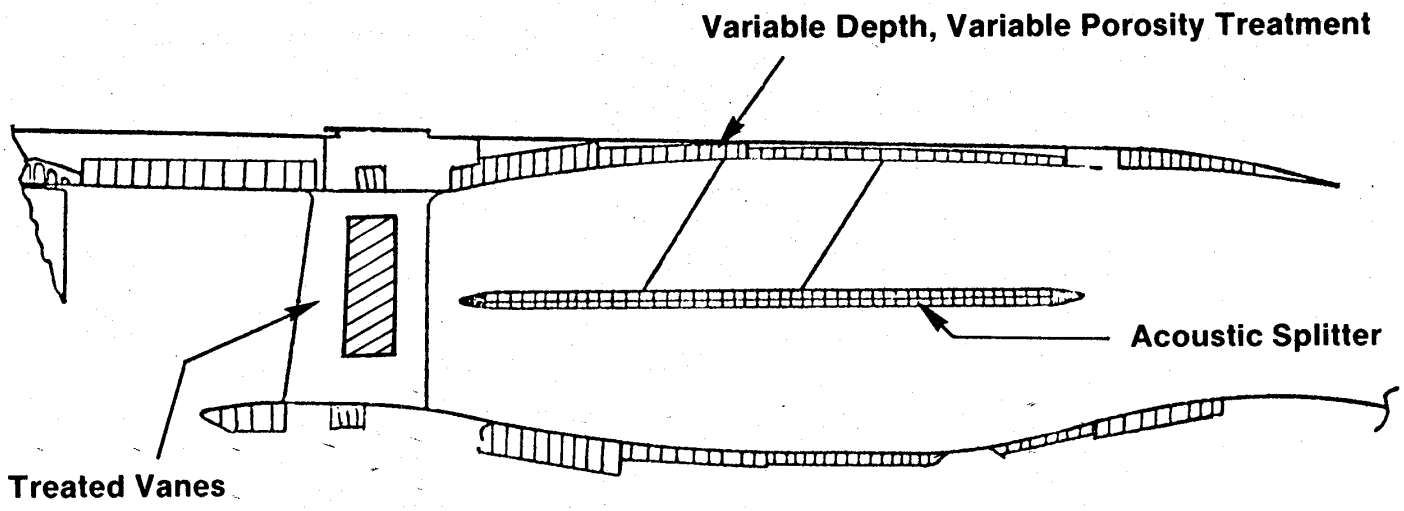

Figure 117. Fan Exhaust Treatment Configuration.

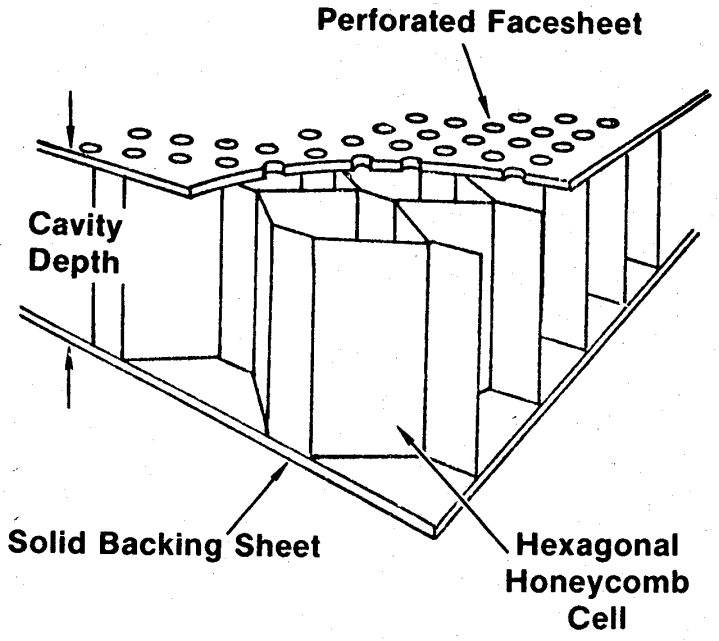

Wall Treatment

Facesheet Porosity	10 to 22%
Cavity Depth	1.9 cm to 5.1 cm (0.75 to 2.0 in.)

Acoustic Splitter

Facesheet Porosity	11.5%
Cavity Depth	1.27 cm (0.5 in.)

Figure 118. Single-Degree-of-Freedom Exhaust Acoustic Treatment.

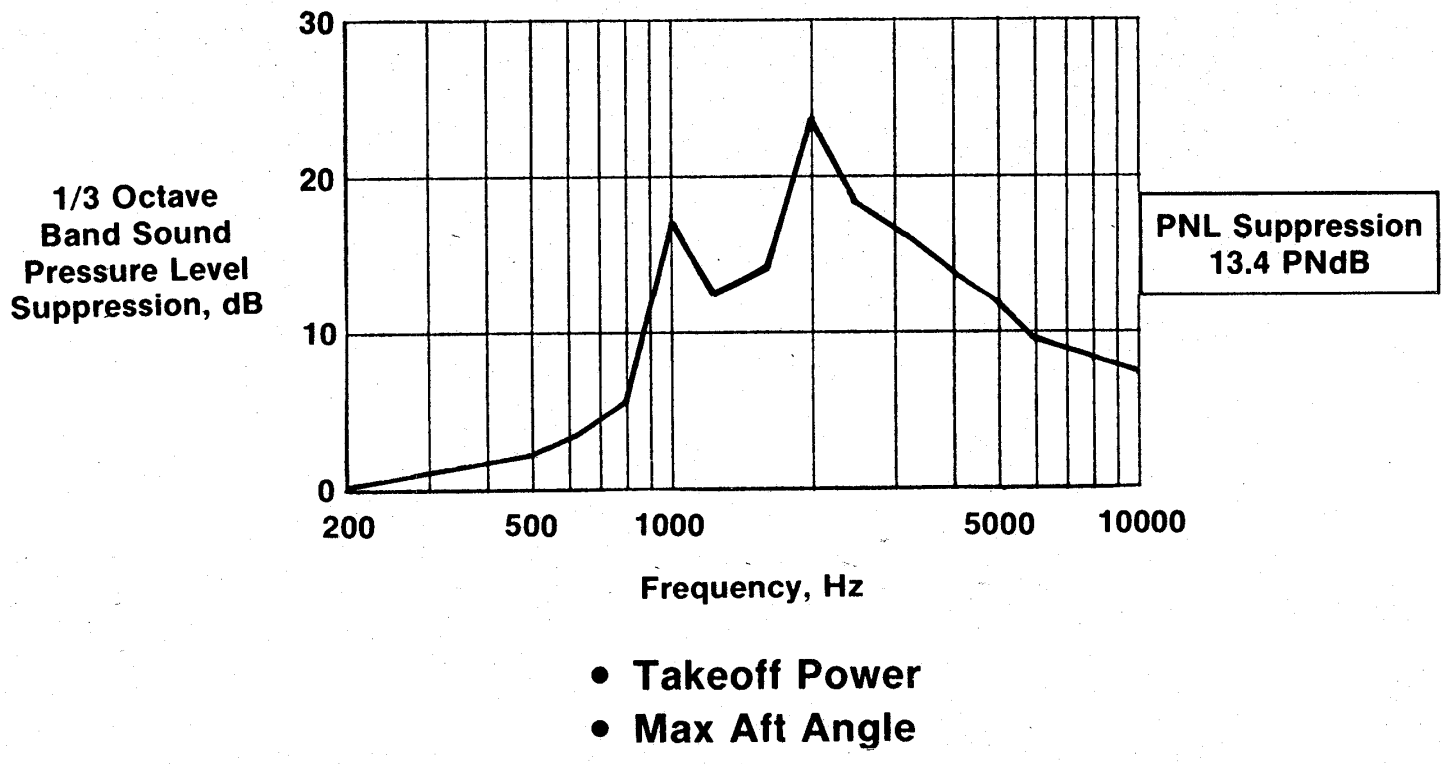

Figure 119. Predicted UTW Fan Exhaust Suppression.

from the combustor. To attain any meaningful noise reduction, the suppressor must attenuate both the high- and low-frequency noise levels. Physical constraints on the engine prevented sufficient amounts of thick (low frequency) and thin (high frequency) treatment from being installed in tandem to give adequate suppression. It was decided to adopt a new concept as shown in Figure 120 and employ a "stacked" treatment design. In this concept, the thin turbine treatment is placed along the duct walls. Thick combustor treatment is then placed behind this turbine treatment and communicated to the duct by means of tubes passing through the turbine treatment. Figure 121 shows the treated QCSEE core plug. Note the larger diameter holes which communicate to the combustor treatment.

A model of this advanced concept was built and tested in the General Electric High Temperature Duct Facility. Results from these tests are shown in Figure 122; they indicate that the stacked treatment would provide the required levels of suppression of 5.1 and 9.89 PNdB in the low- and high-frequency regimes.

3.10.5 QCSEE UTW System Noise Predictions

Since the engine noise levels were to be measured during static testing, a procedure for determining in-flight noise levels from static data was completed as a part of the design effort. This procedure includes the following:

- Jet/flap noise-calculation procedure
- Extrapolation procedures
- Corrections for engine size
- Doppler shift corrections
- Corrections for number of engines
- Dynamic effect correction
- In-flight clean-up and up-wash-angle correction
- Relative velocity correction for jet/flap noise
- Fuselage shielding and OTW shielding
- PNL to EPNL calculation

Calculated jet/flap interaction noise was used to replace the jet noise on the static engine; however, an advanced-technology allowance was assumed on jet/flap noise of 3.5 PNdB on the UTW and 2.5 PNdB on the OTW to account for anticipated reduction in jet/flap noise by the 1980's when QCSEE-powered aircraft might be flying.

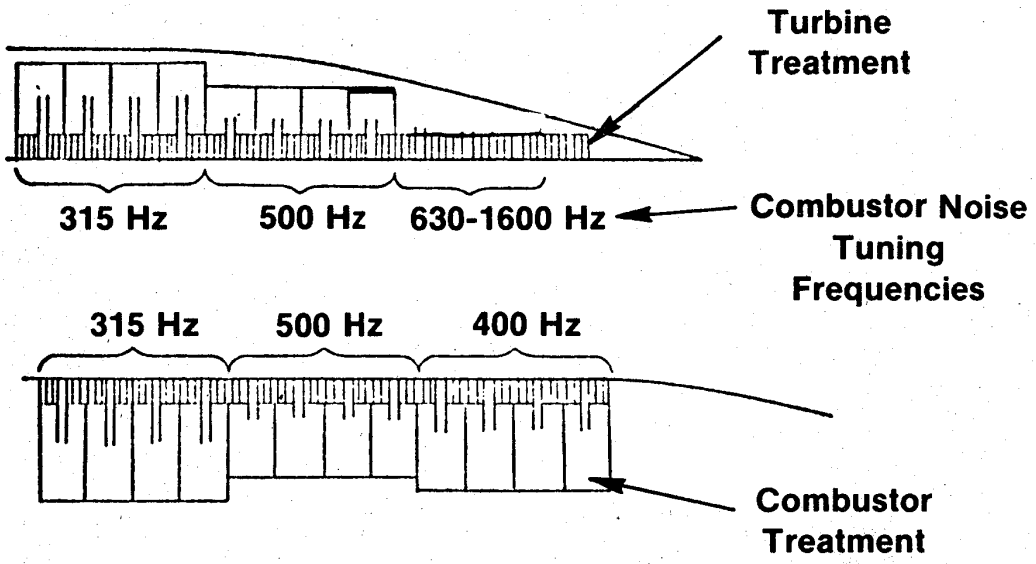

Figure 120. Core Stacked-Treatment Suppression.

Figure 121. QCSEE Core Exhaust Nozzle.

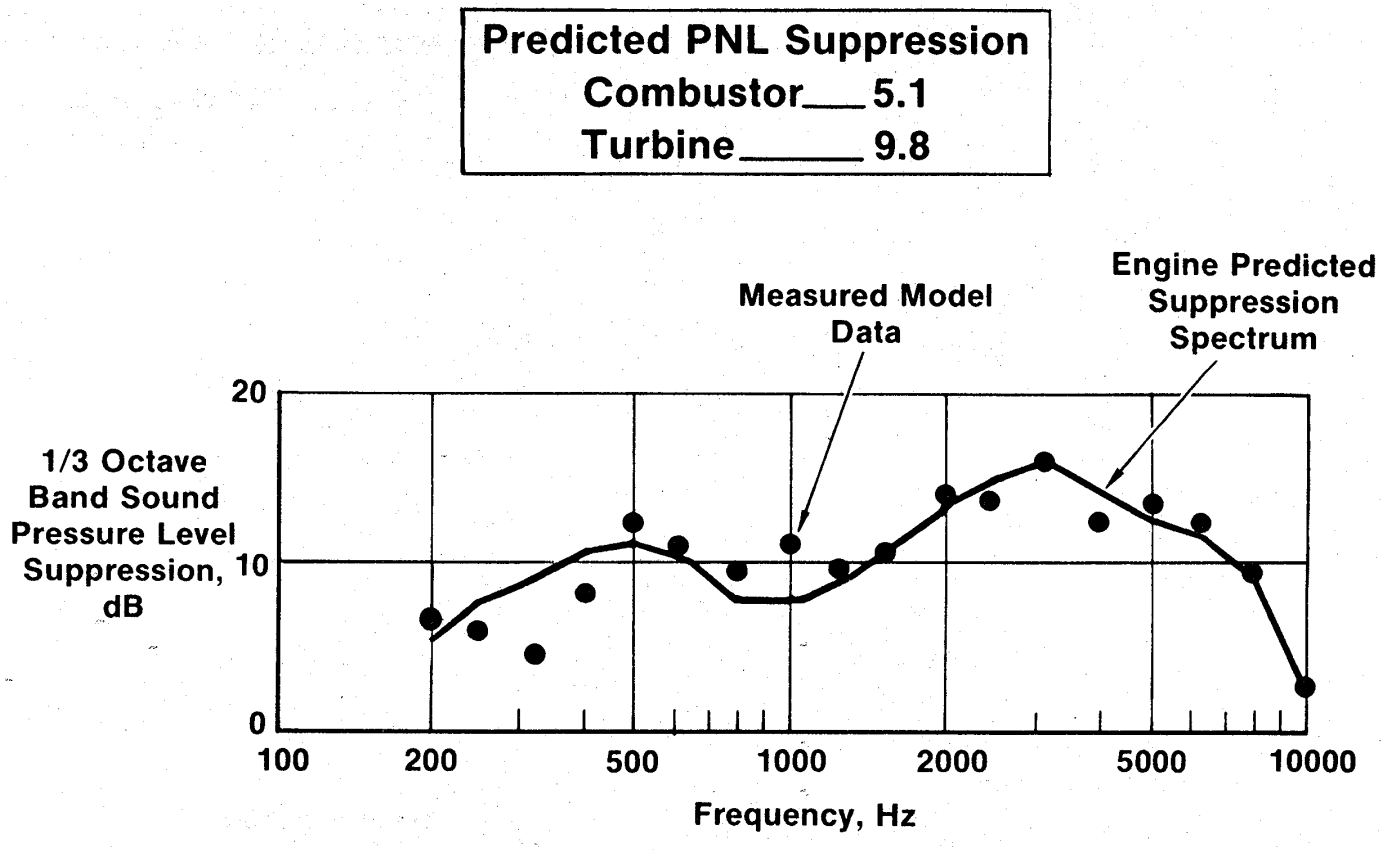

Figure 122. Hot Duct Model Test Data.

System noise levels for the UTW QCSEE are presented in Figure 123 at the takeoff condition. Unsuppressed noise is dominated by the fan in both the forward and aft quadrants. The suppressed levels are balanced between fan, jet/flap, and combustor noise in the aft quadrant and dominated by jet/flap noise in the forward quadrant. The predicted EPNL for the four-engine UTW configuration at takeoff is 93.6 EPNdB compared to the goal of 95.0 EPNdB on a 152-m (500-ft) sideline.

To obtain 65% of takeoff thrust at approach, the UTW QCSEE with its variable-pitch fan may be operated at a variety of fan speed, blade-pitch angle, and fan-nozzle-area combinations. For these acoustic predictions, the fan speed was held at a takeoff speed to minimize engine-response time in the event of a waveoff during landing. Fan nozzle area was wide open to lower jet velocity, and hence jet/flap noise, and the blade-pitch angle was closed down to give the required thrust. In such a mode of operation, unsuppressed noise, Figure 124, is dominated by fan noise in both the forward and aft quadrants. Suppressed, the forward quadrant is dominated by fan noise while the aft quadrant has a balanced design with fan, combustor, and jet/flap noise about the same level. Estimated EPNL for approach is 93.3 compared to the goal of 95.0 EPNdB.

In reverse thrust, Figure 125, the UTW noise levels are dominated by the forward-quadrant fan noise both unsuppressed and suppressed. These levels, based on the 50.8-cm (20-in.) model tests, indicate that in reverse thrust the engine will be 103.9 PNdB on a 152-m (500-ft) sideline or 3.9 PNdB over the goal of 100 PNdB. It would be difficult to obtain more fan-inlet suppression without degrading the suppression at takeoff and approach and eroding the margin present at those conditions. This treated, composite-nacelle design provides the most balanced approach to meeting the three noise goals.

3.10.6 QCSEE OTW System Noise Predictions

System-noise levels for the OTW QCSEE were also predicted. At takeoff (Figure 126), unsuppressed fan noise controls forward and aft quadrants. In the suppressed configuration, fan and jet/flap noise are about the same level. The resulting system EPNL is 95.4 EPNdB, only slightly above the goal of 95. Any reduction to lower the level to 95.0 EPNdB must include jet/flap noise reduction since it is a major contributor.

At approach (Figure 127), fan suppression has lowered the dominant unsuppressed fan noise to the level of jet/flap noise. These two sources, suppressed fan and jet/flap, combine to give a predicted EPNL of 90.0 EPNdB which is well under the goal of 95.0.

For reverse-thrust operation, the OTW engine utilized a target reverser. General Electric had conducted tests on a 1/6 scale model of the OTW target thrust-reverser system. On the basis of these tests, it was realized that the jet noise levels of the target reverser were much higher than anticipated, and only a reduction in fan pressure ratio was likely to produce a significant reduction in reverse-thrust noise. With this in mind, the predicted OTW reverse-thrust noise level in Figure 128 is 106.4 PNdB or 6.4 PNdB above the goal.

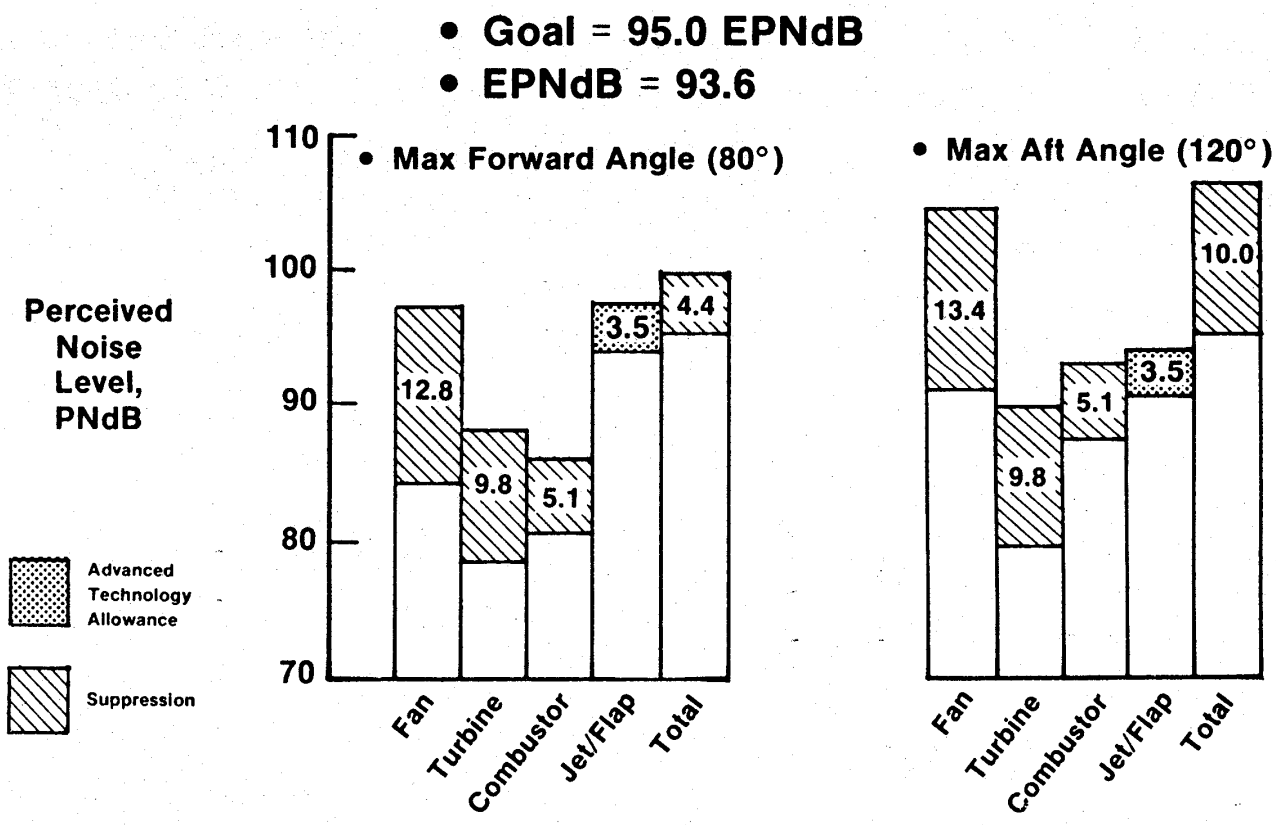

Figure 123. UTW Takeoff Noise Predictions.

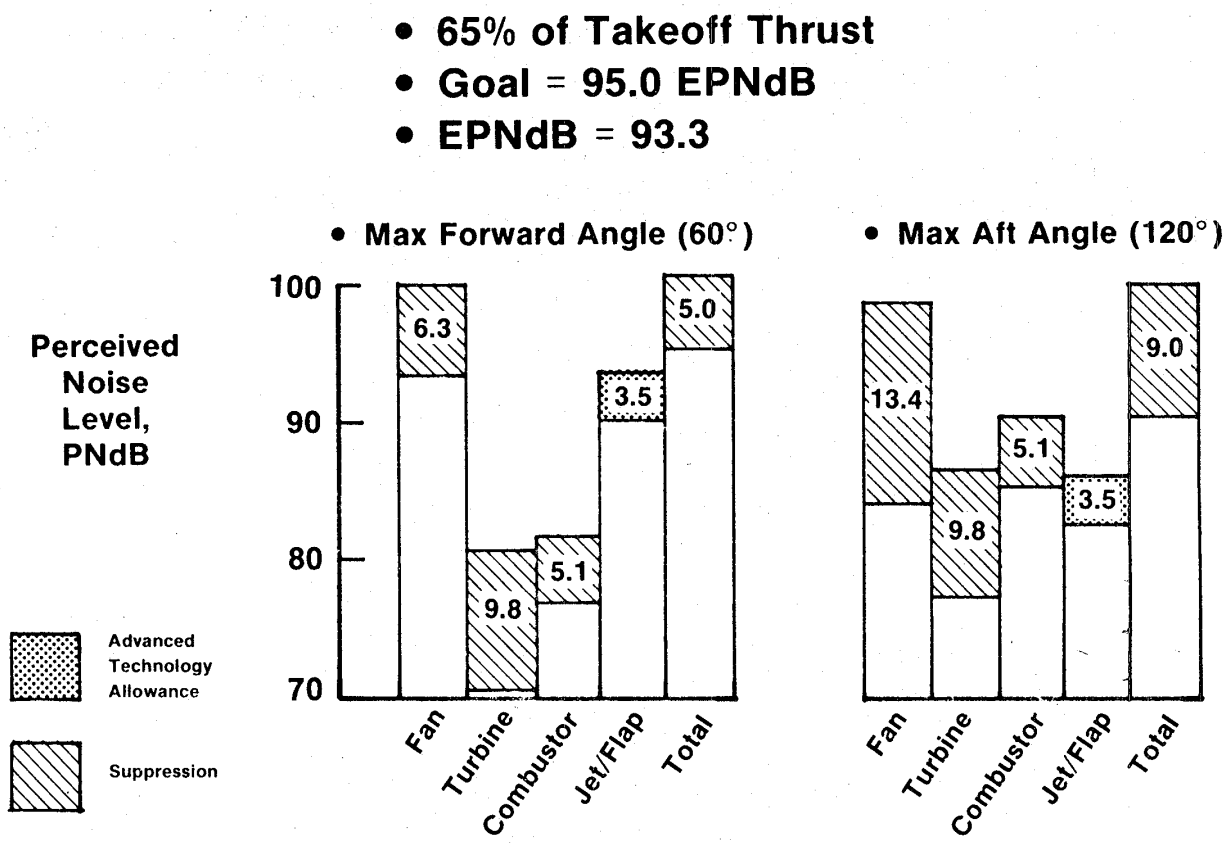

Figure 124. UTW Approach Noise Predictions.

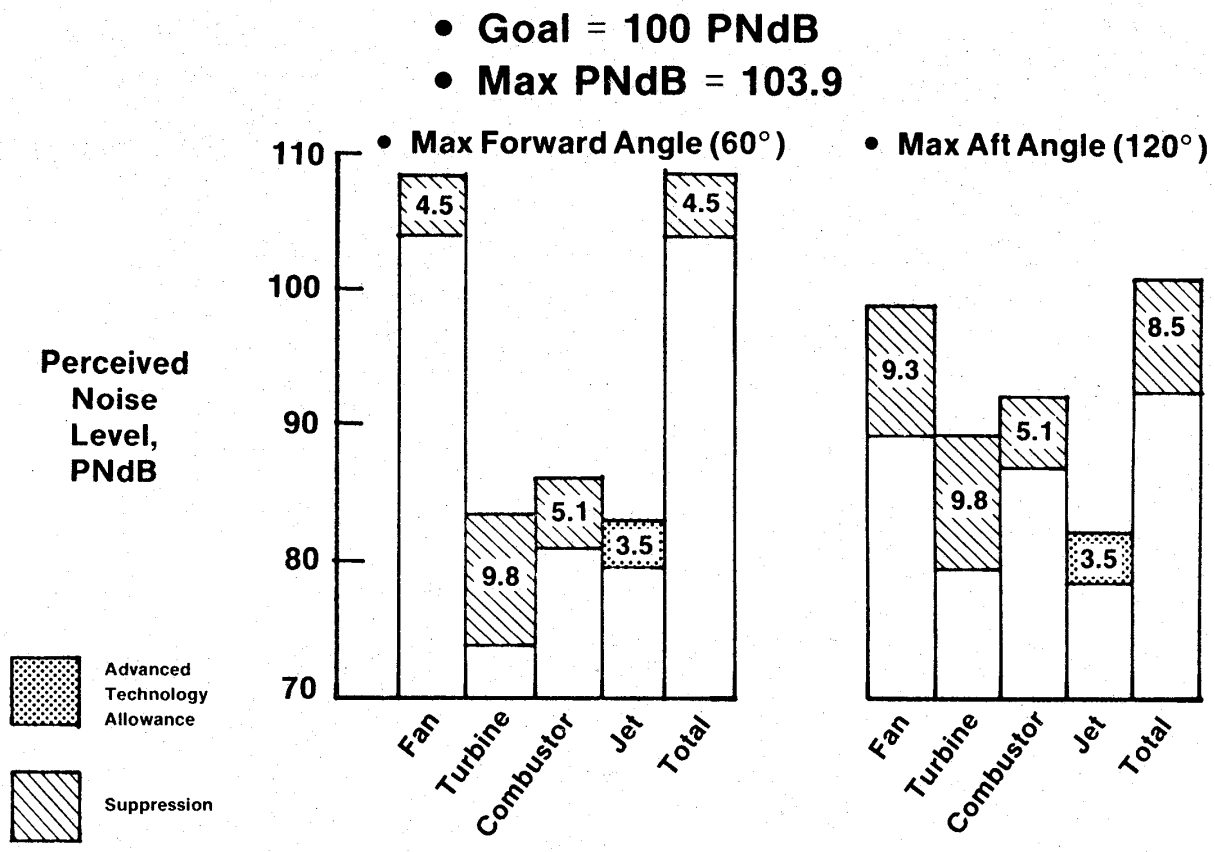

Figure 125. UTW Reverse-Thrust Noise Predictions.

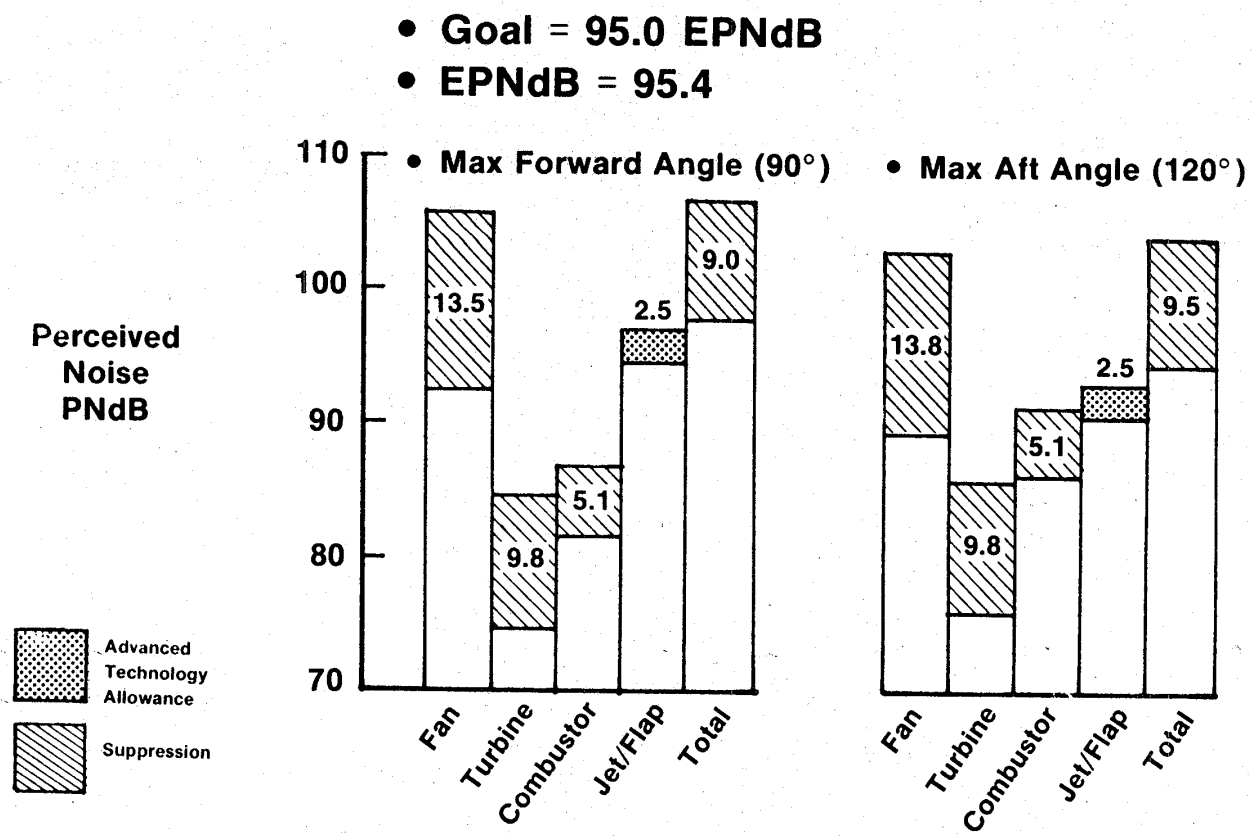

Figure 126. OTW Takeoff Noise Predictions.

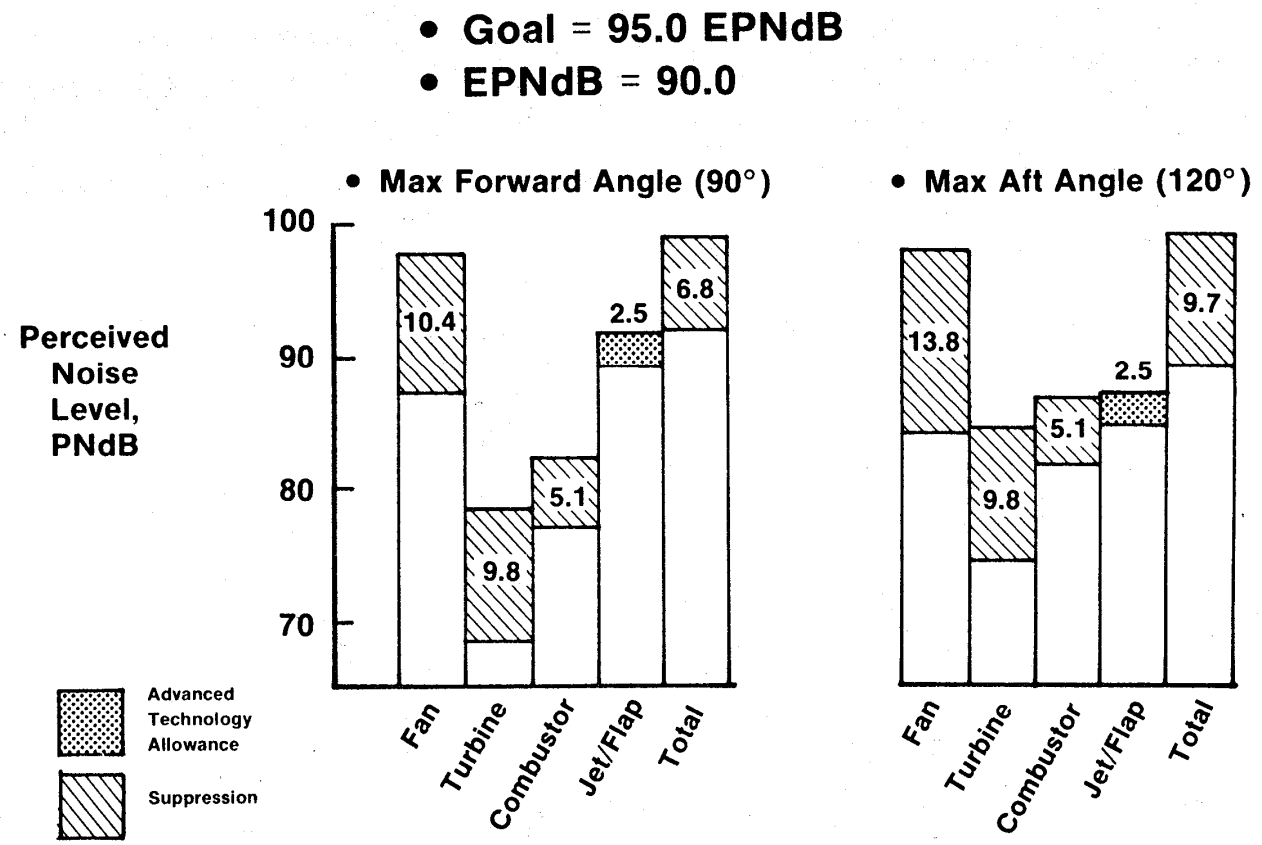

Figure 127. OTW Approach Noise Predictions.

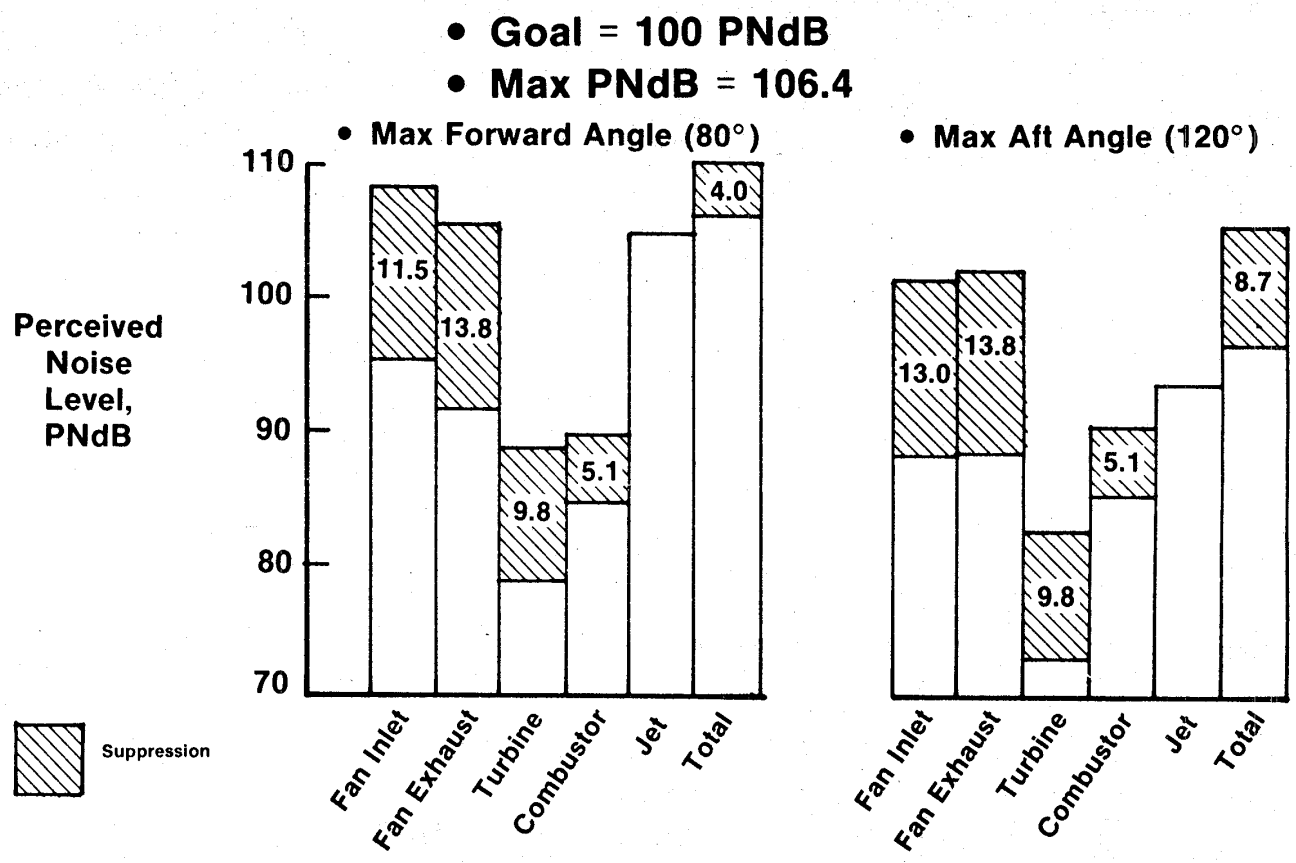

Figure 128. OTW Reverse-Thrust Noise Predictions.

4.0 ENGINE TEST RESULTS

This section presents and discusses the results of testing UTW and OTW propulsion systems. All testing was conducted at General Electric's Peebles, Ohio outdoor test site 4D. This site includes an overhead engine-support structure with all necessary fuel, lubrication, air, and electric facilities. An adjacent control room is linked to the Evendale computer by an automatic data-handling system using leased telephone equipment. The test site includes an acoustic field for recording far-field acoustic data over a 150° arc.

The history of UTW testing is summaried in Table XXIV. Testing was initiated on 2 September 1976 with boilerplate nacelle components and using the cam/harmonic pitch-actuation system. Mechanical and performance testing was completed except for the planned reverse-thrust test. During this phase of testing, an exhaust nozzle support-ring attachment failure occurred, allowing one nozzle flap to be drawn into the engine and causing secondary damage to the fan blades.

Damaged parts were repaired or replaced, and the engine was reinstalled in September 1977 for completion of the test program. The second installation included the ball spline pitch-actuation system and the entire composite nacelle. Planned testing, including acoustic measurements, was completed in July 1978. The engine was then refurbished and delivered to NASA for further testing at the Lewis Research Center.

The history of OTW testing is summarized in Table XXV. The entire test program was conducted on this engine between 6 April and 9 June 1977. All testing included the boilerplate nacelle and "D" shaped exhaust nozzle. The OTW engine was refurbished and delivered to NASA in July, 1977.

4.1 OVERALL ENGINE PERFORMANCE

4.1.1 UTW Performance Test

Figure 129 shows the UTW engine as it was initially tested with a bellmouth inlet for airflow calibration and to establish uninstalled performance levels with essentially 100% ram recovery. The high throat Mach number inlet, shown in Figure 130, was then used to determine installed performance with realistic induction losses.

Measured uninstalled thrust with the bellmouth inlet is shown on Figure 131 as a function of airflow for operating lines established by four fan-exhaust-nozzle areas. Points along each operating line represent various combinations of blade angle and fan speed that can pump the indicated airflow. Thus, the curve is independent of blade angle and speed. The goal thrust level could be reached with a variety of settings of the controlled parameters.

Table XXIV. UTW Test History.

Boilerplate Nacelle, Cam-Harmonic Pitch Actuation

47 Hours (9/2/76 — 12/17/76)

- Mechanical and Controls Checkout
- Aero Performance Mapping — Bellmouth Inlet
- Performance Ratings — High Mach Inlet
- Reverse Thrust Test (Incomplete)

Composite Nacelle, Ball Spline Pitch Actuation

106 Hours (9/8/77 — 4/27/78, 7/13/78 — 7/21/78)

- Mechanical and Performance Checkout
- Acoustic Baseline — Bellmouth/Hardwall
- Suppressed Acoustic Test — High Mach Inlet, Treatment
- Reverse Thrust Performance and Acoustics
- Acoustic Technology and Control Tests

Table XXV. OTW Test History.

Boilerplate Nacelle

58 Hours (4/6/77 — 6/9/77)

- Mechanical and Controls Checkout
- Aero Performance Mapping — Bellmouth Inlet
- Performance Ratings — High Mach Inlet
- Reverse Thrust Performance
- Acoustic Baseline — Bellmouth, Hardwall
- Suppressed Acoustics — High Mach Inlet, Treatment
- Transient Thrust Response

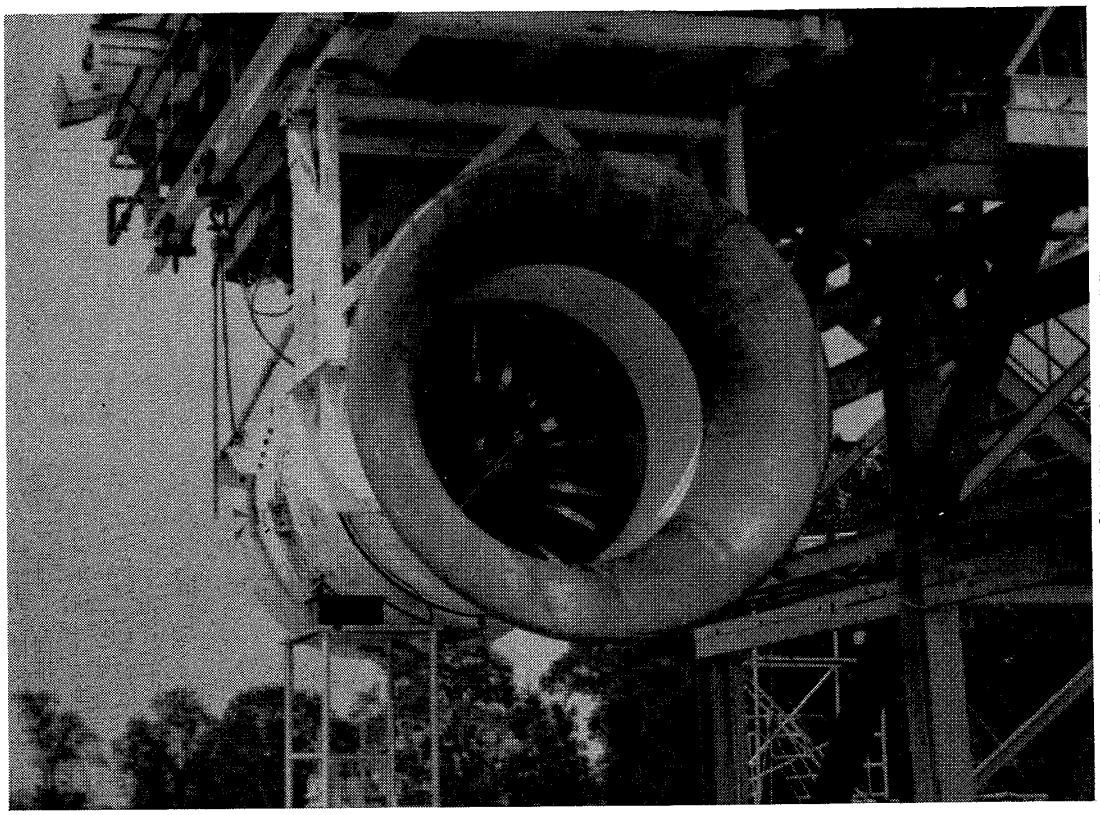

Figure 129. UTW Engine with Bellmouth Inlet.

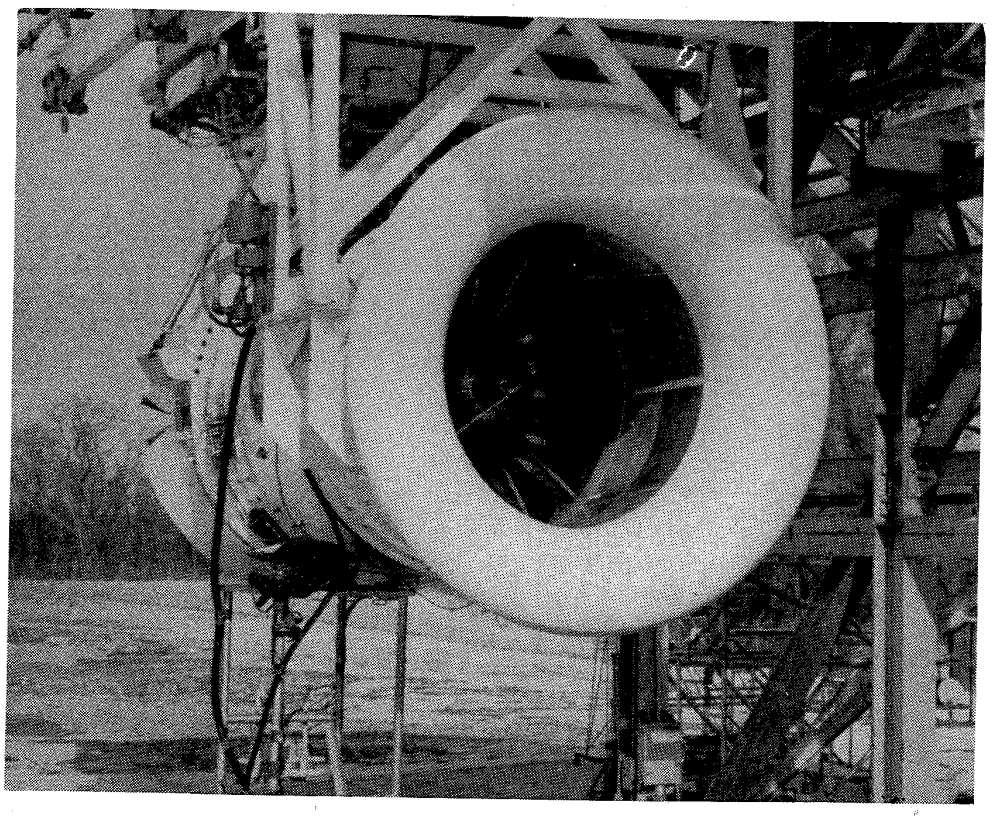

Figure 130. UTW Experimental Propulsion System Test Installation.

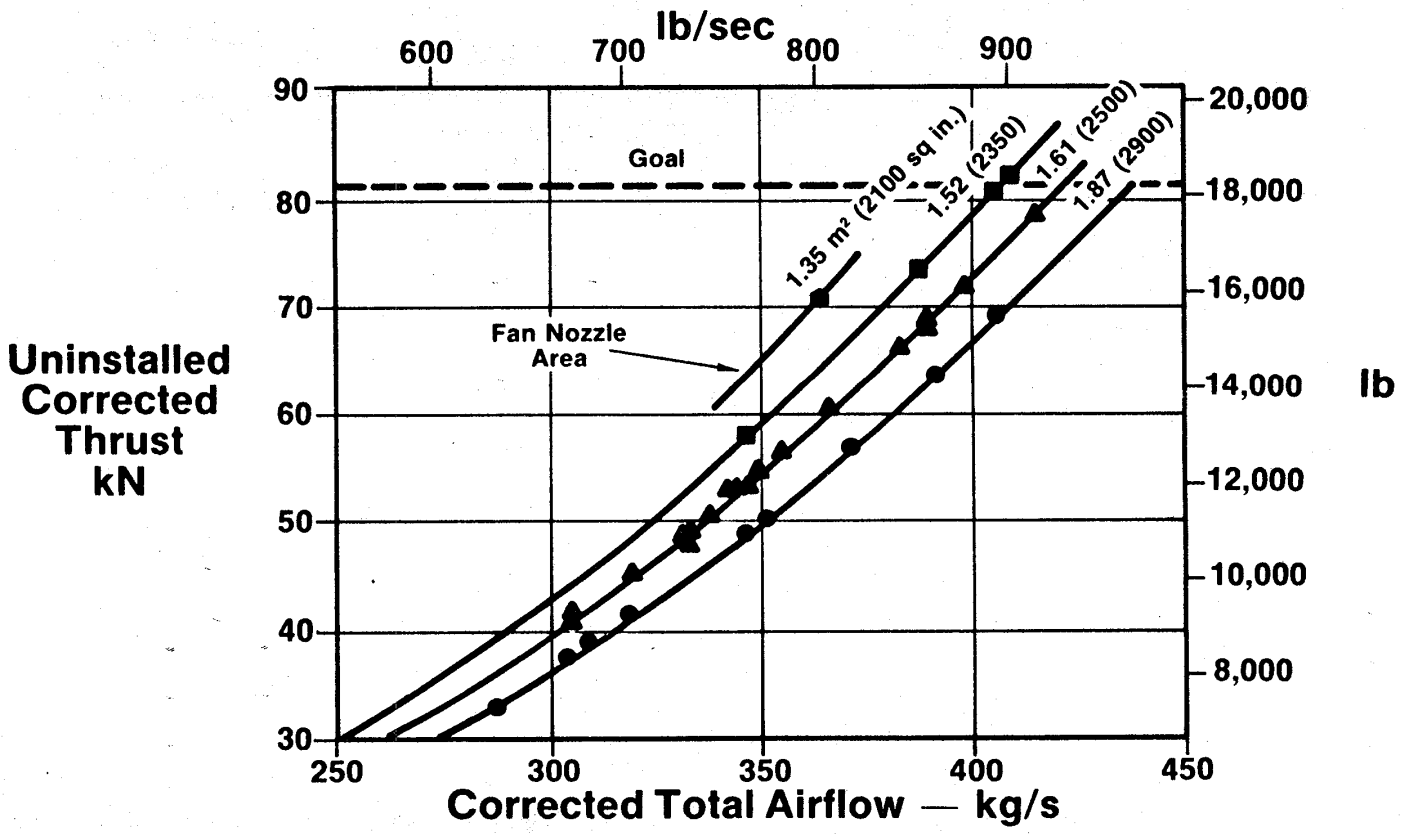

Figure 131. UTW Measured Thrust, Bellmouth Inlet.

Figure 132 shows the same parameters, thrust versus airflow, but at a constant 97% corrected fan speed. Curved lines represent three fan-blade angle settings. The sensitivity of thrust to blade angle is apparent in the three settings. No data points are shown, but the curve represents the best fit of all the data, crossplotted to eliminate scatter. The goal thrust was reached at this fan speed with about 4° open blade setting over a more limited range of nozzle areas.

Typical sfc buckets are shown on Figure 133, again as a function of the same three blade-angle settings. The curve shows that at an open-pitch setting of about 4°, the sfc goal can be met at rated thrust. Since acoustic data did not indicate a significant difference in noise signature over a limited range of fan-blade angles, the rating point was selected at 97% rather than 100% corrected speed and at the slightly opened pitch setting. Installed data with the high throat Mach number inlet yielded similar results but with thrust levels slightly reduced by the lower ram recovery of the flight-design inlet.

Figure 134 shows the UTW engine with the exhaust nozzle in the flared position, acting as an inlet for reverse-thrust testing. The engine was started and accelerated with the blades at the reverse setting, so no transitions were made from forward to reverse.

Figure 135 shows the reverse-thrust performance with the blades set 95° and 100° open. Blade-angle movement to these open angles indicates passage through aerodynamic stall rather than through flat pitch. This was the direction indicated by the scale-model fan test to provide the greater reverse thrust. The open 95° position is nearer to the stall line and produced a higher thrust per pound of airflow, but in both cases the turbine discharge-temperature limit was reached before the 35% reverse-thrust goal was achieved.

It was thought that the acoustic splitter might be channeling the flow in the outer annulus of the duct and increasing the pressure loss into the core, so a run was made with the splitter removed. This did increase the reverse thrust by about 2%, but again the turbine discharge limit prevented reaching the goal. Further work would be required to increase the reverse-thrust capability.

Table XXVI summarizes the UTW performance goals and the demonstrated performance levels. The engine met both the uninstalled and the installed forward-thrust and sfc goals. The reverse-thrust goal was not reached, as noted above, because operational limits were reached first; however, it did produce a potentially useful amount of reverse thrust. Aircraft studies indicated that the 27% reverse thrust achieved with the 100° open blade setting may be acceptable for stopping the airplane on a 915-m (3000-ft) runway.

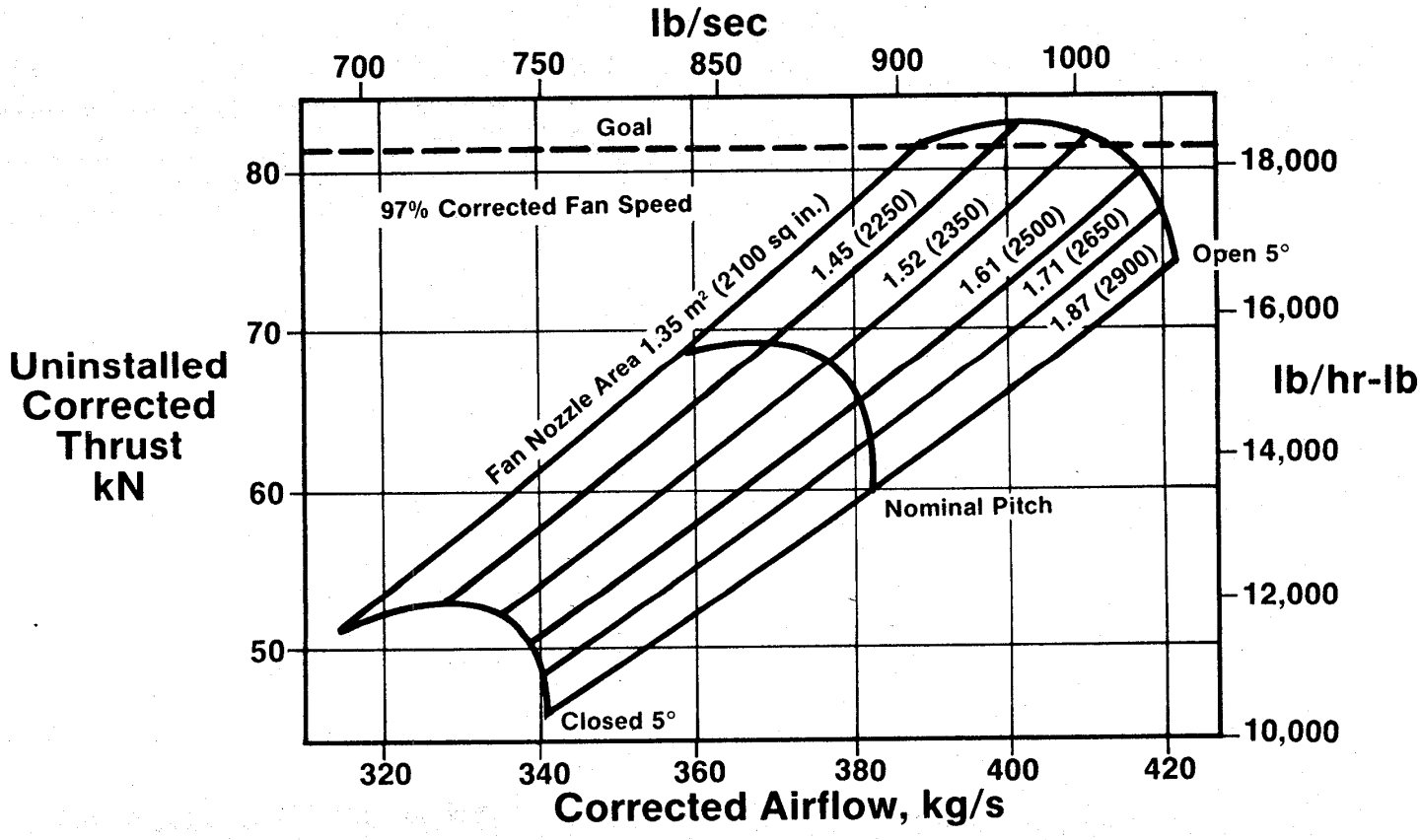

Figure 132. UTW Measured Thrust, Bellmouth Inlet, 97% Corrected Fan Speed.

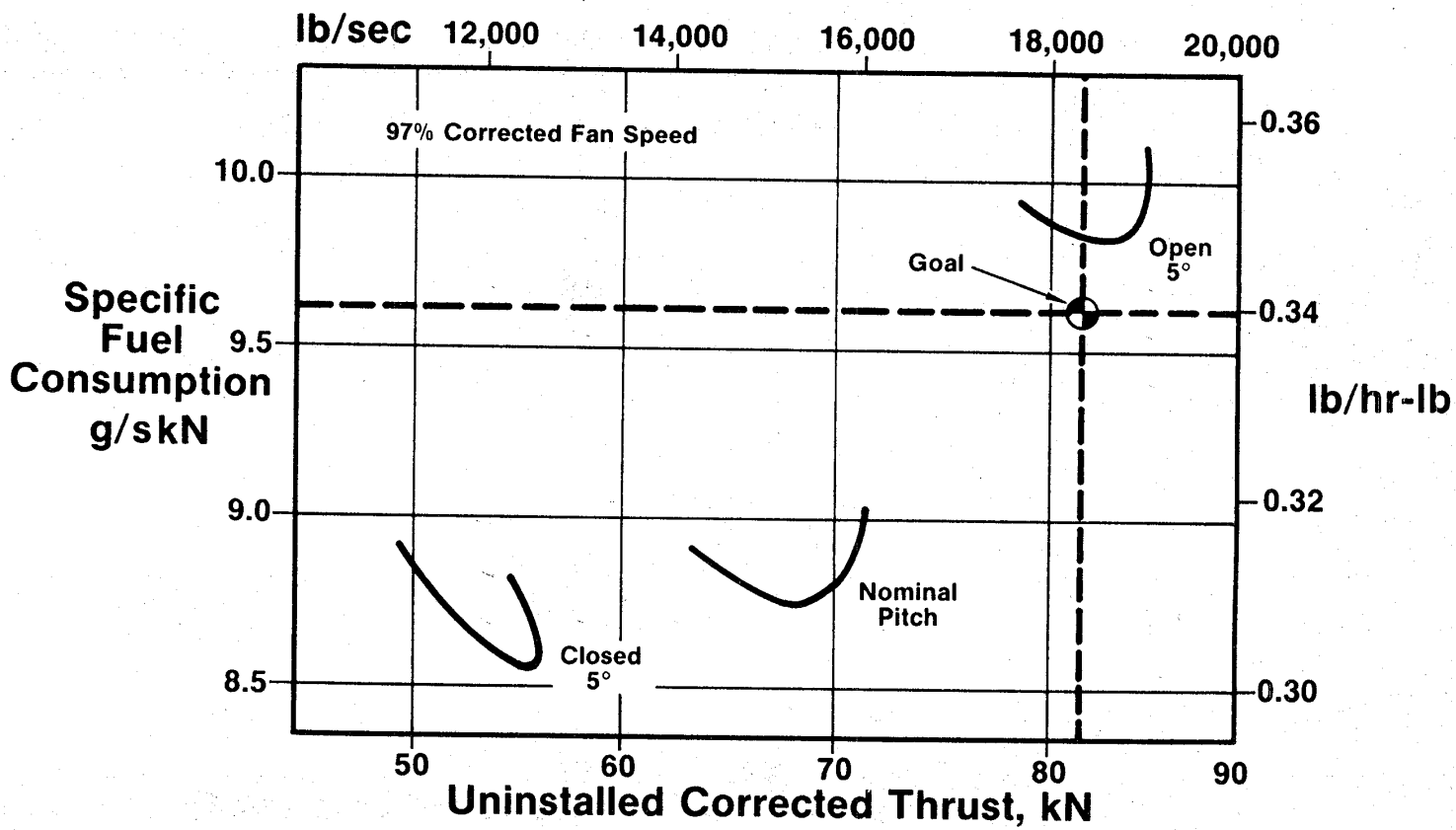

Figure 133. UTW Thrust/SFC, Bellmouth Inlet.

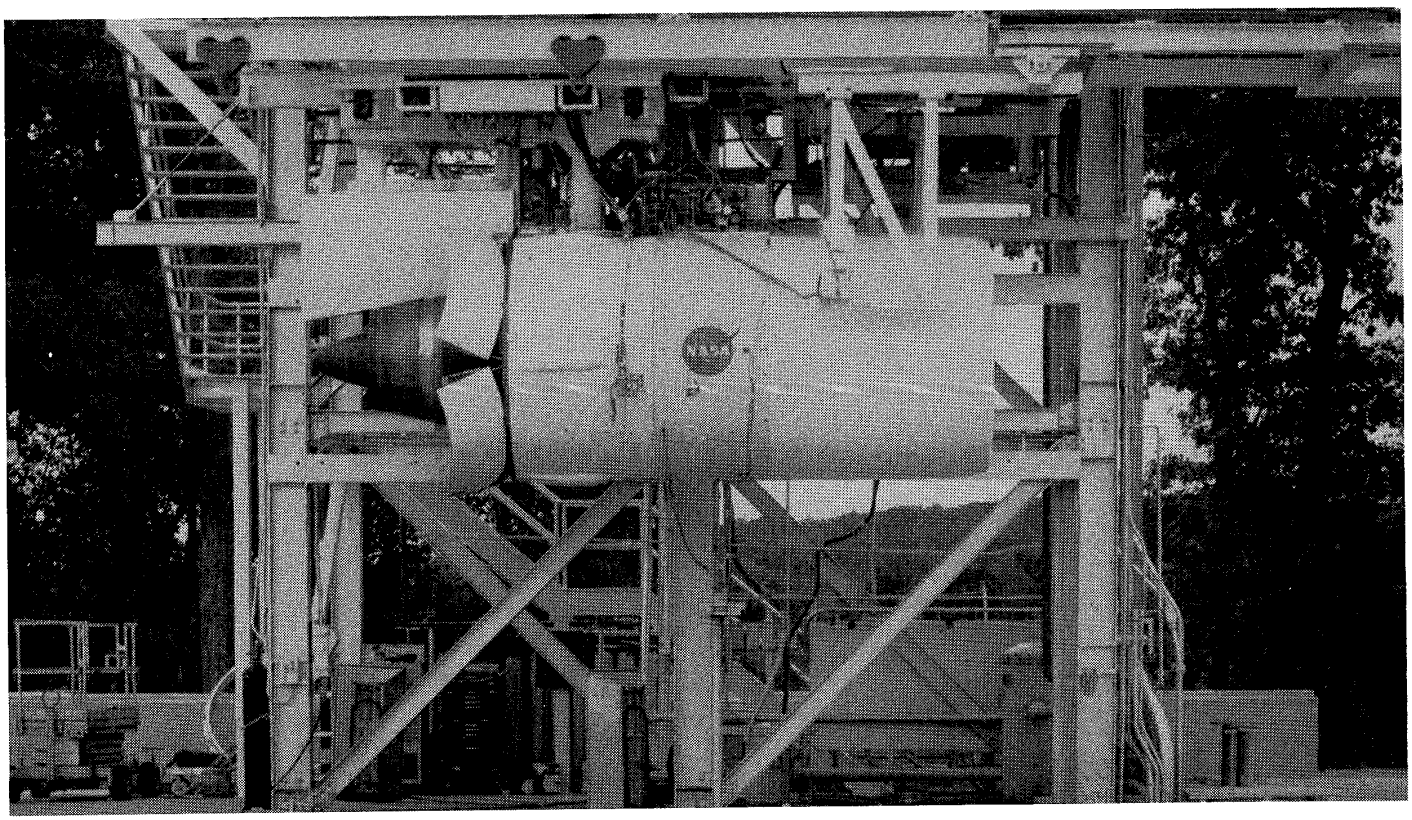

Figure 134. UTW Reverse-Thrust Test.

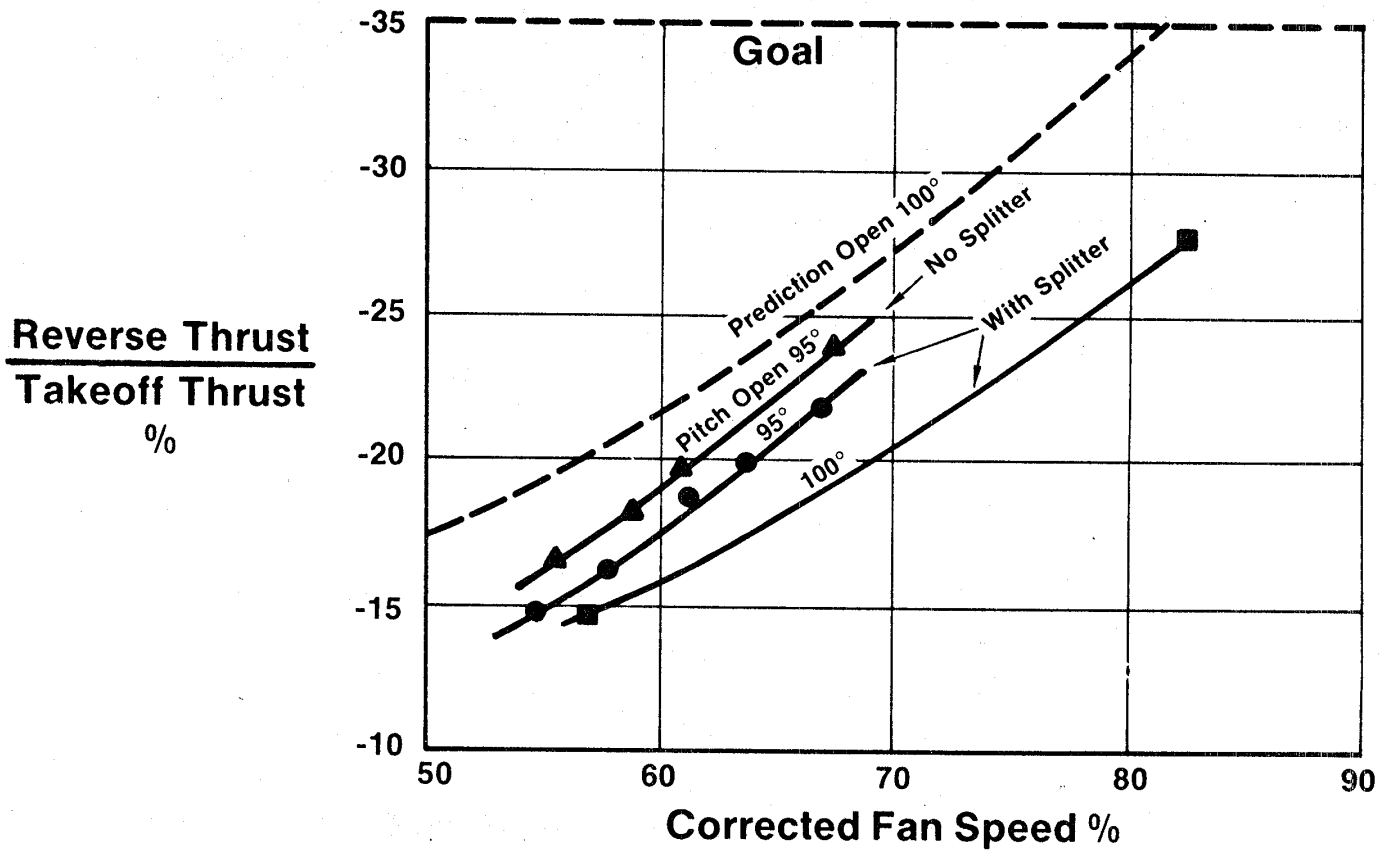

Figure 135. UTW Reverse Thrust.

Table XXVI. UTW Measured Performance, Sea Level Static, 305.5 K (90° F) Day.

	Goal	UTW Engine
Forward Mode		
• Uninstalled Thrust kN (lb)	81.4 (18,300)	81.4 (18,300)
• Uninstalled SFC, g/sN (lb/hr/lb)	0.0096 (0.34)	0.0096 (0.34)
• Installed Thrust, kN (lb)	77.4 (17,400)	77.4 (17,400)
• Bypass Ratio	11.8	11.6
• Cycle Pressure Ratio	13.7	15.2
Reverse Mode		
• Installed Thrust, % Max Fwd.	35	27

4.1.2 OTW Performance Test

Figure 136 shows the OTW engine which was also tested with both the bell-mouth and boilerplate high throat Mach number inlets.

Measured axial thrust values are shown on Figure 137 as a function of corrected airflow. The effect of side-door setting on exhaust-nozzle area is apparent in the three different operating lines. Data include both inlet configurations; fan inlet pressure has been corrected to sea level. Excellent agreement is shown between the two inlets.

The "D" shaped exhaust nozzle was designed to turn the exhaust down over the wing/flap surface. Since the thrust meter was capable of reading the horizontal component only, goals were based on an equivalent conical exhaust nozzle having a velocity coefficient of 0.995.

Figure 138 shows specific fuel consumption versus equivalent-conical-nozzle thrust for the same nozzle areas. The areas corresponding to 11-1/2° and 25° side-door settings are seen to meet the thrust goal and to better the sfc goal by about 3%. The 25° setting was selected for establishing the engine takeoff rating.

The exhaust nozzle was run in the inverted position so that, in the reverse-thrust configuration, the jet efflux would be directed forward and into the ground rather than into the overhead test facility and instrumentation lines. To avoid reingestion of hot exhaust gases and kicked-up debris, a long reingestion shield was used as shown in Figure 139. The effect of the shield on thrust-meter reading was first calibrated in the forward-thrust mode to establish a correction for the reverse-thrust data.

Figure 140 shows the measured axial component of reverse thrust as a function of airflow for the two blocker-door angles tested. While both angles exceeded the desired 35% reverse thrust, pressure loss in the turn was greater than expected. This caused a back pressurizing of the fan and required a greater fan speed than expected. Although the 115° blocker angle produced more turning, and more reverse thrust per pound of airflow, it also produced a higher pressure loss. Both angles required 82% corrected fan speed to reach the 35% thrust goal. The turning loss could be reduced by increasing the bypass-duct area and lowering the Mach number entering the turn. This would have a beneficial effect on reverse-thrust noise by reducing both the jet velocity and the fan speed.

The OTW engine met its uninstalled and installed forward-thrust goal and exceeded its reverse-thrust goal and sfc goal as shown in Table XXVII.

4.2 FAN AERODYNAMIC PERFORMANCE

4.2.1 UTW Fan

Full-scale fan performance was evaluated during tests of the UTW demonstrator engine. The engine, shown during build-up in Figure 141, was fully

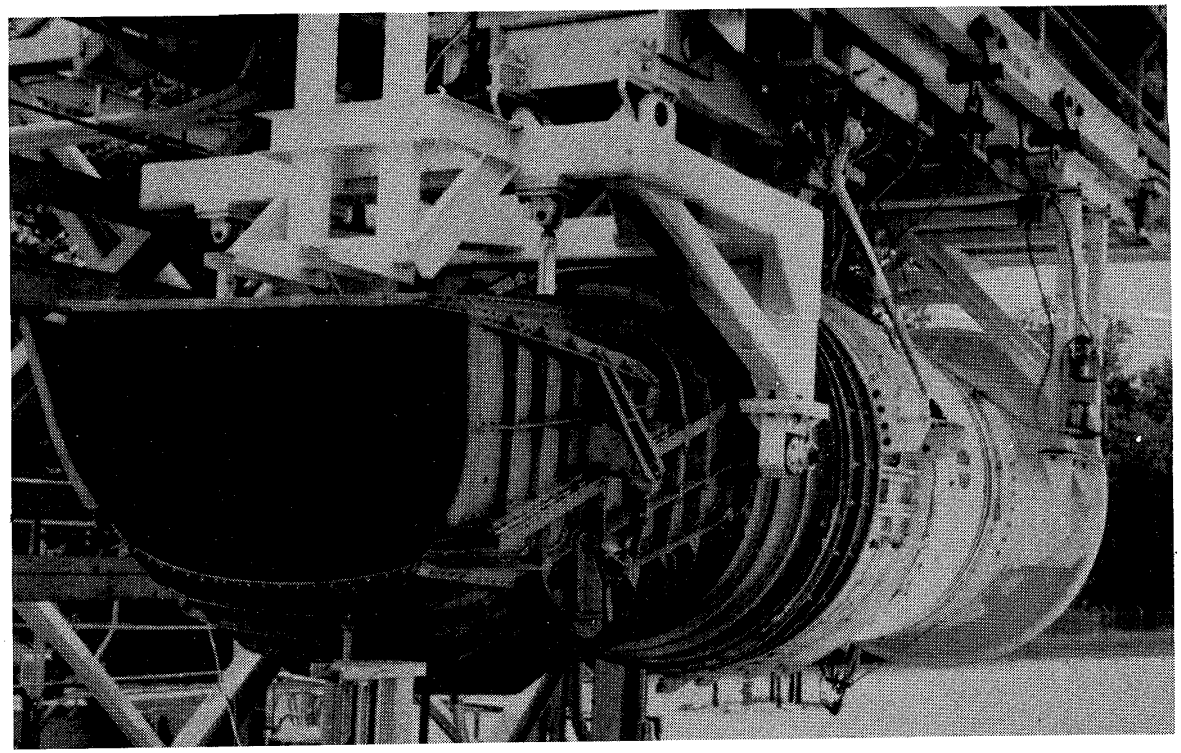

Figure 136. OTW Experimental Propulsion System Installation.

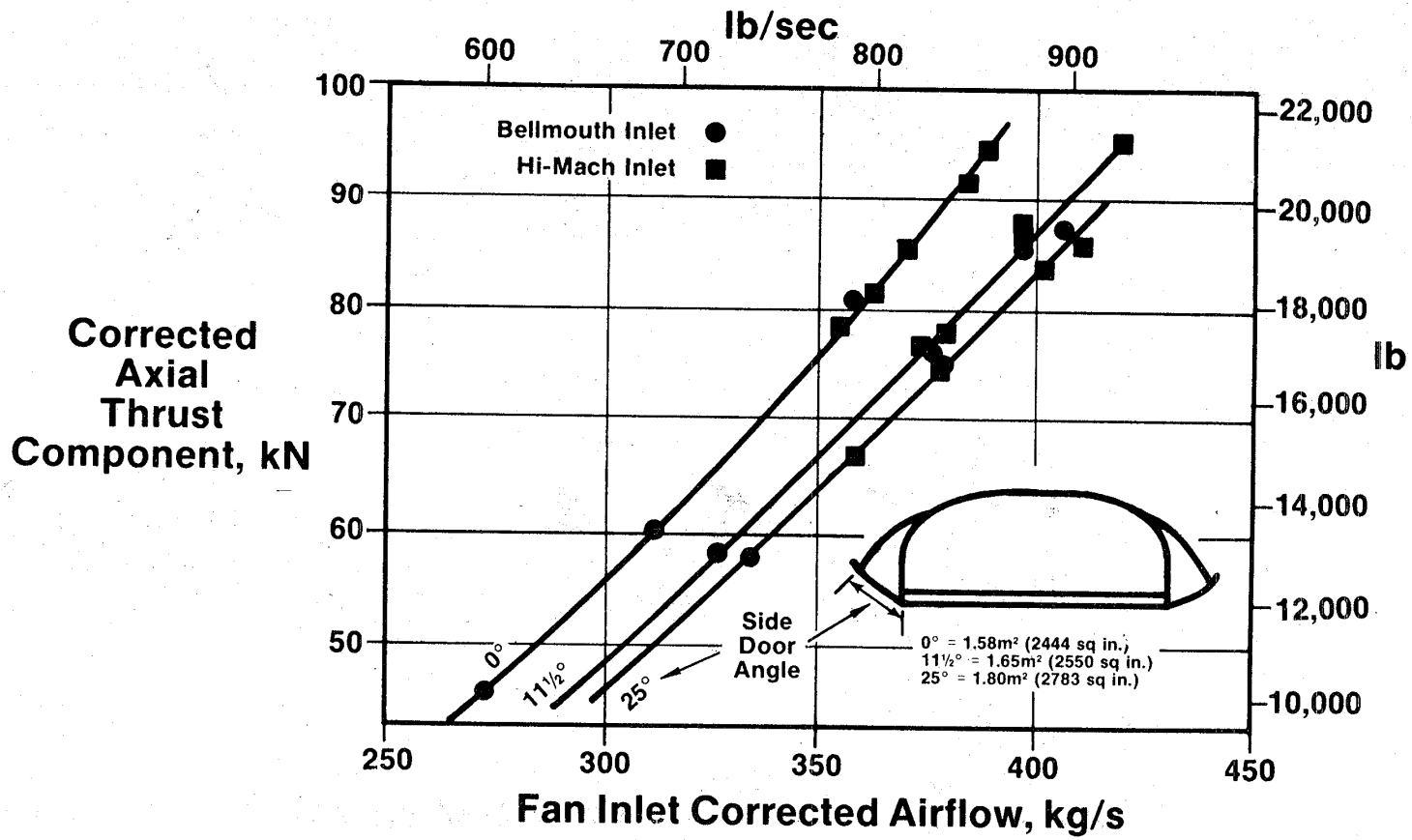

Figure 137. OTW Measured Axial Thrust, "D" Nozzle.

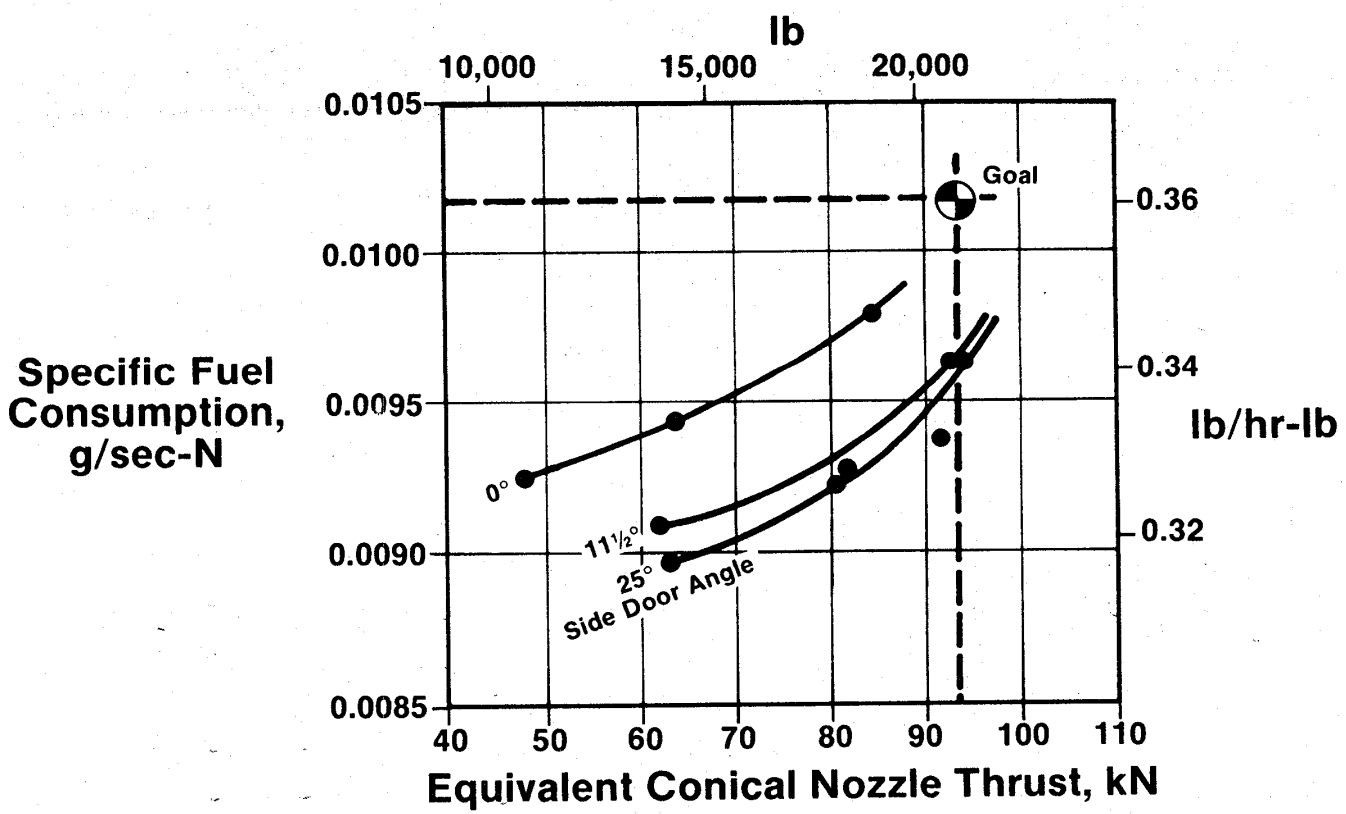

Figure 138. Uninstalled SFC Vs. Thrust.

Figure 139. Inlet Reingestion-Shield Installation.

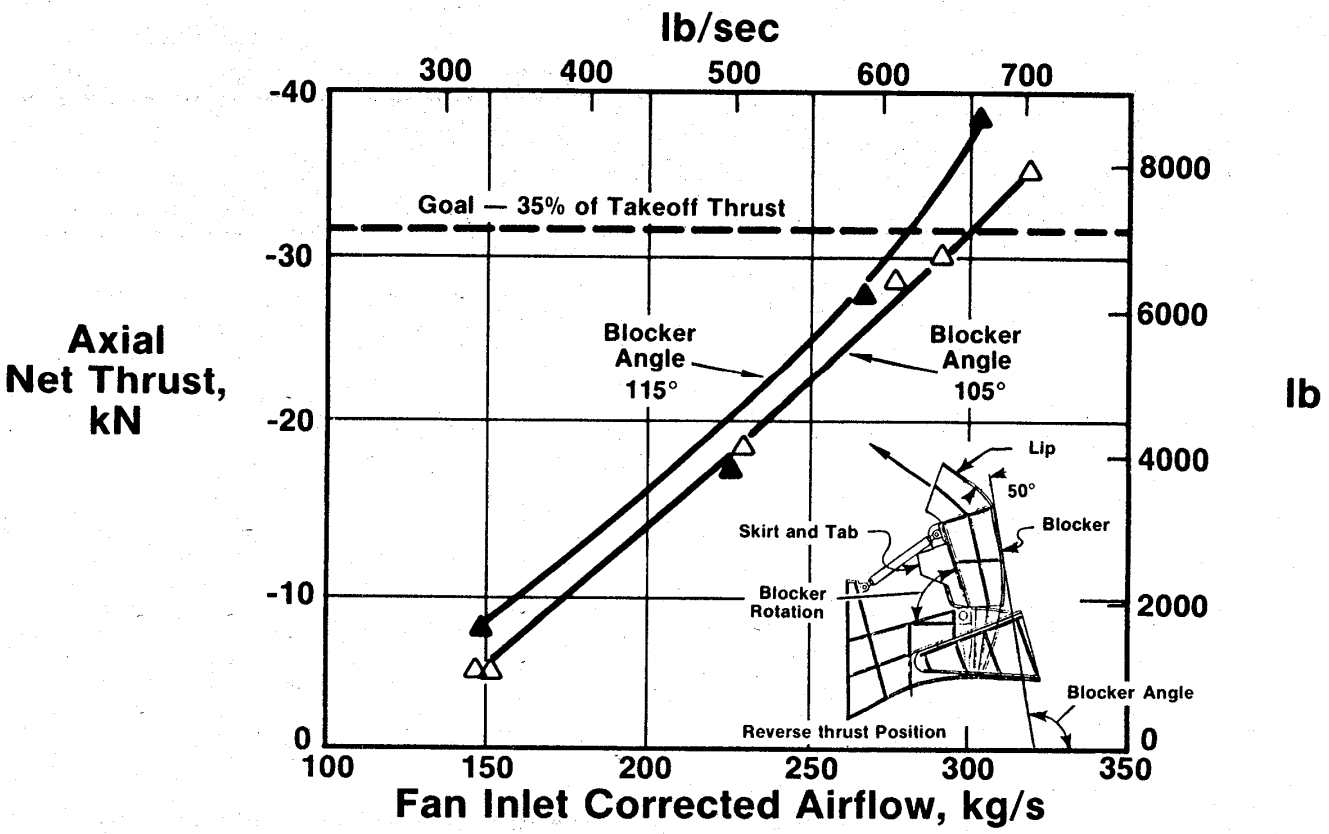

Figure 140. Reverse Thrust Vs. Airflow.

Table XXVII. OTW Measured Performance, Sea Level Static, 305.5 K (90° F) Day.

(Based on Equivalent Conical Nozzle, CV = .995)

	Goal	OTW Engine
Forward Mode		
Uninstalled Thrust, kN (lb)	93.4 (21,000)	93.4 (21,000)
Uninstalled SFC, g/sN (lb/hr/lb)	0.0102 (0.36)	0.0099 (0.35)
Installed Thrust, kN	90.3 (20,300)	90.3 (20,300)
Bypass Ratio	10.2	10.3
Cycle Pressure Ratio	15.5	17.2
Reverse Mode		
Installed Thrust, % Max Fwd.	35	35

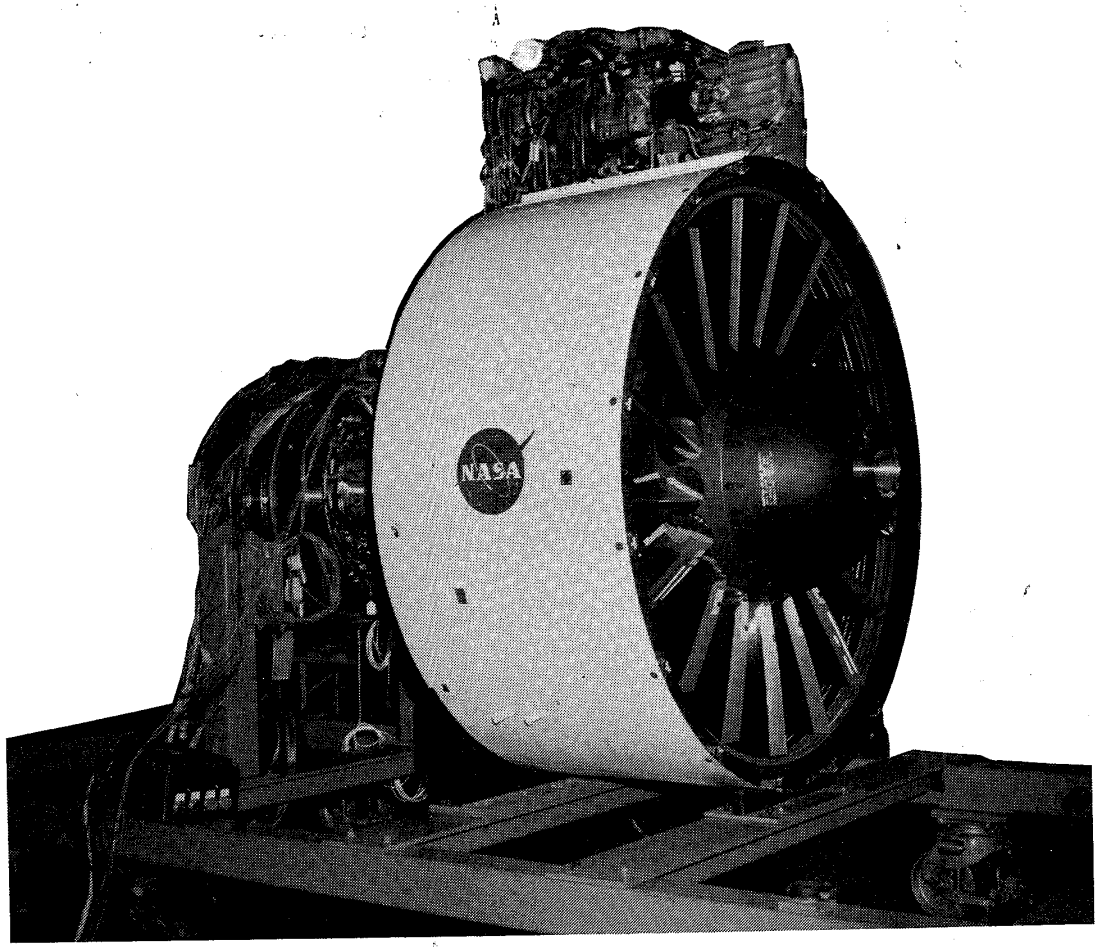

Figure 141. UTW Fan.

instrumented for performance testing, and data were recorded both in forward- and reverse-mode operation. Since all tests were conducted at sea level static inlet conditions, emphasis was placed on determining performance on lower operating lines near the takeoff power setting.

Fan bypass-stream performance in the forward mode of operation is shown in Figure 142. All data points are at the objective takeoff corrected speed, 95% of the aerodynamic design value, and are at three different rotor-pitch-angle settings. The solid speed lines in the background indicate performance measured during scale-model tests. The full-scale fan performance on the engine was very close to that expected as a result of the scale-model tests; efficiency appeared to be slightly better than in the scale model, especially with the rotor closed 5°. Full-scale fan tests confirmed that the fan take-off-flow and pressure-ratio goals could be met at 95% speed with approximately a 3° open rotor-pitch-angle setting. Similar good agreement with the scale-model-test results was obtained over the entire range of speeds and pitch angles that could be evaluated in the engine.

Full-scale fan hub performance at 95% corrected speed for the same three pitch angles is shown in Figure 143. In the engine tests, fan hub data were recorded at the inlet of the core engine rather than behind the fan inner stator, and (thus) stator exit total pressure was reduced by an estimated 1.5% transition-duct pressure loss. At the low pressure ratio of the fan hub at the takeoff condition, this duct loss reduced the efficiency by approximately seven points. The fan hub turbomachinery efficiency at takeoff pressure ratio was actually about 80% rather than being in the low 70's as shown in Figure 143 for the overall hub compression. As shown in the figure, the fan hub performance in the engine was better than in the scale-model tests, particularly at closed rotor-pitch angles, and the core engine supercharging goal was exceeded.

A limited amount of reverse-through-stall-pitch testing was conducted on the engine with the aeroperformance instrumentation installed. The results are shown in Figure 144 plotted as overall pressure ratio from atmospheric engine inlet to fan rotor exit versus total engine flow corrected by engine inlet conditions. The upper family of curves indicates reverse-mode performance predicted from the scale-model tests; the symbols indicate engine test data. Although flow at a given speed and pitch angle was within a few percent of the scale-model level, the fan overall pressure ratio was noticeably lower than expected for the engine. Since the inlet pressure was taken as atmospheric, higher flow-induction losses in the exhaust duct would have contributed to the low apparent fan pressure ratio. Limited traverse data taken in the aft engine duct during reverse-thrust operation indicated that pressure recovery was 1 to 2% lower than measured in the fan scale-model tests, and the recovery could well have been even lower than the traverse data indicated. The apparent low fan operating line could also be the result of the effective discharge area being larger in the engine than in the scale model. The blockage due to fan-exit pressure rakes was less in the engine than in the scale model, but this difference alone was not sufficient to fully account for the low operating line. A final possibility is that some

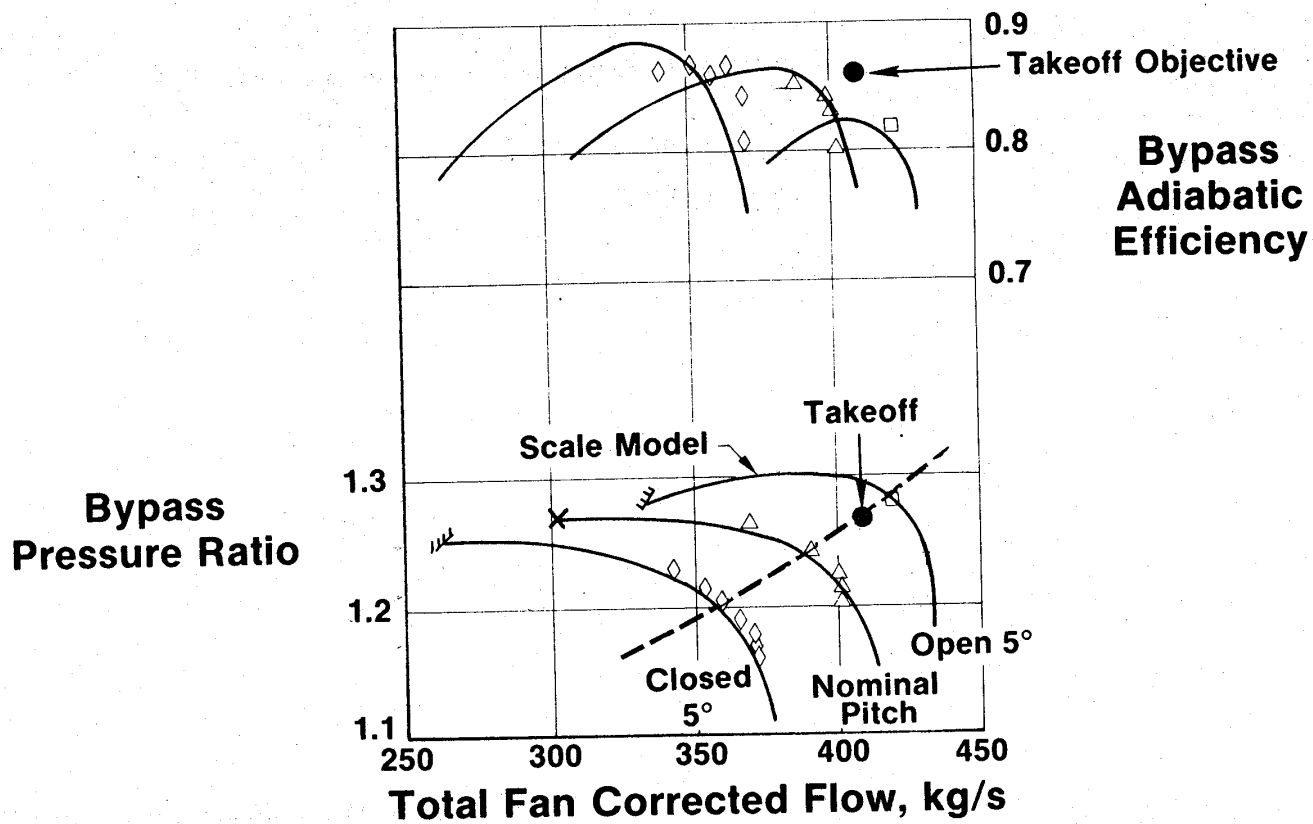

Figure 142. UTW Fan Bypass Performance at 95% Speed.

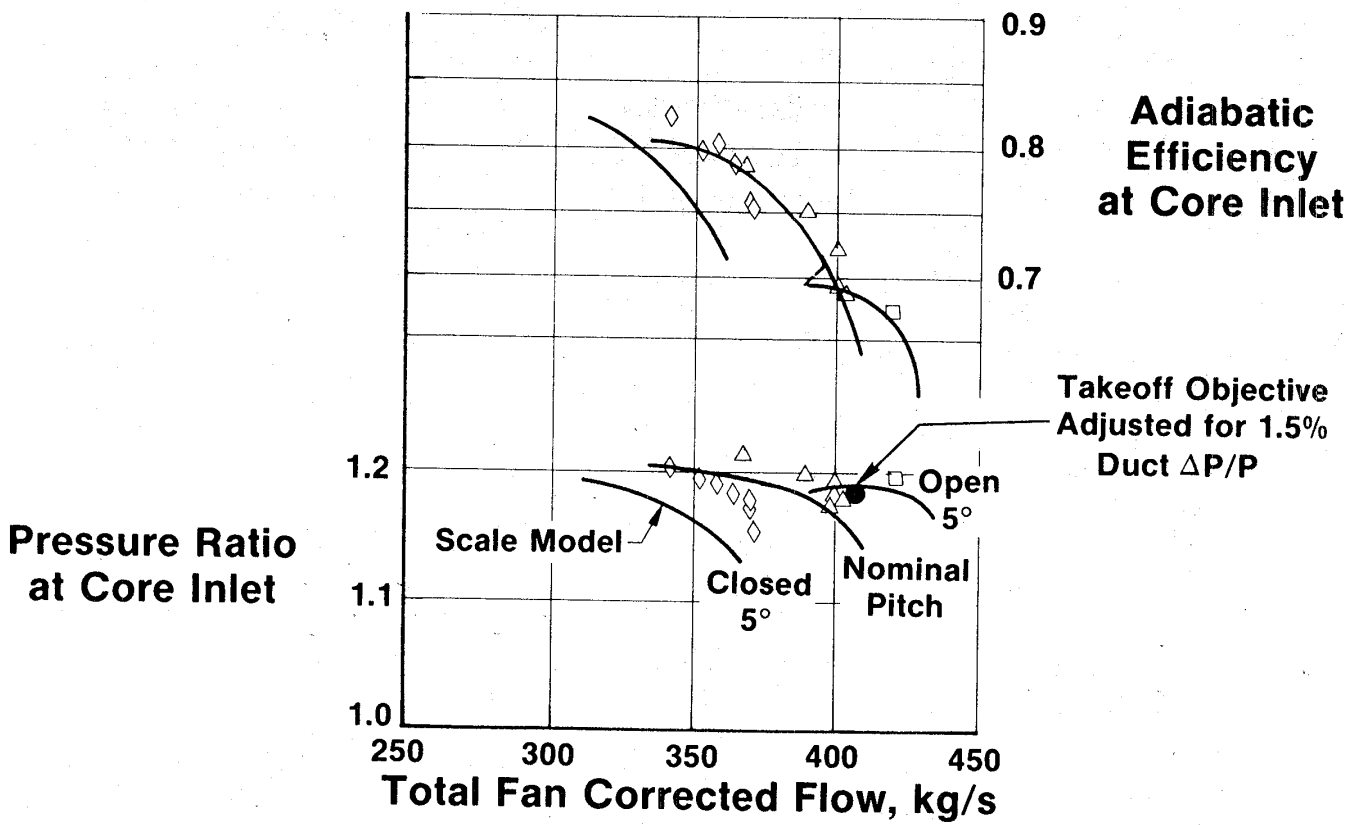

Figure 143. UTW Fan Hub Performance at 95% Speed.

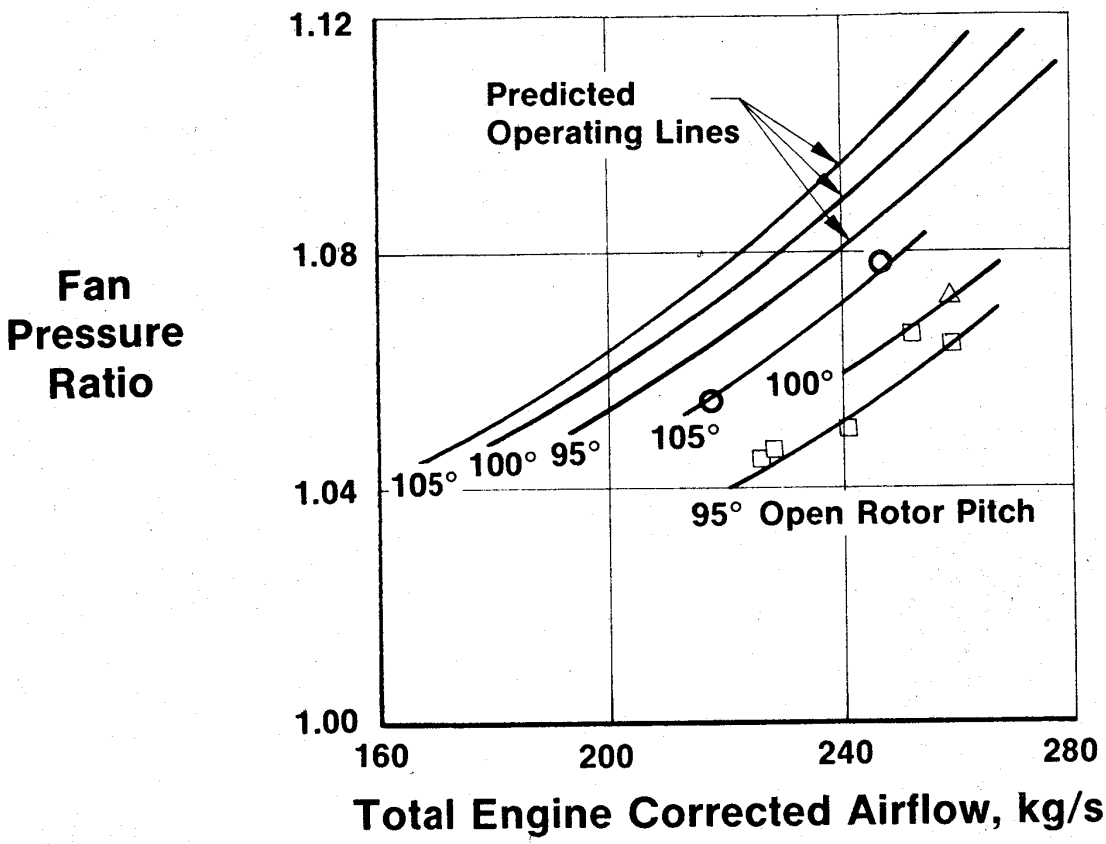

Figure 144. UTW Fan Reverse-Thrust Performance.

other factor may have affected the size of the stagnant-flow region along the centerline of the engine inlet, thus altering the effective discharge area of the fan. Possible causes of this effect include differences in the ratio of core-engine flow to fan flow and differences in fan rotor hub platform shapes. Although insufficient data were recorded during engine tests to resolve this question, it is an area that deserves further testing and analysis since it directly affects the ability to predict the reverse-mode performance of this type of fan.

Although fan pumping in reverse mode was less than expected, the engine system was able to produce 27% of takeoff thrust in reverse, compared to the goal of 35%. While less than the goal, this level of reverse thrust is believed to be sufficient for many applications.

4.2.2 OTW Fan

Fan performance was evaluated during tests of the OTW engine. There was no scale-model component test conducted for the OTW fan. A photograph of the OTW engine during build-up is shown in Figure 145. A full complement of fan-performance instrumentation was installed during the engine tests.

Fan bypass-stream performance data from the engine tests are shown in Figure 146. At 100% design corrected speed, the fan exceeded flow and pressure-ratio goals by 2 to 3%. The 86.5% bypass-stream efficiency goal for the demonstrator engine was met or exceeded along an operating line through the design point. Peak fan efficiency was on a lower operating line than the lowest tested, possibly near the takeoff operating line, so the exact level of peak efficiency at high speed was not determined. No stall testing was attempted during the engine-performance runs, and no fan stalls were encountered. It was thus not possible to determine if the fan was able to meet the stall margin objectives, although 10% stall margin was demonstrated at 95% corrected speed.

Fan hub performance results are shown in Figure 147. These were based on measurements recorded at the core-engine inlet, so the design objective pressure ratio and efficiency on this performance map (indicated by the target symbols) have been lowered consistent with an estimated 1.5% transition-duct pressure loss. Hub performance results were quite encouraging in that the high level of core supercharging was achieved at 100% speed. Efficiencies at the design operating line were approximately equal to the goal (78% for the turbomachinery alone) and were significantly higher than the goal at higher operating lines.

4.2.3 CONCLUSIONS

The OTW and UTW fans both performed satisfactorily during sea level engine tests, and most of the fan aerodynamic-performance goals established for the demonstrator engine programs were met. Some further development of the UTW fan would be required to meet altitude-cruise performance goals, and

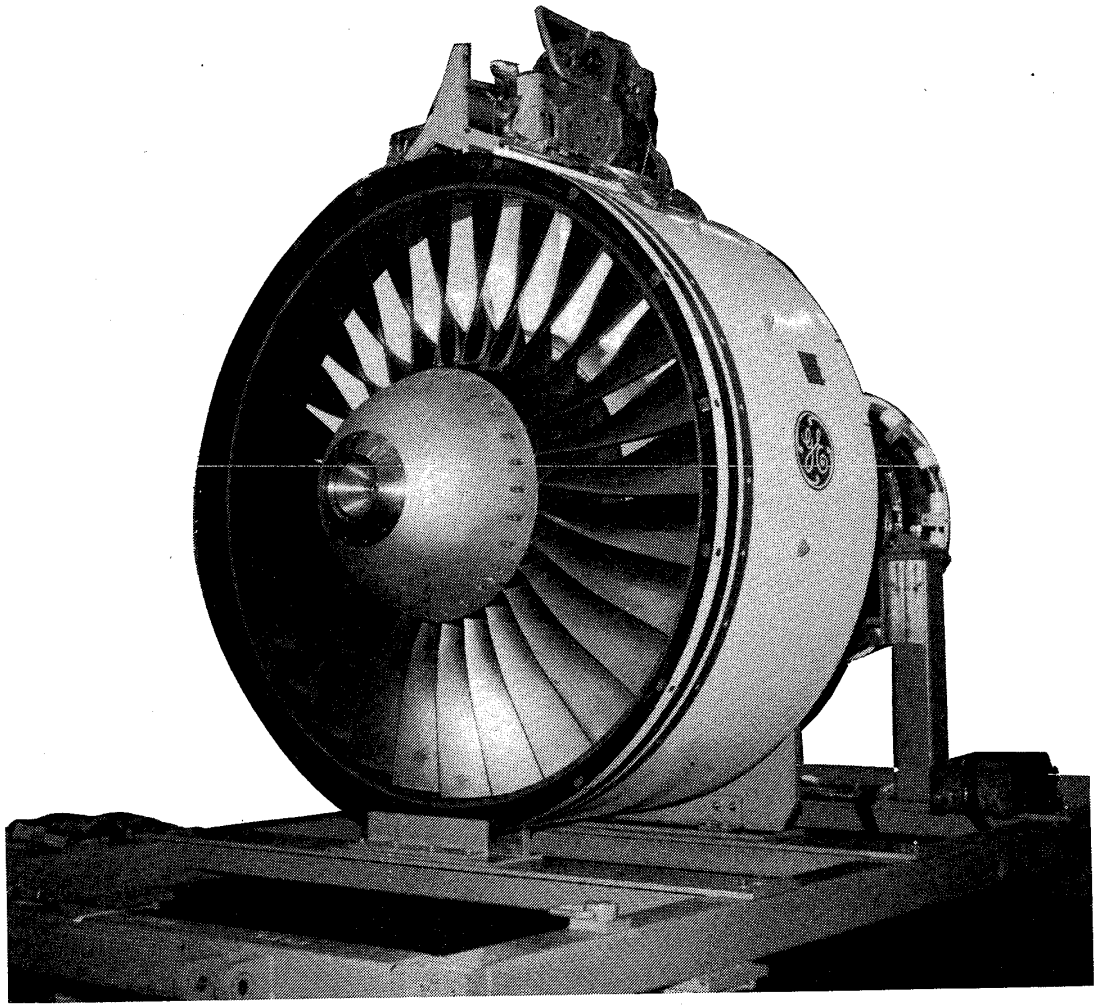

Figure 145. OTW Fan.

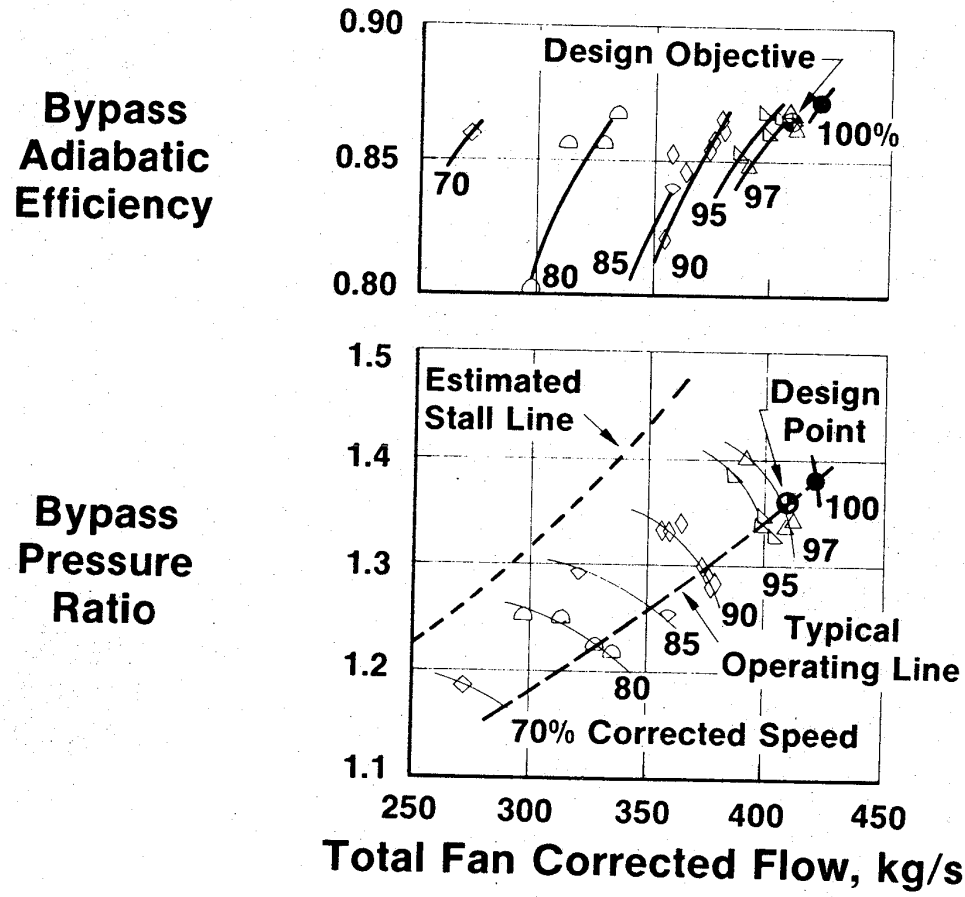

Figure 146. OTW Fan Bypass Performance.

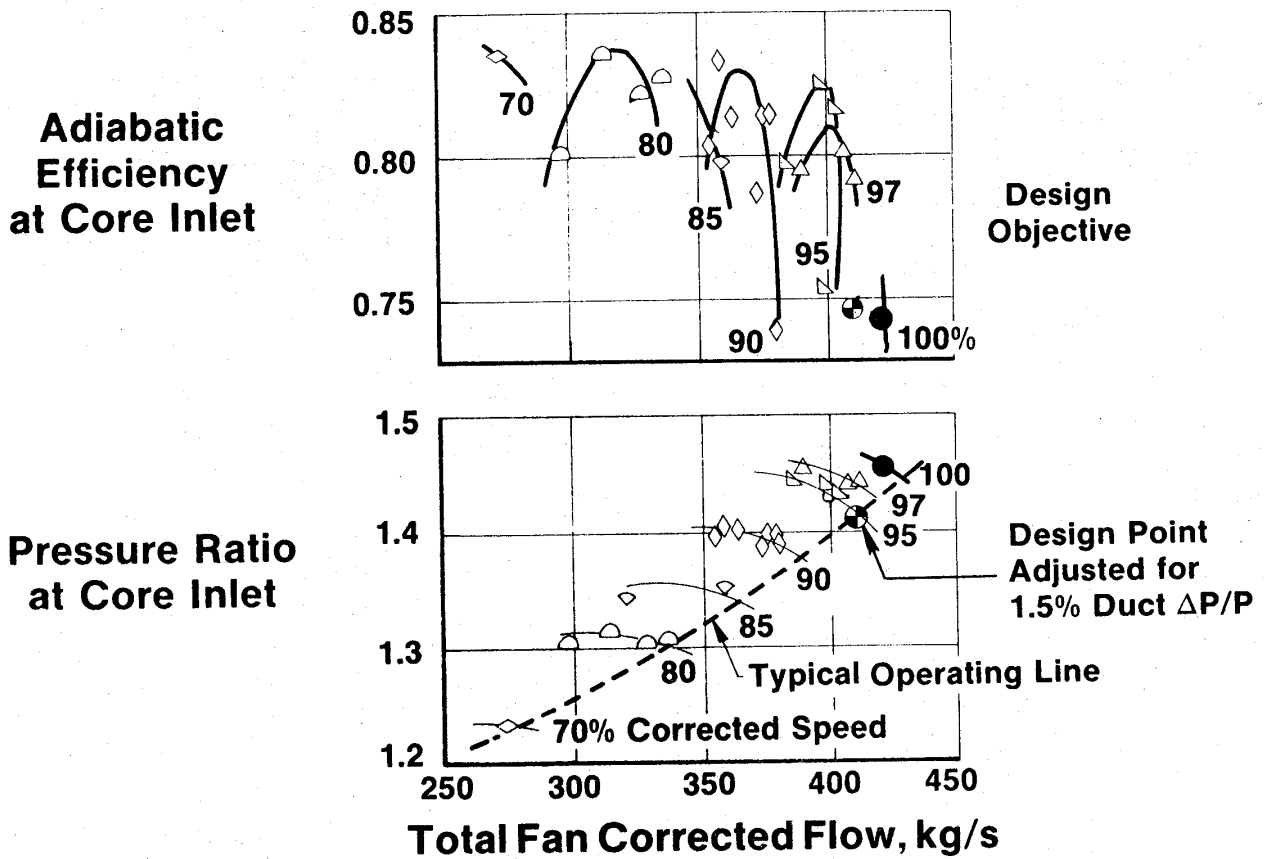

Figure 147. OTW Fan Hub Performance.

the reduced pumping of this fan during engine reverse-mode tests needs to be understood and improved. Important advances in fan aerodynamics were demonstrated during the QCSEE program, and these advanced fan features can be used with confidence in future turbofan engines for short-haul aircraft.

4.3 MECHANICAL PERFORMANCE

4.3.1 COMPOSITE FAN BLADES

Although it was recognized that the QCSEE composite blades were not flightworthy, because of insufficient FOD resistance, they were judged to be suitable for development engine testing.

The blades performed acceptably during experimental engine test. The steady-state stress levels were low, and there were no indications of torsional instability. The only problems encountered were that the blade vibratory-stress levels exceeded scope limits at the 2 per rev/first-flex crossover, and high first-flex vibratory stresses were also noted due to crosswind and tailwind test conditions at speeds above the 2/rev crossover. It should be pointed out that the scope limits defined for the composite blade were very conservative, and no blade delamination occurred. Further, the OTW titanium blades were also excited by crosswinds and tailwinds, although they remained well within established scope limits.

4.3.2 Variable-Pitch Actuation Systems

The Hamilton Standard cam/harmonic and the General Electric ball spline systems were both engine tested. Figure 148 shows the fan rotor with the cam/harmonic system installed. Clearly visible are the nested lever arms and the spherical cam that drives the blades in unison as the cam rotates with respect to the fan disk.

The cam/harmonic system completed 47 hours of engine testing. It accurately positioned the fan blades at lower speeds, but could not move the blades against the load when operating above 85% fan speed. Since this system handled the simulated blades during whirl-rig testing, it was concluded that actual blade torques exceeded design estimates.

The ball spline system completed 106 hours of engine testing. Motor torque was increased 16% prior to engine test, and the system crisply actuated the blades at all speeds. There was an indicated 1.3° system hysteresis, based on airflow measurements, when the direction of blade movement was reversed while operating near nominal. This was again attributed to excessive actuator clearances and presented no operational problems.

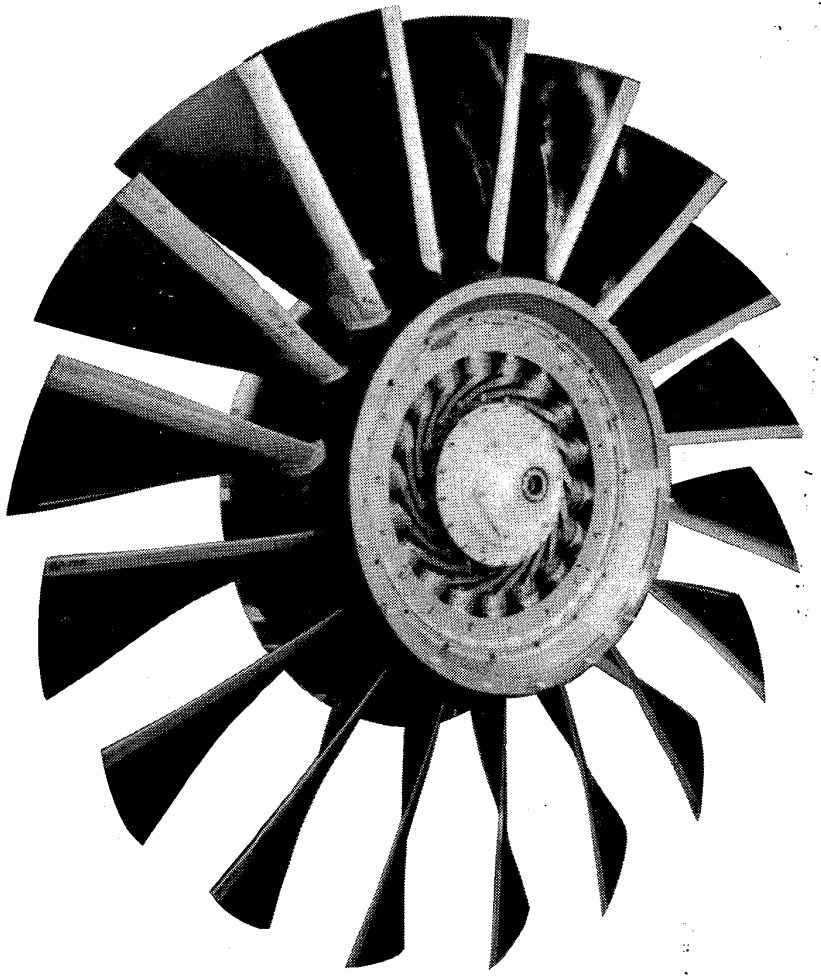

Figure 148. Fan Rotor with Cam/Harmonic System.

4.3.3 Main Reduction Gear

Figure 149 shows the UTW reduction gear, including the fan pitch-change-mechanism support, installed in the engine but with the fan shaft and ring gear removed.

There were no operational problems with either the UTW or the OTW gearsets during engine operation. The indicated reduction gear efficiency of 97.7% in the engine was somewhat lower than that experienced in the rig tests, but this is attributed at least in part to inaccuracies in the method of estimating the sources of heat rejected to the oil and oil-flow distribution from several sources within the engines. It is believed some development effort related to the placement of the oil supplied to the gears and the scavenging characteristics both within and surrounding the gearset can improve the efficiency to a value even better than that previously shown for the rig tests.

Another item of interest in the engine test was gear noise. The gear-noise level, even at meshing frequencies, appeared to be below that of the rest of the engine and indiscernible.

The UTW reduction gearset was inspected at an interim point in the engine operation. All parts passed Magnaflux satisfactorily, and tooth wear patterns were uniform. Slight corrosion was apparent on the ring gear due to inadequate removal of fingerprints, and slight evidence of bearing skidding was noted.

Neither engine was disassembled following the completion of testing; consequently, further gear inspections have not been possible. However, at this time, over 40 hours of additional testing of the OTW engine have been done at Lewis Research center with no gear problems.

4.3.4 Composite Frame

The two composite fan frames built under this program were used throughout the engine-test phase of the UTW and the OTW engines. No structural problems resulted from these tests. Both the mount region and the bypass vanes were instrumented and monitored during engine testing. The indicated stress levels were very low but were in good agreement with the analysis for the conditions run.

The main problem encountered during engine operation was oil leakage from the sump; adequate sealing of all the penetrations for lines and tubes could not be maintained. This problem was alleviated by filling the core struts and other selected areas with adhesive to provide an external seal. This was done on the test stand. Secondary FOD damage was also repairable on the stand.

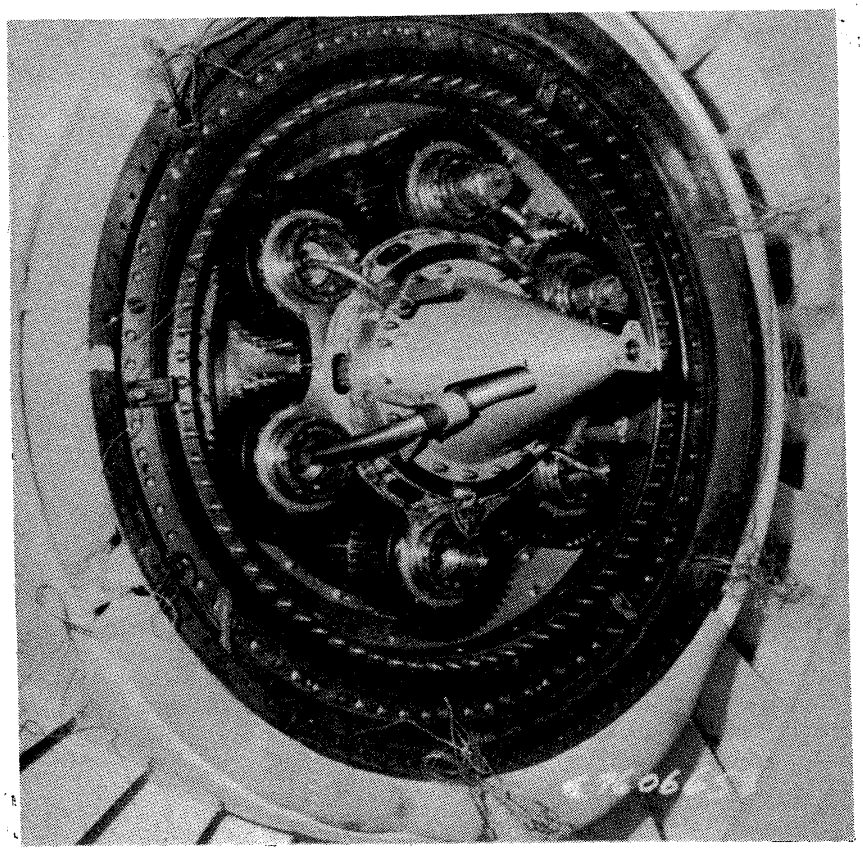

Figure 149. UTW Reduction Gear.

4.3.5 Composite Nacelle

The composite nacelle components were run on the UTW engine with the following results:

- No problems were encountered with the inlet.
- No problems were encountered with the inner core cowl.
- No problems were encountered with the outer fan cowl.
- No problems were encountered with the fan nozzle when it was installed on the composite outer cowl; however, this nozzle was also used on the boilerplate outer cowl where the hinge ring was bolted to the rear of the outer cowl rather than being bonded in. This hinge ring (due to a poorly designed bolted joint to the boilerplate outer cowl) came off during reverse-thrust testing, terminating the boilerplate nacelle tests.
- No environment degradation was noted during engine operation.

4.4 CONTROL SYSTEM TEST RESULTS

4.4.1 UTW Engine

Several control-system experiments were conducted during the overall engine test program. As noted earlier, the system is designed to hold the inlet throat Mach number constant at high power settings by variation of the fan nozzle area. Figure 150 shows the results of an inlet Mach number control experiment. The figure shows the results of a slow power increase. The control system inlet Mach number reference was set at 0.75. As the power setting was increased, the fan nozzle automatically closed to maintain the inlet Mach Number essentially constant at 0.75.

Figure 151 shows the results of a fan-speed control experiment. As noted earlier, the digital control will automatically vary fan pitch angle to hold fan speed constant. In this experiment the fan speed reference was set at 2985 rpm. As the power setting increased to demand a higher thrust level, the fan pitch automatically opened to hold the fan speed essentially constant. Actual fan-speed variation was approximately plus or minus 0.5% during the power advance. The fan pitch changed from approximately 2° closed to 3° open during the power change. The nonlinearity in pitch angle change between 85% and 90% power demand is associated with an interaction between the fan pitch and fan nozzle control systems. Between 85% and 90% power demand, the fan nozzle opened to the maximum open area, and a relatively large pitch-angle change was required to maintain fan speed. Above the 90% power setting the nozzle closed, and smaller changes in pitch angle were required to maintain control of fan speed.

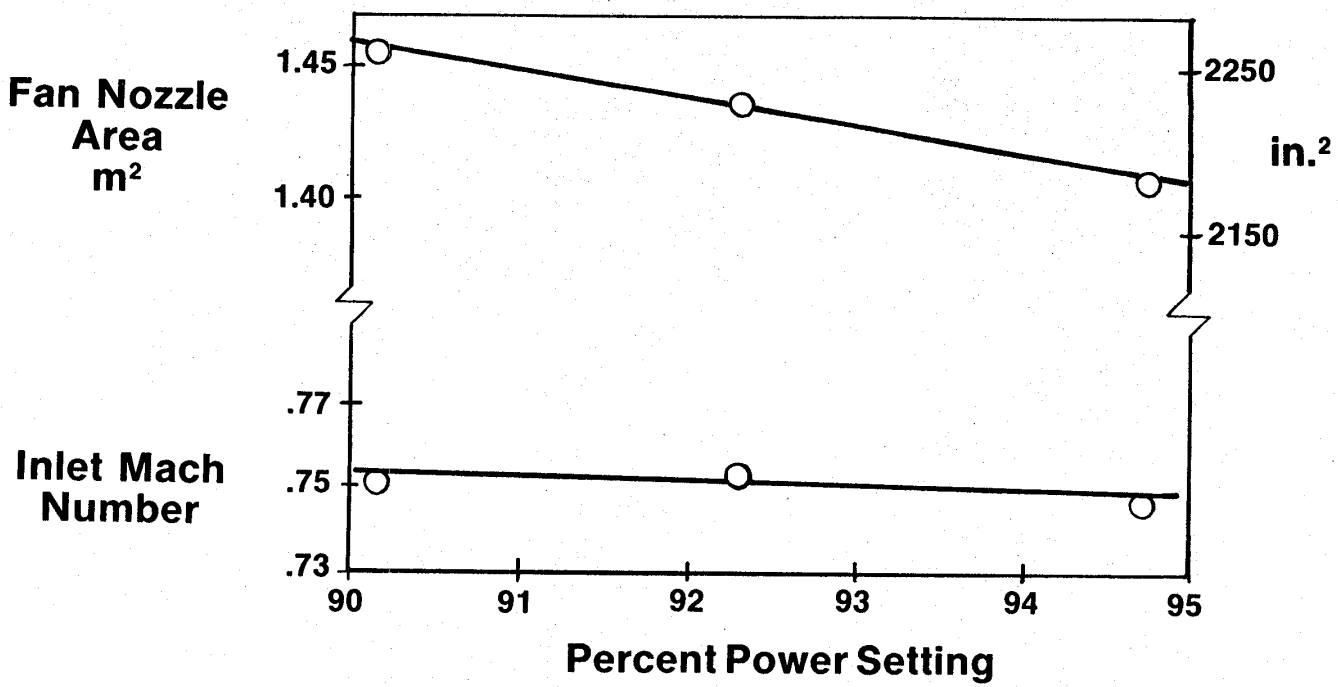

Figure 150. UTW Inlet Mach Number Control.

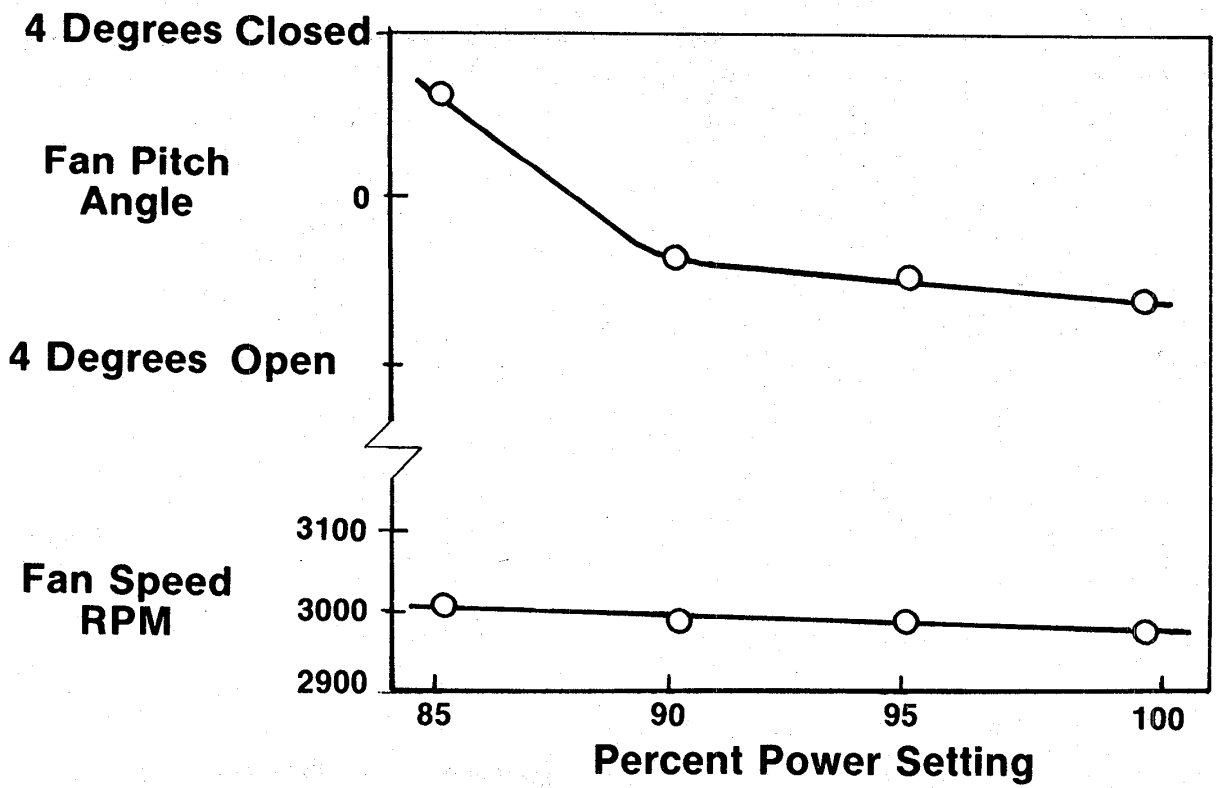

Figure 151. UTW Fan Speed Control.

Figure 152 shows the results of another experiment on inlet Mach number control. In this experiment, the engine power demand was held constant, and the desired inlet Mach number reference was varied. As the inlet Mach number reference in the digital control was changed by an on-line adjustment, the fan nozzle opened to hold the requested inlet Mach number.

Recorded data were examined to determine the steady-state stability of the control system when it was operated with the closed-loop controls noted above. Throughout all of the closed-loop operation the steady-state stability of the controlled variables (pressure ratio, inlet Mach number, fan speed) was excellent. Table XXVIII shows typical steady-state stability results.

Sensor accuracy is an important element in the engine control system. To evaluate this element, data measured by the engine control-system sensors were compared to data measured with the experimental engine instrumentation. Table XXIX shows the results of a comparison of digital control sensors and engine instrumentation.

Summary - A multivariable digital control system was designed and engine-tested in the UTW QCSEE program. During the engine-test program, accurate and stable control was achieved in all modes of operation. Closed-loop control was demonstrated on an engine pressure-ratio/fuel-flow loop, inlet Mach number/fan-nozzle-area loop, and a fan-speed/fan-pitch loop. The digital communication link between the engine control and the engine control room was demonstrated, and accurate steady-state sensor performance was obtained.

4.4.2 OTW Engine

As noted earlier, the OTW digital control varied engine fuel flow to hold a scheduled corrected fan speed. Figure 153 shows typical engine-test data. As noted on the figure, scheduled and measured speed are nearly identical. Examination of recorded data also revealed excellent steady-state fan-speed stability.

A second primary function of the digital control was to schedule the variable compressor stators. Figure 154 shows the steady-state schedule and typical data recorded during the engine test program. It should be noted that the corrected core speed is based on a calculated compressor-inlet temperature.

One task of the propulsion control system is to prevent the engine from exceeding physical operating limits. One engine limit incorporated in the digital control memory was turbine inlet temperature. Turbine inlet temperature was calculated from fuel flow, compressor discharge pressure, and compressor discharge temperature. The calculated value of turbine inlet temperature was compared to the limit, and fuel flow was adjusted to prevent overtemperature. The OTW and UTW control incorporated this function. Figure 155 compares on-line turbine inlet temperature calculations by the

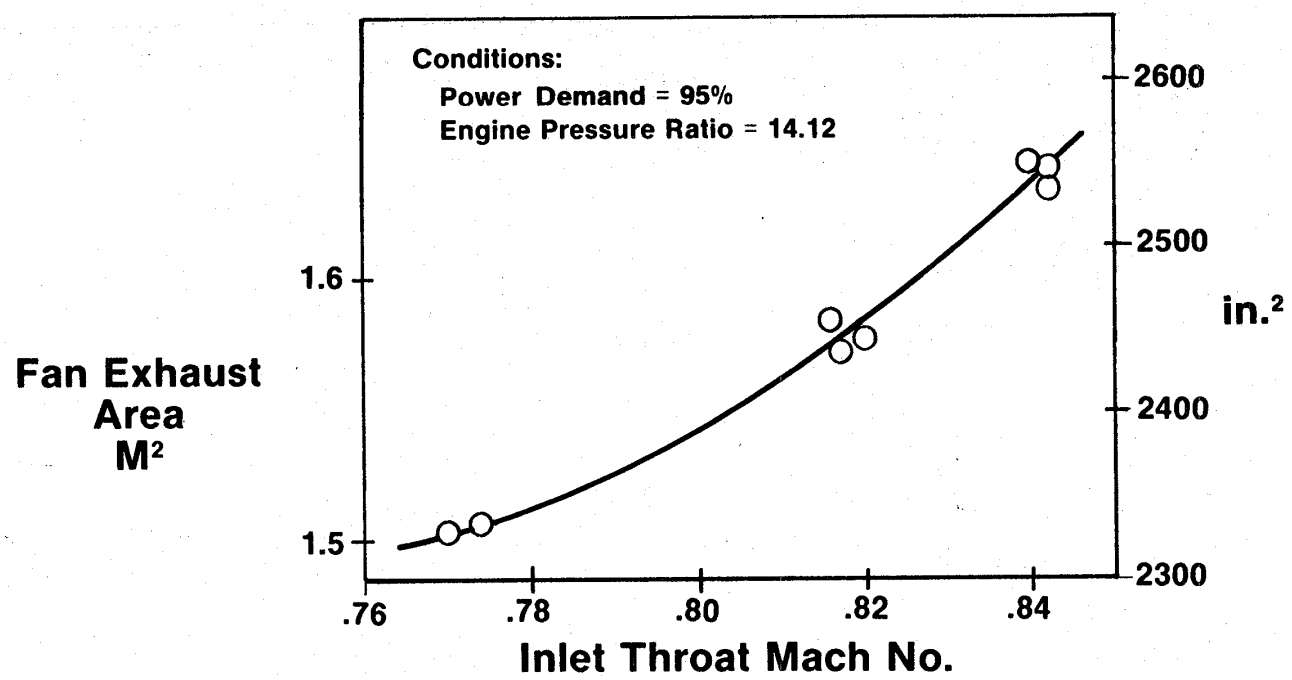

Figure 152. UTW Fan Exhaust Nozzle Tracking.

Table XXVIII. Steady-State System Stability.

	Variation
• Pressure Ratio	$<\pm.05$
• Mach Number	$\pm.005$
• Fan Speed	± 20 RPM

Table XXIX. Sensor Accuracy.

	% Variation
Fan Inlet Temperature	±0.2
Compressor Discharge Temp.	-1.0
Compressor Discharge Pressure	+0.4
Fuel Flow	+1.7
Inlet Static Pressure	+1.0

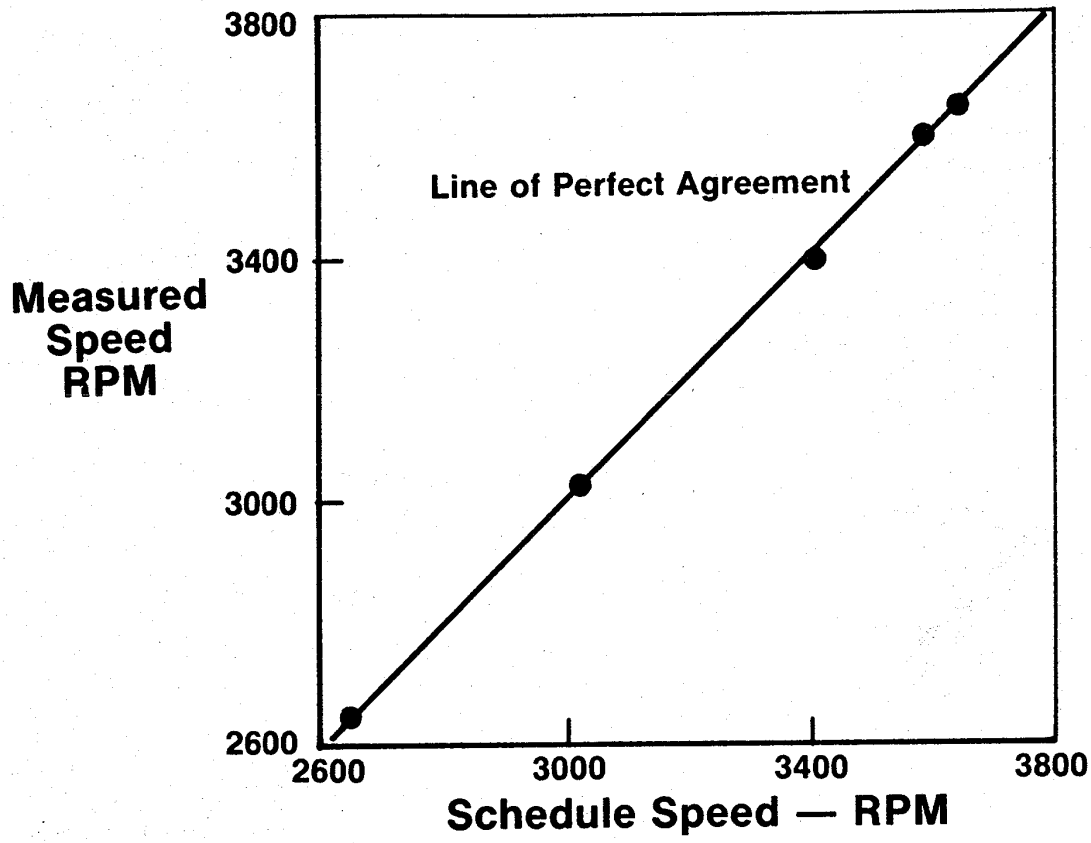

Figure 153. OTW Fan Speed Scheduling.

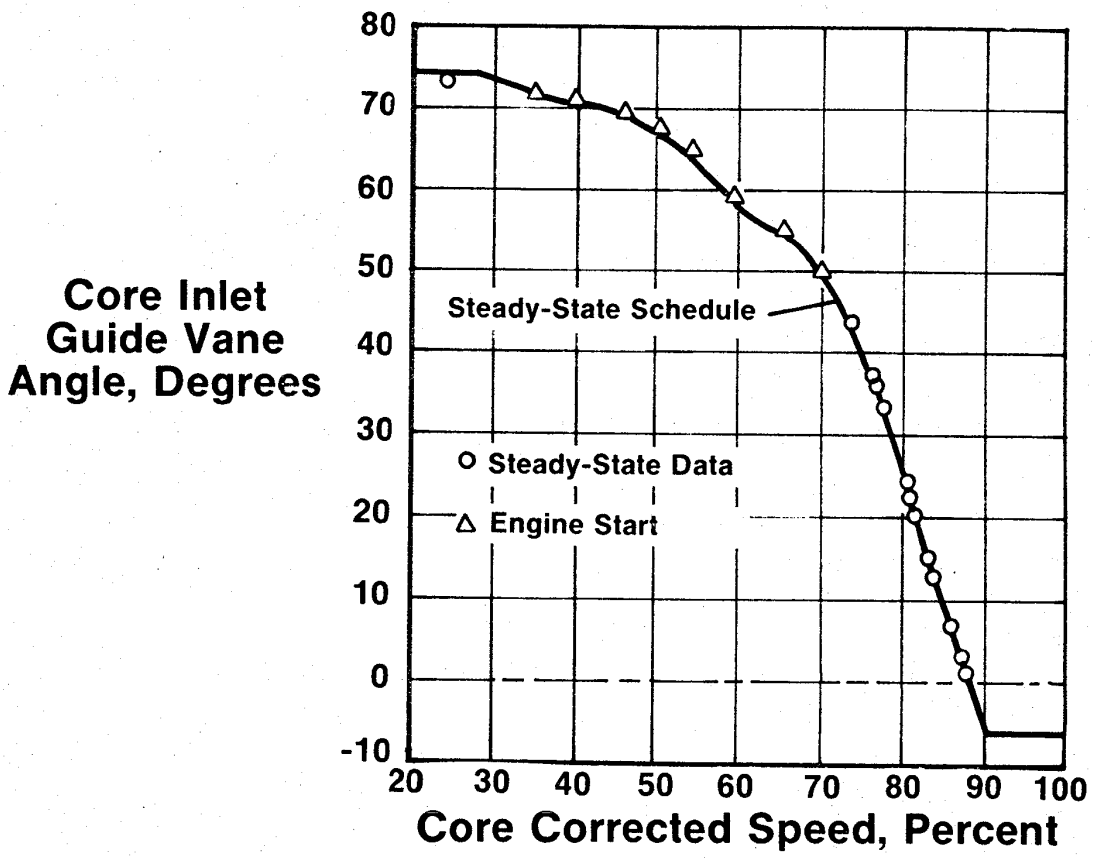

Figure 154. OTW Core Stator Control Performance.

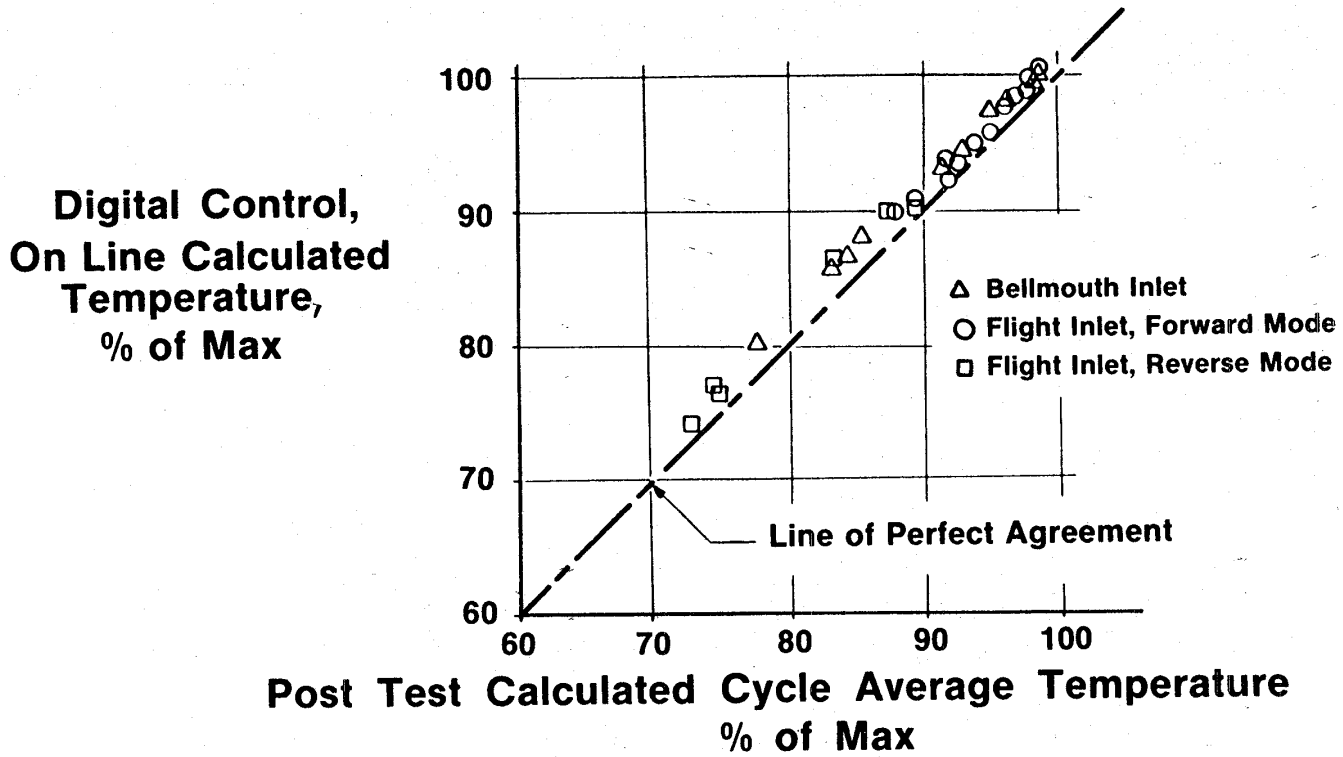

Figure 155. OTW Turbine Inlet Temperature Calculation Comparison.

digital control with posttest calculated values of turbine inlet temperature. The posttest data were calculated from cycle balance, using measured steady-state engine data; whereas, the digital control data were continuously calculated from an empirical equation in the digital control program memory. At the higher temperature levels, where protection is required, the digital control data agree with the posttest data within approximately 1.5%. Examination of recorded data showed that most of this error was associated with an error in fuel-flow measurement. With further development of the fuel-flow sensor an on-line, accurately calculated, turbine-inlet temperature could be implemented in a flight application.

During the engine test program, the engine was operated on the calculated turbine temperature limit. The limit level could be varied through an on-line adjustment. Engine operation on the limit was stable.

During the engine start cycle, the control system schedules engine acceleration fuel flow to prevent compressor stall. As noted earlier, the digital control incorporated the acceleration schedule in a series of polynomial equations. Figure 156 shows a typical start on the OTW engine with the full authority digital control. In this figure, the engine is being motored at core speed of 4000 rpm, at zero time, on the air starter. At approximately 1 second the combustor ignitor is energized, and the fuel stop cock is opened. An engine light is achieved in approximately 2 seconds as indicated by the rise in turbine discharge temperature. Over the next 25 seconds, the engine accelerates to idle speed. Through this period, the digital control is calculating and implementing the acceleration fuel-flow limit.

As noted earlier, the QCSEE's were required to have rapid thrust-response capability. Figure 157 shows the thrust-reponse requirement and the results of one transient-response experiment. The test results were obtained with a 25° core stator reset. As indicated on the figure, the experimental engine met the thrust-response requirement.

Summary - A full-authority, engine-mounted, digital control was designed and tested on the OTW QCSEE. During the engine-test program, the digital control functioned to provide reliable engine starting; it scheduled fan speed and core stator angle accurately. System stability was excellent from idle to full power. The calculated turbine inlet temperature concept was evaluated, and the control system manipulated the engine variables to demonstrate the transient-response requirement.

4.5 ACOUSTIC TEST RESULTS

The QCSEE acoustic-test program was conducted to measure the system-noise levels of the UTW and OTW engines and to evaluate the component-technology features on both engines. Both forward- and reverse-thrust noise levels were measured with the engine alone, i.e., without a wing-flap system in place. Where possible the component source levels and suppression have been assessed, but in some cases the noise reduction achieved by the total system will be presented.

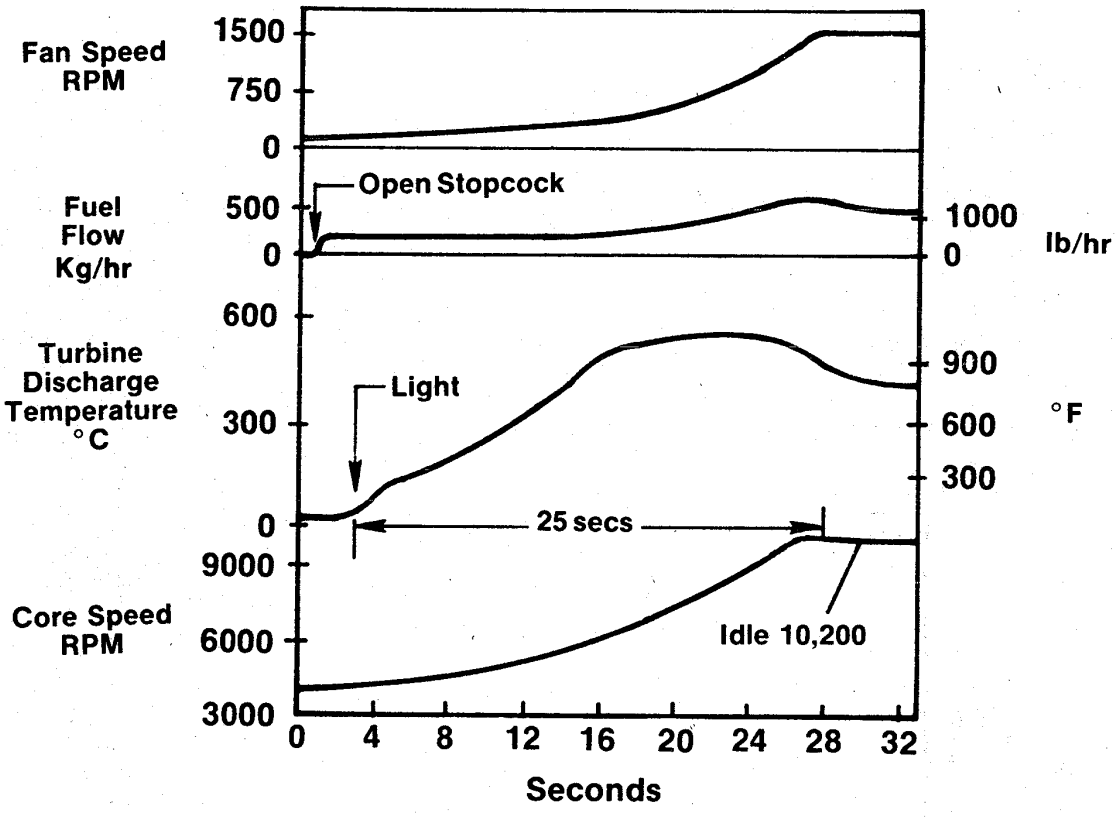

Figure 156. OTW Typical Engine Start.

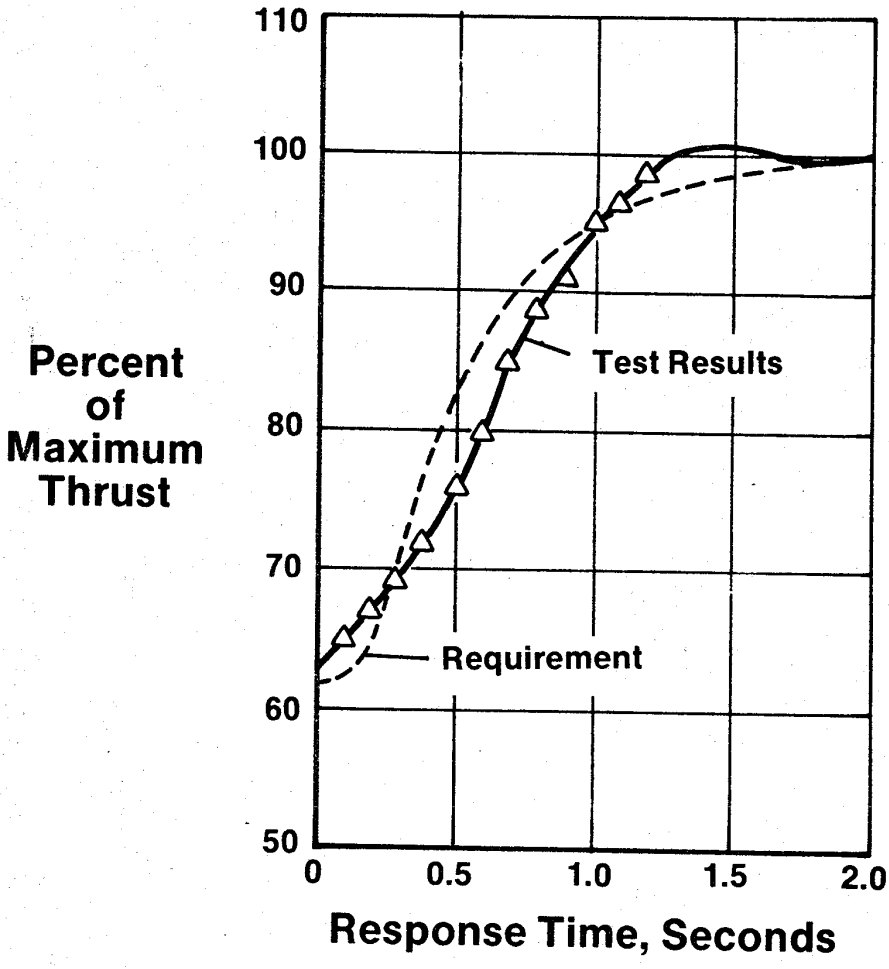

Figure 157. OTW Thrust Response.

The UTW acoustic test program was carried out with the composite nacelle mounted as shown in Figure 158 on the acoustic test pad. The engine centerline was 3.96 m (13 ft) from the ground. Since data were taken without the wing-flap system in place, the noise produced by the jet-flap interaction source had to be calculated and added to the measured engine-noise level in order to calculate the aircraft system noise for comparison to the program noise goals.

4.5.1 Test Configuration and Measurements

The five test configurations shown in Figure 159 permitted evaluation of the basic UTW engine noise levels as well as assessment of the major noise components. The baseline configuration was untreated with the exception of the fan frame between the rotor and OGV's, treatment on the OGV's, and in the core compressor inlet. Configuration No. 2 was the same as the baseline with the exception that the vanes were taped to determine the effect of this treatment. Both of these configurations were run with an untreated bellmouth inlet, and the resulting data were used to define the baseline system and fan-component-noise levels. The fully suppressed nacelle was run both in forward and in reverse thrust. Configurations 4 and 5 were tested with the fan-exhaust splitter and the core suppressor removed, respectively, to determine the impact of these two suppression elements. All configurations were operated over a range of engine conditions including speed variation, blade angle setting, and nozzle area.

All noise testing was done on the acoustic pad at the Peebles test facility. The ground surface shown in Figure 160 is concrete, but most of the testing was carried out with a gravel field surface. Noise measurement instrumentation locations, shown in Figure 161, consisted of a far-field microphone arc at 46.5 m (152.4 ft) with microphones on 12.2-m (40-ft) towers, every 10°. The acoustic directional array, which was used at six angles to separate engine sources and aid in component-suppression evaluation, is a highly directional receiver mounted on a movable cart. Internal engine instrumentation was also used and consisted of sound-separation probes and wall pressure transducers in the fan inlet and fan exhaust ducts.

4.5.2 UTW Results

Prior to test, the major noise-component spectra were estimated using calculation procedures for the jet noise, combustion noise, and turbine noise and scaling fan-noise spectra from previously measured fixed-pitch-fan noise data. Fan pressure ratio and tip speed were the primary scaling parameters used to obtain estimates of both inlet-radiated and exhaust-radiated fan noise. Each of these component spectra are plotted in Figures 162 and 163 at the maximum forward and aft angles of noise radiation for the takeoff power setting of the UTW engine. The heavy line on each plot is the logarithmic sum of these individual spectra and is an estimate of the measured baseline engine spectra at 46.3-m (152-ft) radius. The symbols on Figure 162

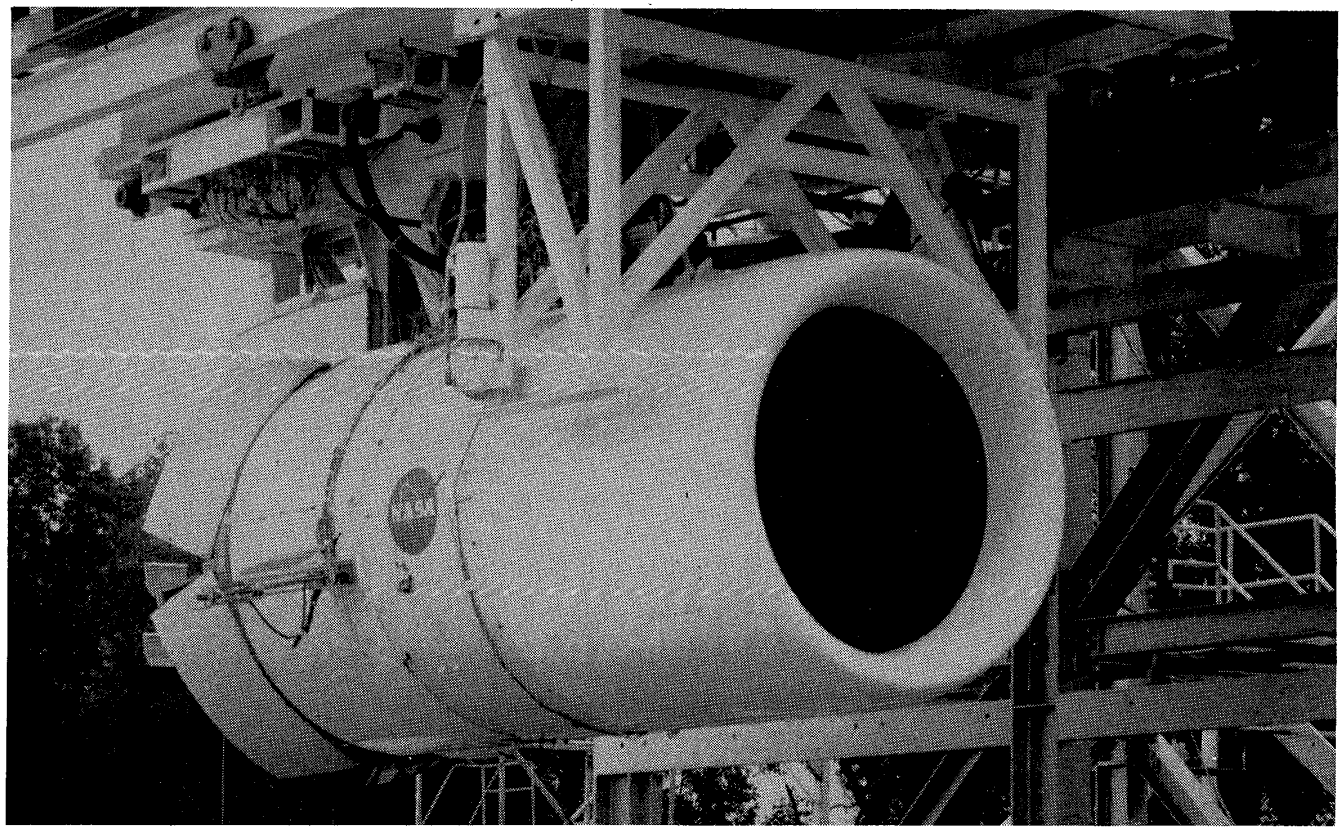

Figure 158. UTW QCSEE.

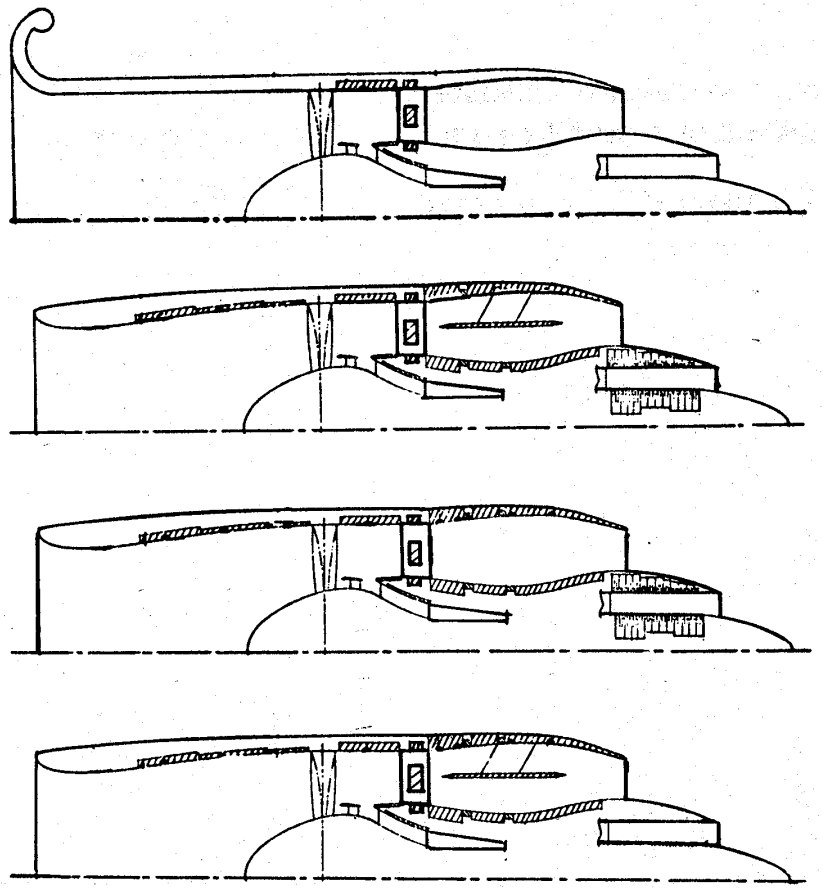

1. Baseline (Untreated Except for Treated Frame and Vane)
2. Baseline with Untreated Vanes
3. Fully Suppressed (Forward and Reverse Thrust)
4. Without Fan Exhaust Splitter
5. Without Core Treatment

Figure 159. UTW Acoustic Test Configurations.

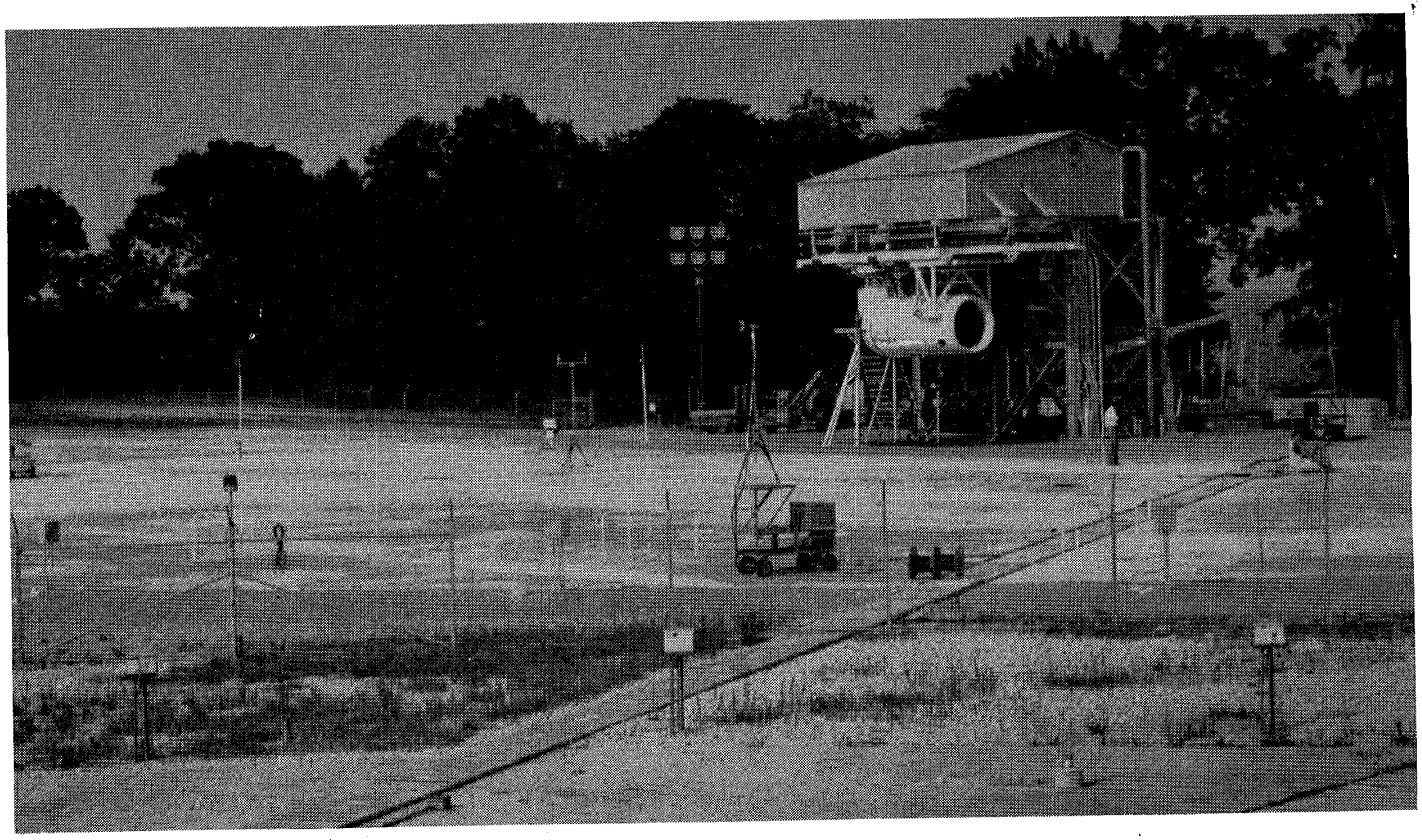

Figure 160. Acoustic Test Site.

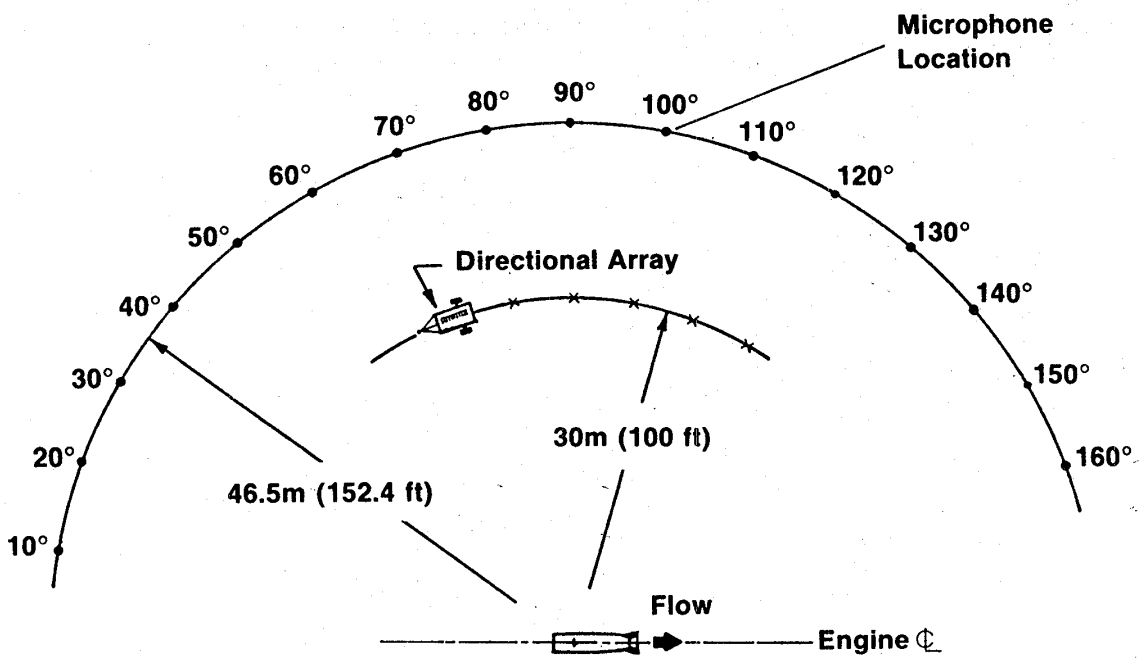

Figure 161. Peebles Acoustic Test Sound Field.

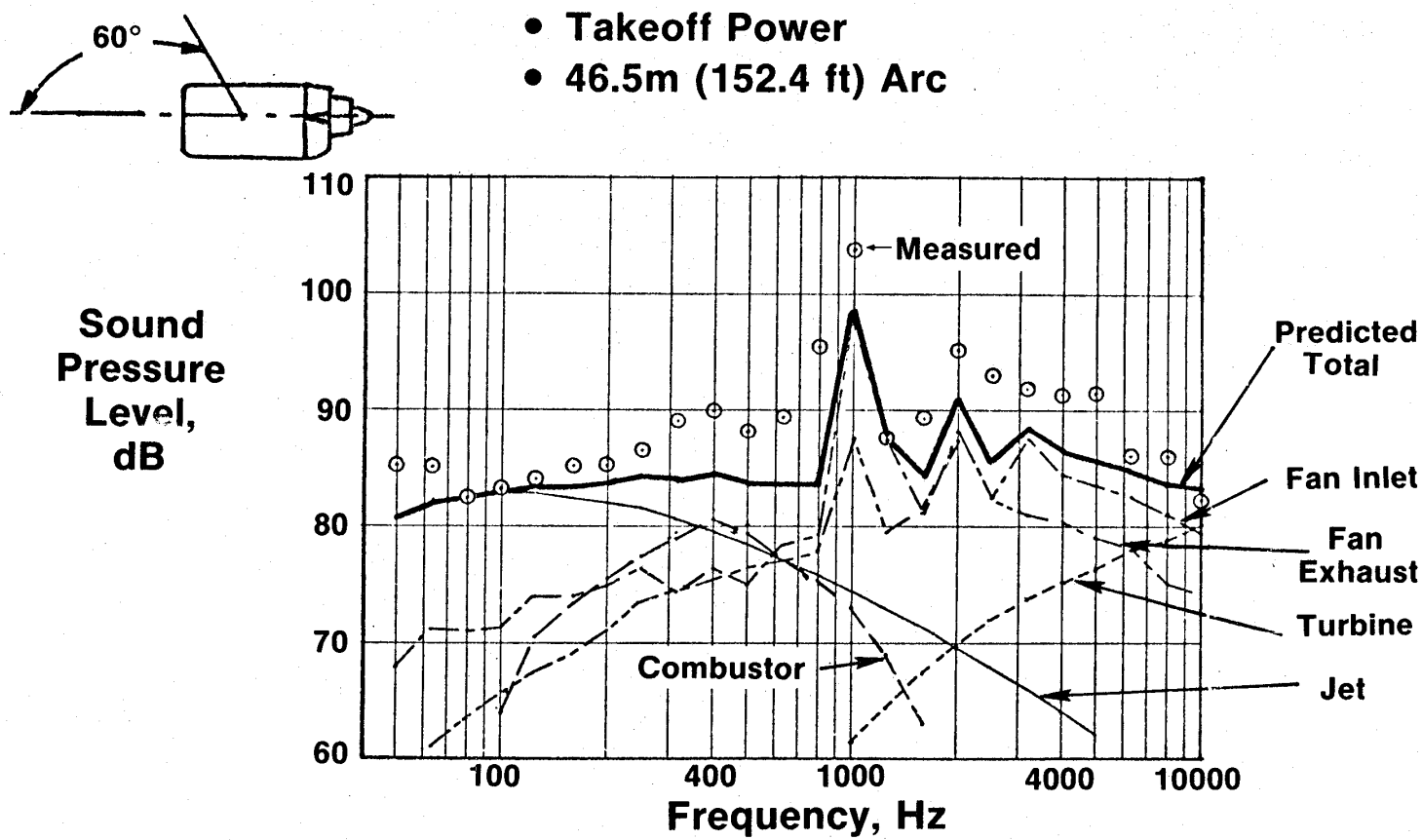

Figure 162. UTW Inlet-Radiated Baseline Noise.

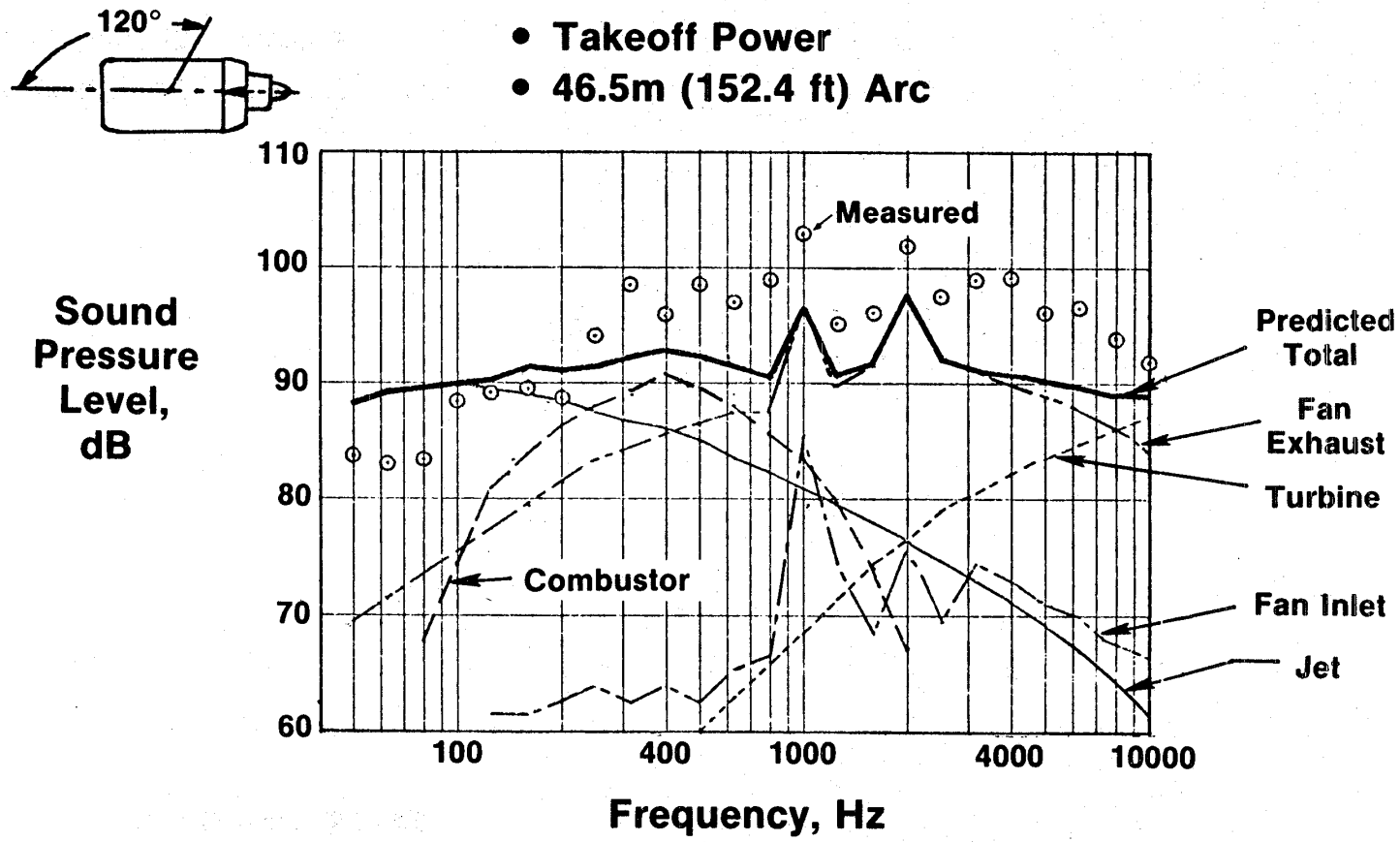

Figure 163. UTW Exhaust-Radiated Baseline Noise.

and 163 are the measured data from the baseline test. In general, the measured levels are on the order of 5 dB higher than expected over the entire high-frequency spectrum. Since the system noise above 800 Hz is controlled by fan noise, it appears that the estimates based on the fixed-pitch-fan data cannot be used to reliably predict variable-pitch-fan designs; i.e., solidity, blade number, and perhaps the vane-frame design are probably causing this divergence, and the exact cause needs to be the focus of additional investigation.

One of the potential advantages of a variable-pitch fan was thought to be the capability to minimize noise by continuously optimizing blade incidence angle and loading over the fan-speed range. Data shown in Figure 164, taken at forward and aft max angles, takeoff and approach thrusts, show no tendency to identify a minimum noise point. These data represent a range of incidence angles and loading large enough to reveal any acoustic advantages which might be present. Fan-source mechanisms are many and varied for the static test case. For example, one of the major noise-source mechanisms statically is known to be the interaction of the rotor with inlet turbulence. This source appears to be made up of both a dipole source and a quadrapole source; one varies with blade loading, and one is independent of loading. If, for this fan design, the dipole, rotor/turbulence interaction source controls, then no change with blade angle would occur. In flight, however, the ingested turbulence is no longer affected by the contraction ratio of the static inlet, and this rotor-turbulence interaction noise is reduced. Therefore in the flight case the effect of blade angle may be important.

The inlet design, which has been described previously, is shown in Figure 165 in cross section. The treatment begins 11.2 cm (4.4 in.) downstream of the high Mach number throat and is designed to produce 12.8 PNdB suppression at takeoff and 6.3 PNdB suppression at approach, both at the maximum forward-radiation angle on a 152-m (500-ft) sideline.

The suppression results of this inlet design are shown in Figure 166; the sideline PNL has been plotted as a function of throat Mach number for the baseline test and the fully suppressed configuration. (The baseline data taken with the cylindrical inlet is plotted at equivalent fan rpm points since, of course, the inlet Mach numbers are quite low.) Several sets of data with different blade angle settings make up the fully suppressed line. The indicated suppression at a throat M_n of 0.79 is only 9 PNdB and is changing very slowly with increasing throat M_n. This trend is contrary to the scale-model results, but additional analysis with the directional array revealed the problem. Separating the measured spectrum into noise emanating from the inlet and noise reaching the forward quadrant, but radiated from the fan exhaust, produced the dotted and dashed curves of this figure. It is obvious that the aft-radiated noise, which is increasing with engine speed (and M_{th}), is a "floor" to the inlet-noise reduction. The indicated suppression (baseline to "inlet noise") is now seen to be 14.5 PNdB at the design Mach number.

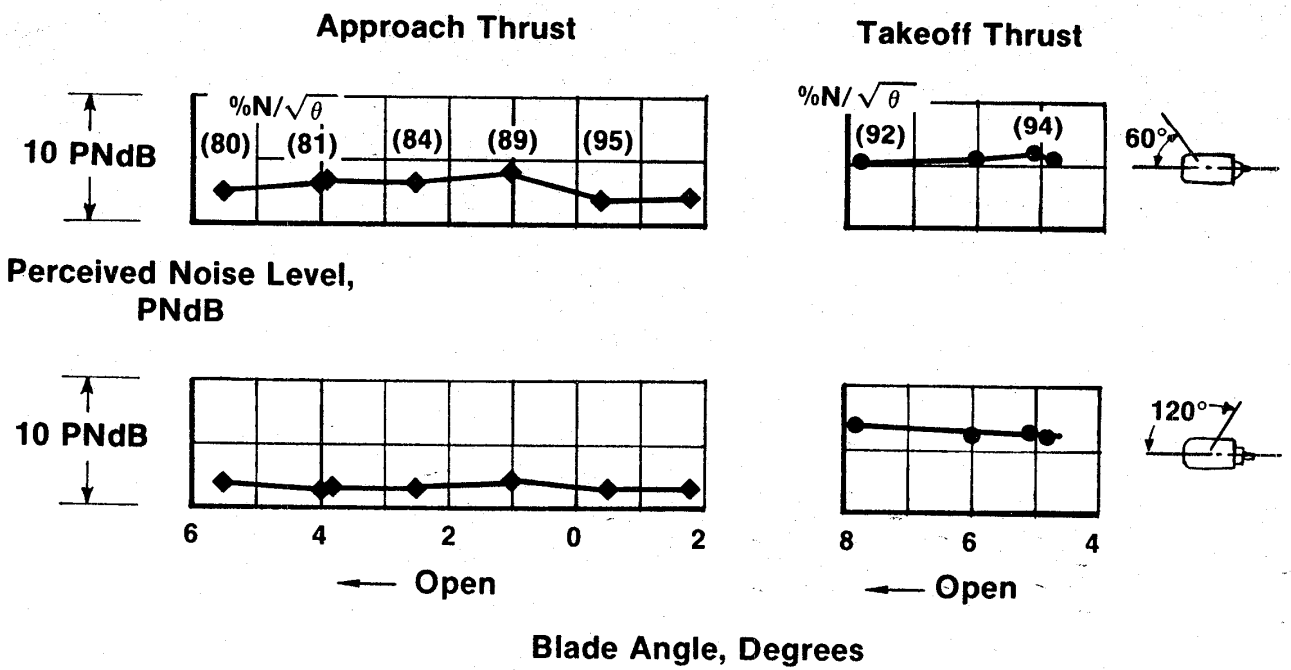

Figure 164. Variation of PNL with Blade Angle.

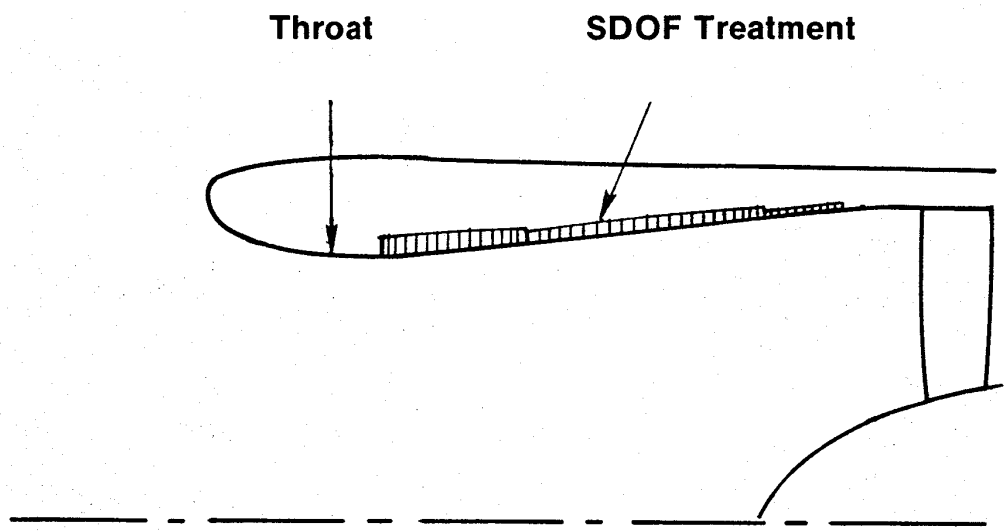

PNL Suppression Prediction

Takeoff	**12.8 PNdB**
Approach	**6.3 PNdB**

Figure 165. UTW Inlet Configuration.

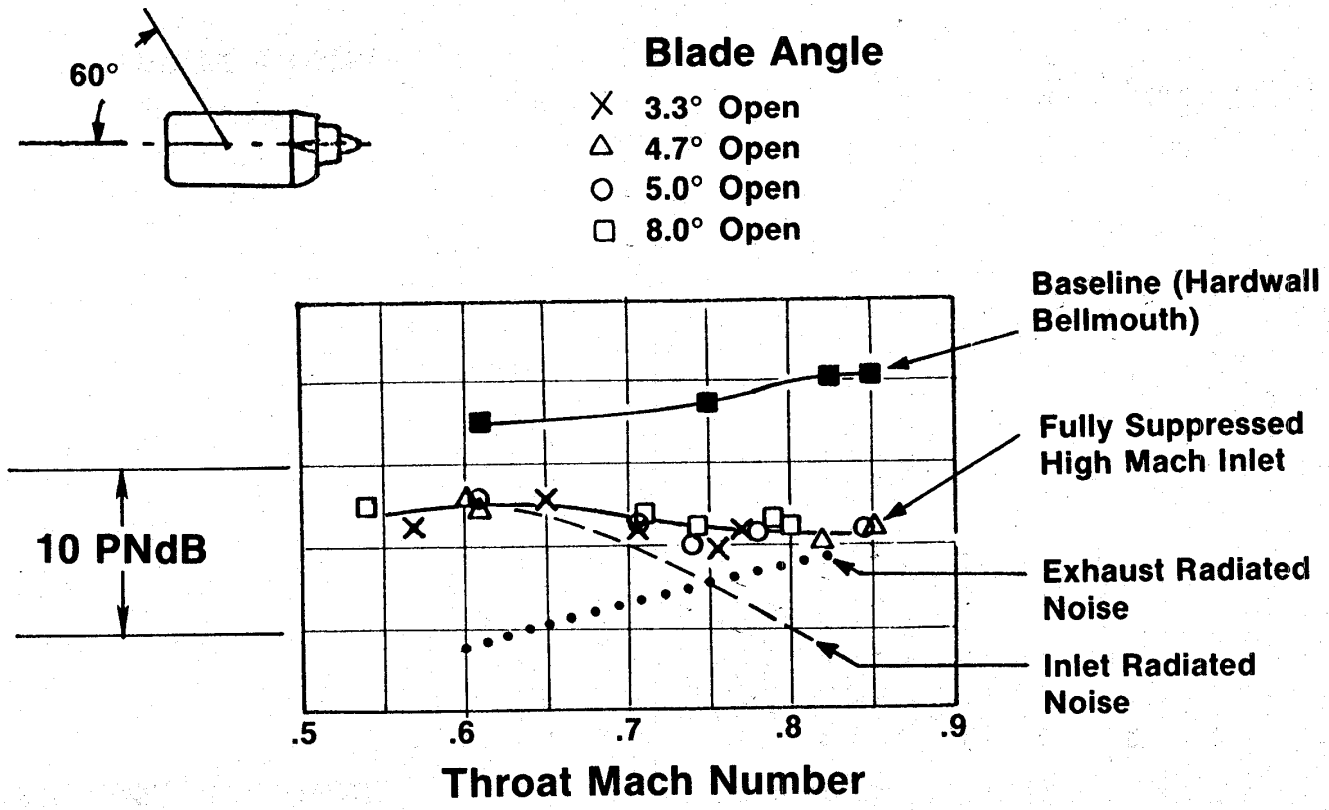

Figure 166. Effect of Inlet Throat Mach Number on PNL.

The aft treatment design is shown in Figure 167 with the predicted system suppression values at takeoff and approach. Due to the large bypass ratio and fan diameter, the fan exhaust passage height is 50.8 cm (20 inches). The desired fan exhaust suppression required the use of a splitter in this large duct. The splitter was removable, and the exhaust suppression was measured with and without the splitter in place. The measured system suppression as a function of engine thrust at the maximum aft-radiation angle is plotted in Figure 168 and shows a value of 8.0 PNdB, roughly constant over the engine power-setting range. The suppression spectra, for the splitter-out case shown in Figure 169 at takeoff and approach, are in good agreement with the prediction but miss the predicted suppression by 2 dB in one critical band (2000 Hz). This results in PNL reduction short of the prediction by about 1.5 PNdB. With the exhaust splitter in place, peak SPL suppression of almost 15 dB was measured at the 120° far-field position, and this is shown in Figure 170. In general, the suppression did not meet expectations at the second-harmonic frequency at approach nor at the fundamental and second-harmonic frequencies at takeoff. There appears to be a flanking transmission path which prevents the full suppression from being measured, and this is the subject of additional data analysis.

Taping the treatment in the vanes provided an opportunity to evaluate the suppression potential of treatment in this location. Total treated area is small, about 0.67 m^2 (7.2 ft^2), and because of treatment-thickness limitations the design frequency was high (about 4 kHz). The measured suppression spectrum (Figure 171) in the aft quadrant shows about 2 dB over a broad frequency range; this could be very beneficial to engine systems with marginal or inadequate suppression.

The core suppressor for the QCSEE was designed to suppress both high-frequency, turbine-generated noise and low-frequency, combustor-generated noise. Since both of these components are marginal in terms of contribution to the total system noise, it was recognized in the beginning of the program that it would be extremely difficult to measure the unsuppressed and suppressed levels of these components. If the fan exhaust suppression levels are achieved, however, this core noise must be reduced to meet the system goals. The difficulty in measurement of the core suppression has been compounded by the fan-source-noise increase (5 dB) which results in aft fan noise levels high enough to completely mask the high-frequency core suppression. In a similar fashion, low-frequency jet noise masks the low-frequency suppression of the combustor noise. The comparison of the measured and predicted core suppression in Figure 172, therefore, reflects the measurement difficulties just described rather than poor performance of the core suppression. Additional engine testing is required to confirm the good performance of the core suppressor indicated from the component test.

Reverse-thrust noise testing of the UTW engine was done with two blade angles over a range of reverse thrust. The measured max PNL values, shown in Figure 173, occurred at an angle of 70° on a 152-m (500-ft) sideline and were substantially above the noise goal of 100 PNdB for 35% reverse thrust. Maximum reverse thrust achieved was 27%, and at this thrust level the 152-m

- **Predicted Exhaust Suppression**
  - **Takeoff 9.2 PNdB**
  - **Approach 9.6 PNdB**

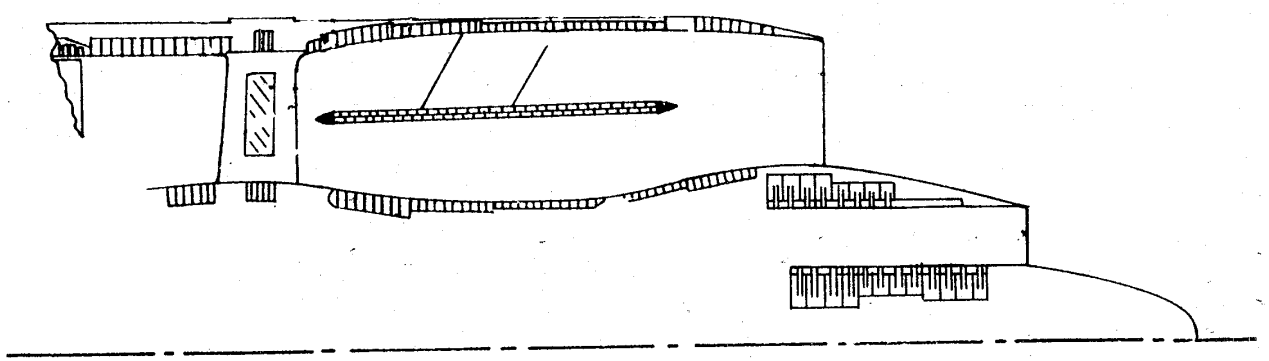

Figure 167. UTW Exhaust Treatment Configuration.

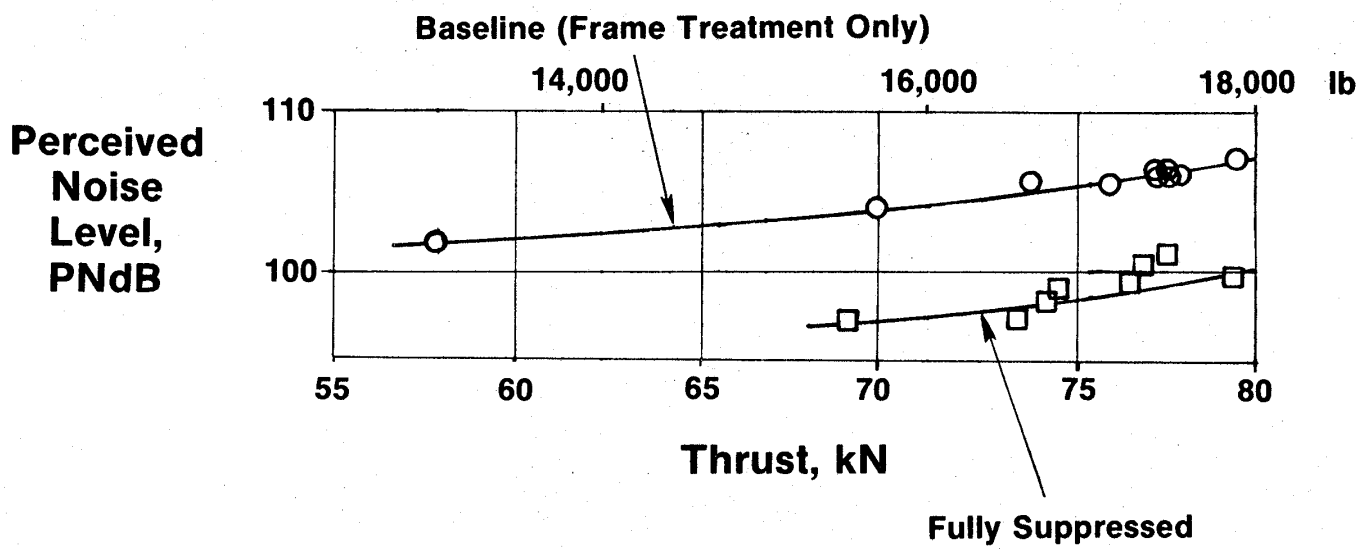

Figure 168. Exhaust-Quadrant PNL Variation with Thrust.

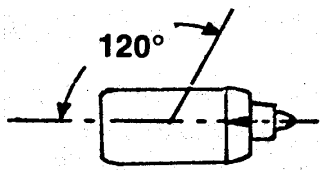

- **Wall Treatment Only**

1/3 OBSPL Suppression, Δ dB

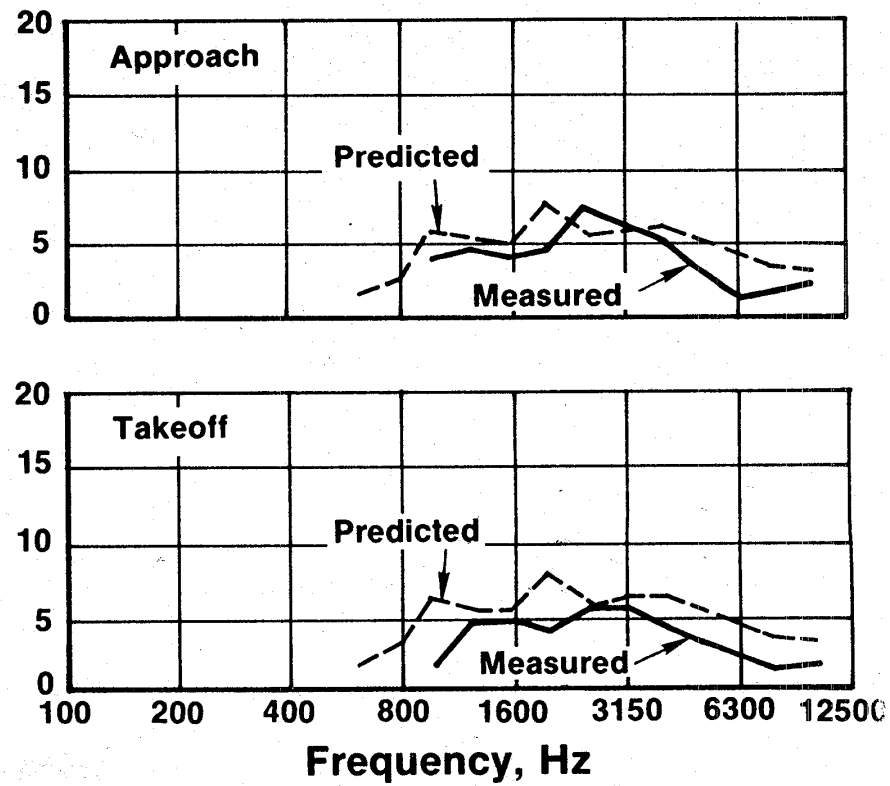

	Δ PNdB	
	Approach	Takeoff
Measured	4.4	4.0
Predicted	5.8	5.4

Figure 169. Exhaust-Quadrant System Suppression Spectra, Wall Treatment Only.

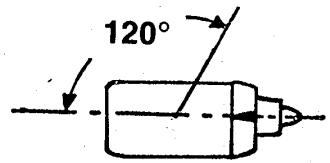

• With Splitter

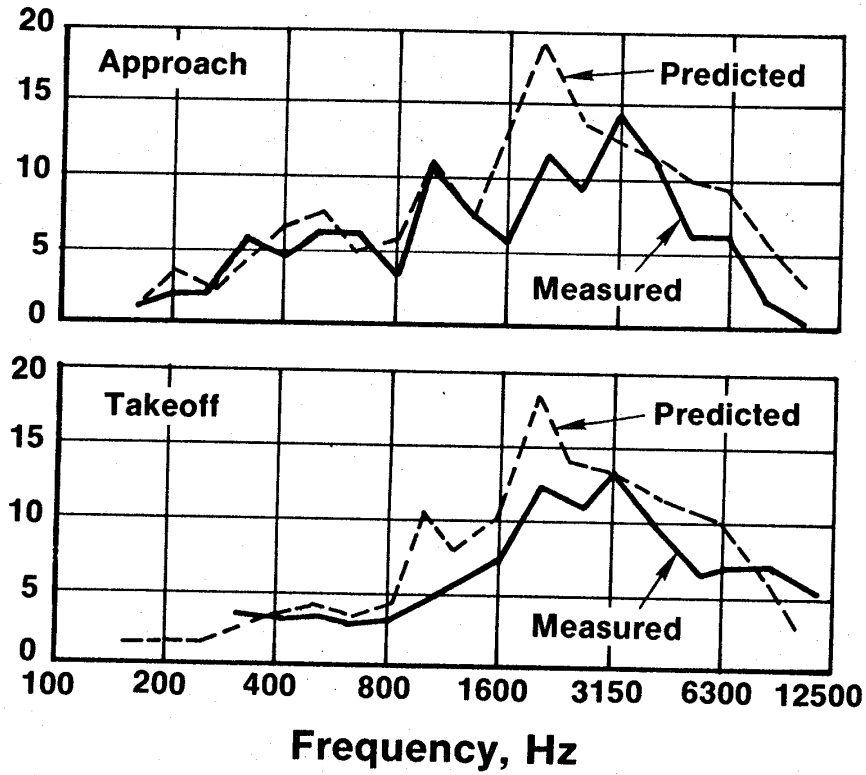

Δ PNdB	Approach	Takeoff
Measured	8.0	7.5
Predicted	9.6	9.2

Figure 170. Exhaust-Quadrant System Suppression Spectra, with Splitter.

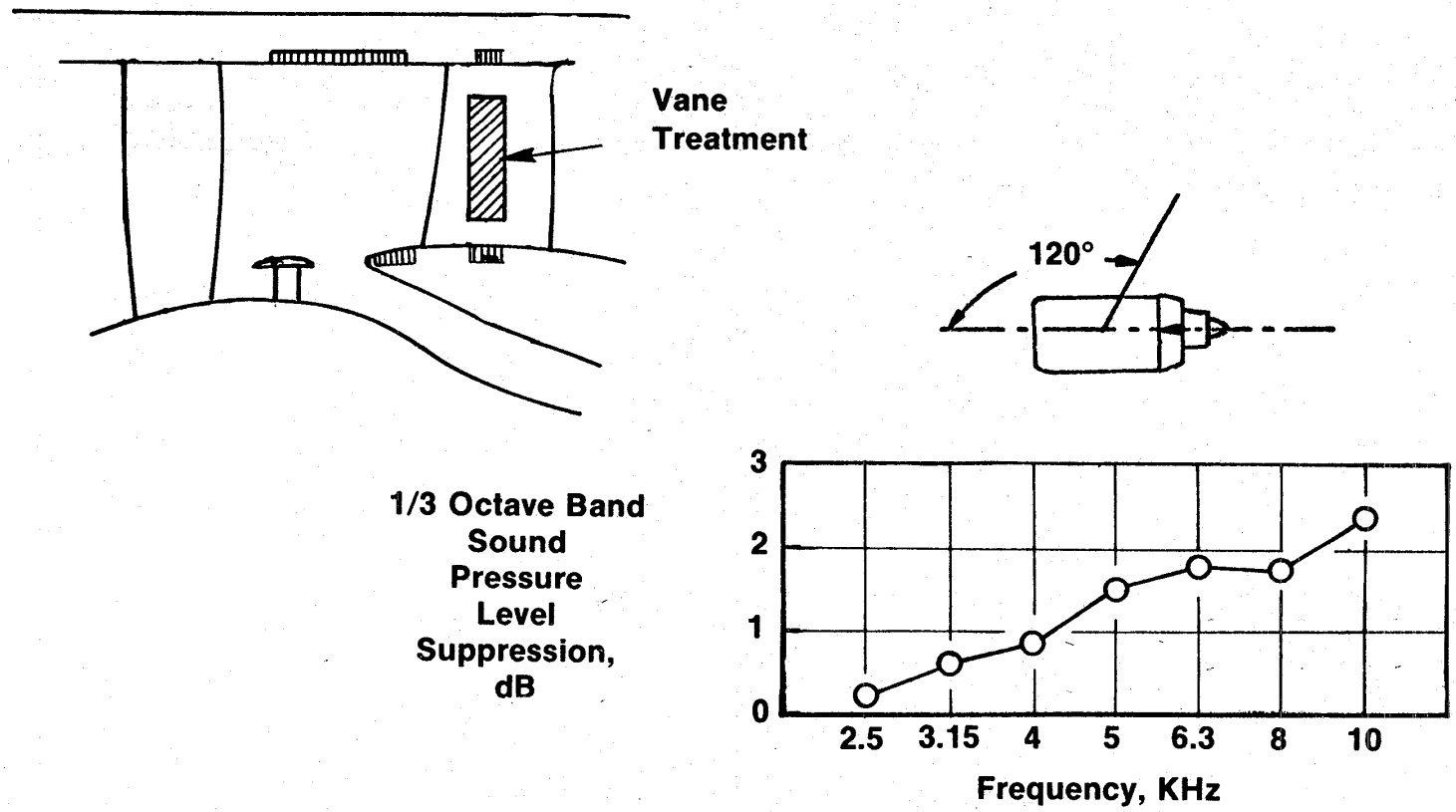

Figure 171. Treated-Vane Suppression.

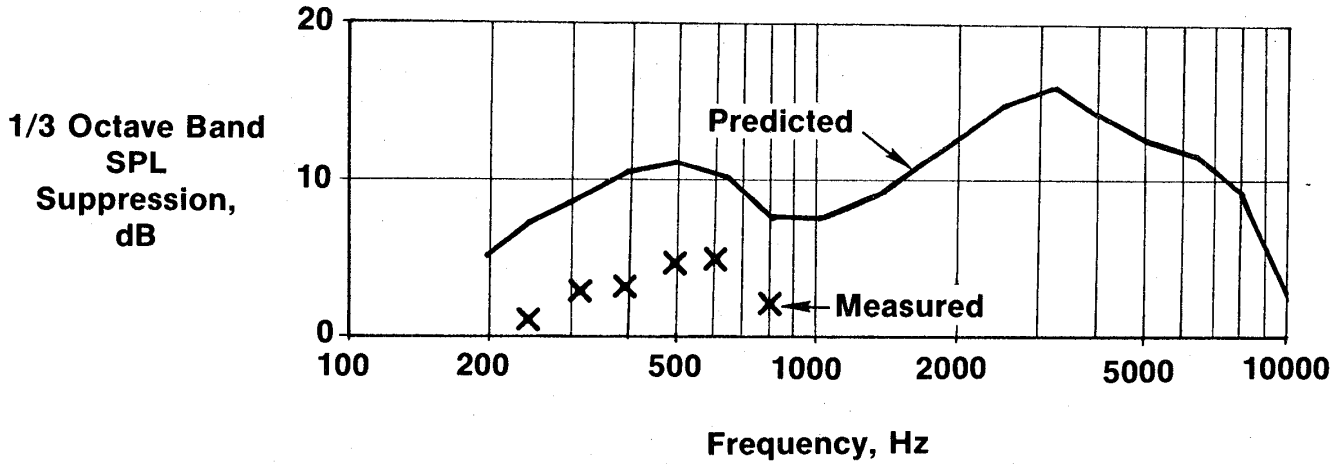

Figure 172. Core Suppression from Far-Field Measurements, Approach Thrust.

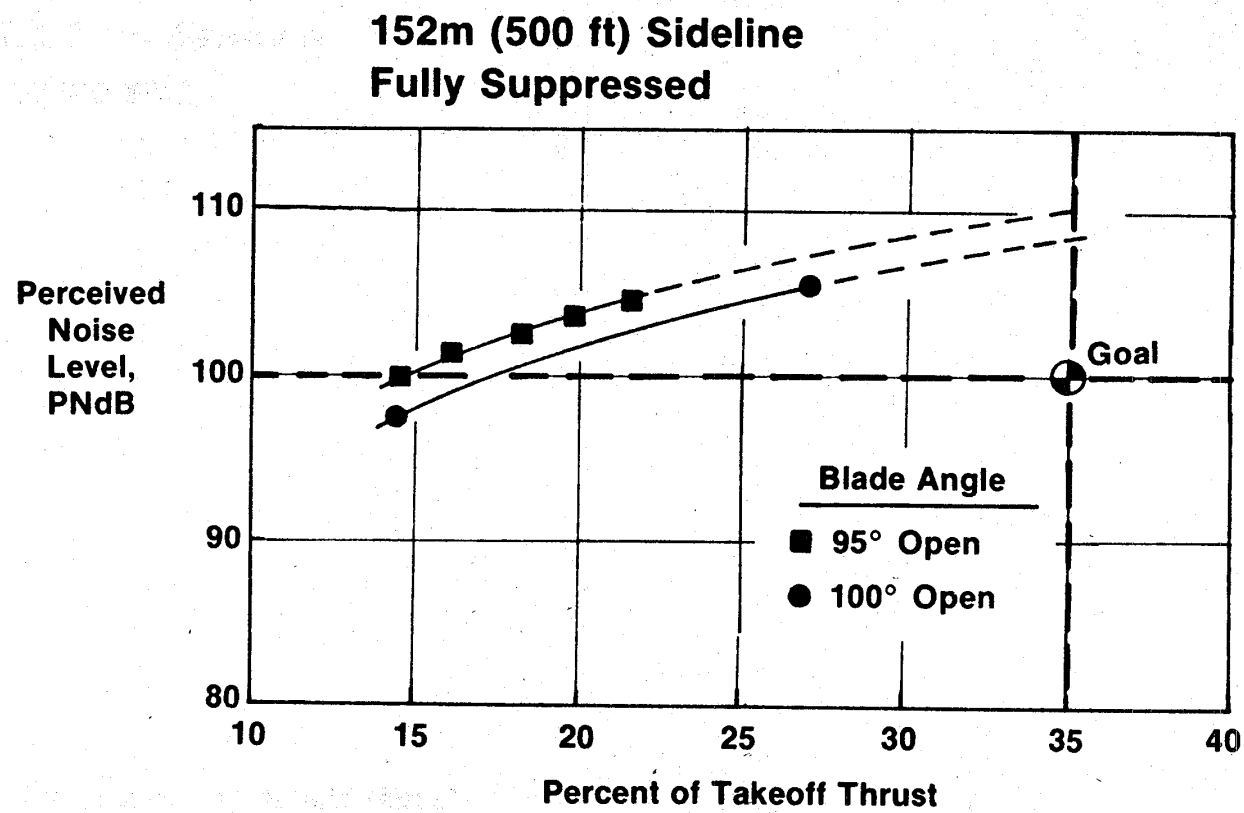

Figure 173. Variation of Peak PNL with Percent Reverse Thrust.

(500-ft) sideline noise is 106 PNdB. Although higher than the goal, this measured reverse-thrust engine-noise level is consistent with the scale-model fan data and collectively provides a good data base for future reverse-pitch-fan noise predictions.

The UTW engine noise summary in Table XXX shows that the aft-radiated engine noise is 9 PNdB higher than the calculated jet-flap component and makes a major contribution to the system EPNL at takeoff. The noise goal was exceeded by 2.2 EPNdB primarily as a result of the unexpected increase in aft fan-source noise. At approach the forward-radiated fan noise is slightly higher than expected due to low approach suppression, but the system noise misses the goal of 95 EPNdB by only 0.7 EPNdB.

4.5.3 OTW Results

The OTW engine was tested in an inverted mode (Figure 174) to permit the deployment of the thrust reverser. Acoustic testing was conducted with five configurations (Figure 175), starting with a baseline which was untreated except for treatment in the frame area and on the vanes. Three forward-thrust configurations were used to determine system-noise levels and to evaluate component suppression. The hybrid inlet was evaluated without treatment in order to determine the acceleration-suppression alone, and a more moderate suppression approach was evaluated by removing the aft fan duct splitter and the core suppressor. The reverse-thrust noise was measured with the fully suppressed nacelle.

The agreement of the measured inlet-radiated baseline levels with the predicted spectrum was excellent as seen in Figure 176. All the major features of the dominant fan-inlet noise are seen to be accurately predicted. The aft-radiated noise shown in Figure 177 was correctly predicted at blade-passing frequency, but SPL's at the second harmonic and above are substantially below predictions. The only factor that appears to explain this over-prediction at high frequency is a very effective suppression characteristic for the frame and vane treatment which was not separately evaluated during the program.

The hybrid inlet for the OTW engine, shown in Figure 178, was constructed with a bulk absorber material for the treated area. A Kevlar felt covered with a perforated plate was used. This very effective treatment was used to improve the approach suppression with the hybrid inlet; 13.5 PNdB suppression was anticipated at the takeoff power setting.

The takeoff suppression spectrum, shown in Figure 179, exceeded the goal slightly, reaching 14 PNdB at the maximum forward angle and suppressing the inlet noise down to the jet-noise floor up to 2500 Hz. Peak suppression at blade-passing frequency was almost 20 dB. The suppression was entirely due to the acceleration effect since the untreated inlet was identical to the treated. At approach, Figure 180, the inlet suppression with the bulk absorber is improved over that achieved with the resonator treatment, but the OTW inlet did not achieve the predicted suppression. The difficulty

Table XXX. UTW Composite Nacelle System Noise.

	Forward Quadrant		Aft Quadrant	
	Engine	Jet/Flap	Engine	Jet/Flap
Takeoff				
PNL	91.7	94.6	99.0	90.0
Quadrant Total PNL	97.0		99.9	
System EPNL	97.2			
Approach				
PNL	96.7	89.8	95.6	82.7
Quadrant Total PNL	97.9		96.0	
System EPNL	95.7			

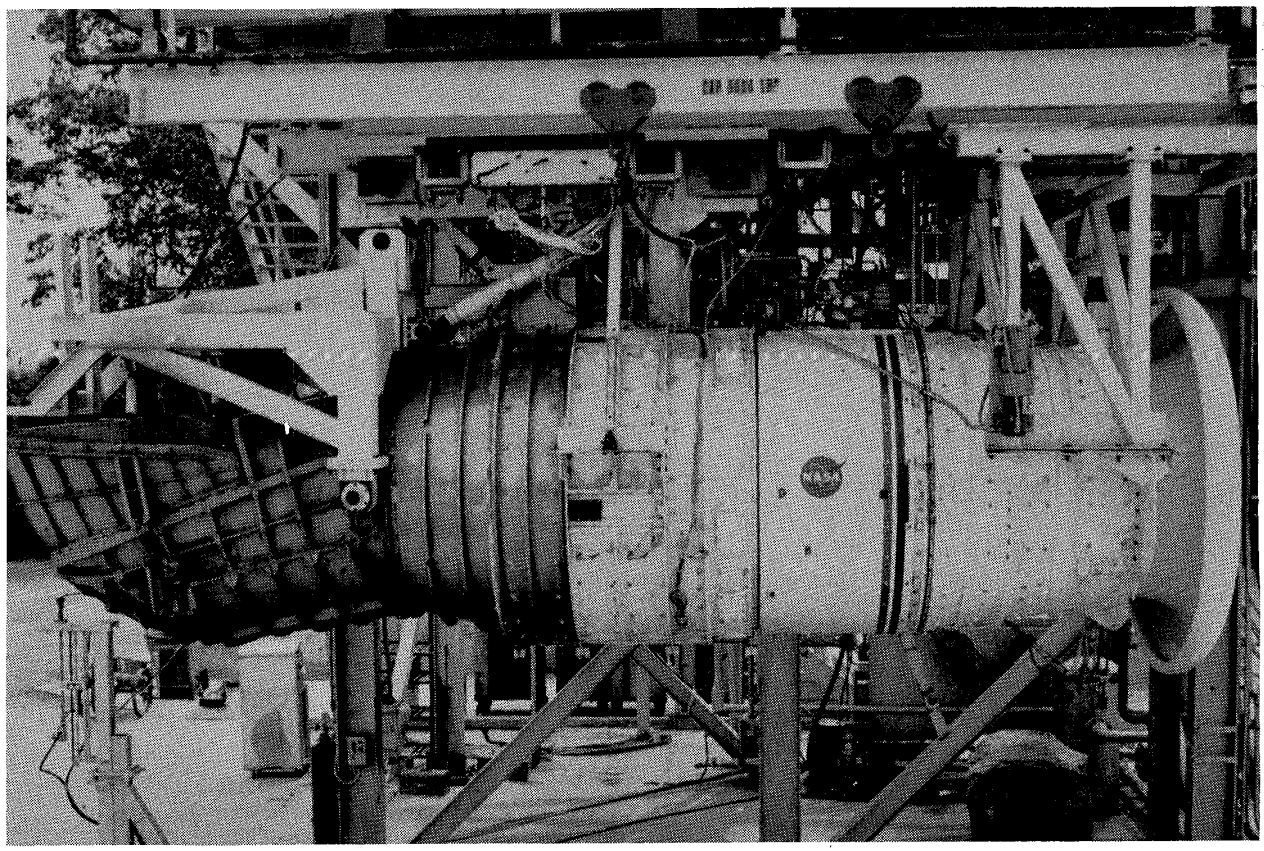

Figure 174. OTW QCSEE.

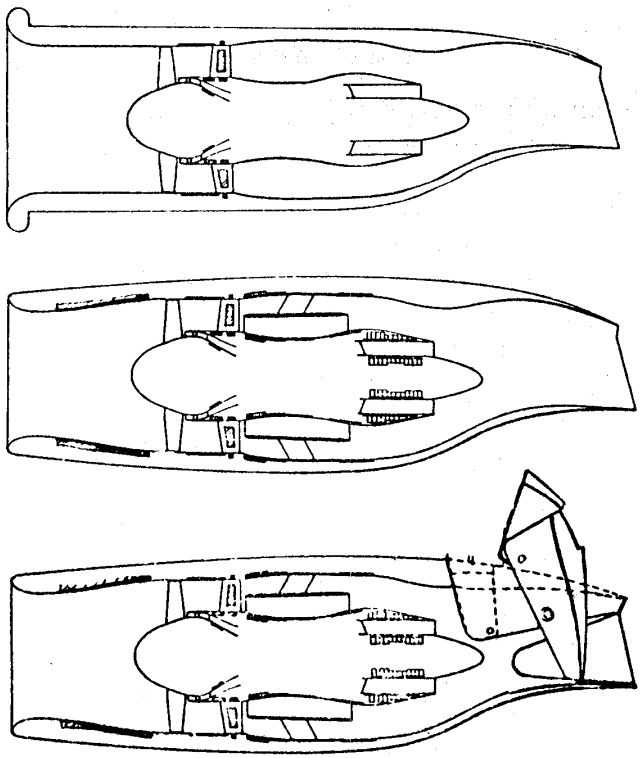

Baseline

1. **Untreated Except for Frame and Vane Treatment**

Suppressed Engine-Forward Thrust

2. **Fully Suppressed**
3. **Untreated High Mach Inlet**
4. **Untreated Core and Splitter Removed**

Suppressed Engine-Reverse Thrust

5. **Fully Suppressed**

Figure 175. OTW Acoustic Test Configurations.

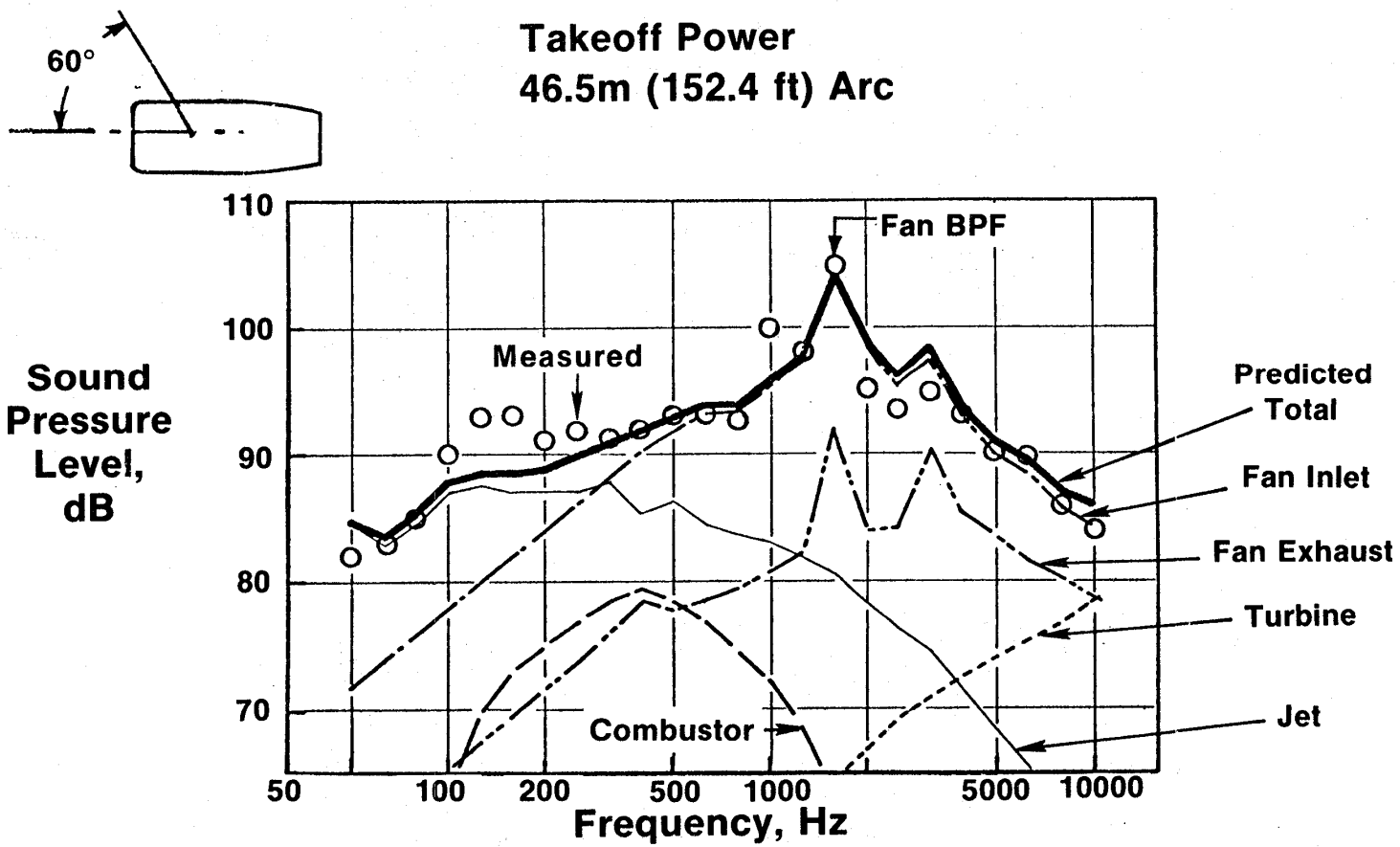

Figure 176. OTW Inlet-Radiated Baseline Noise.

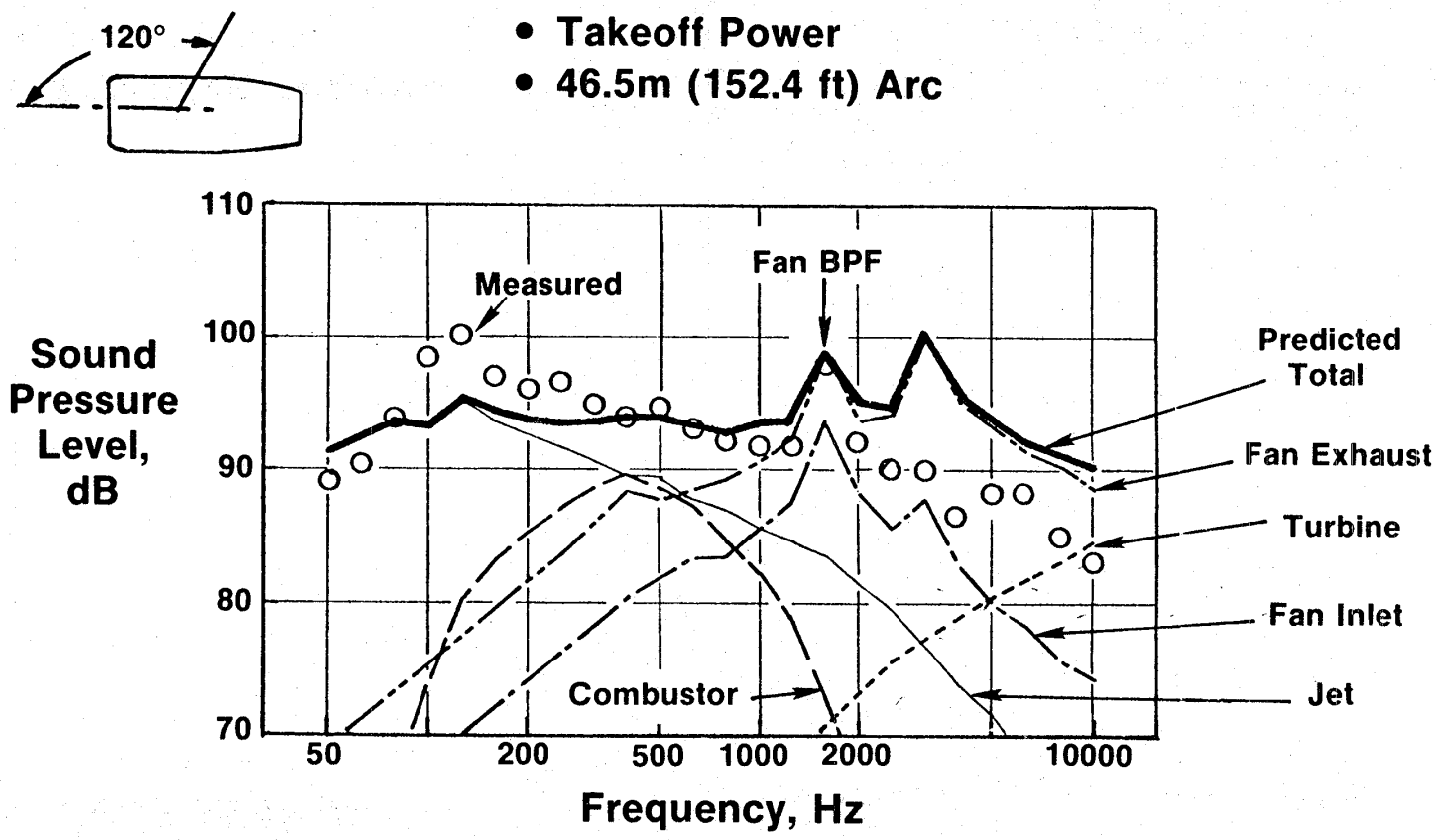

Figure 177. OTW Exhaust-Radiated Baseline Noise.

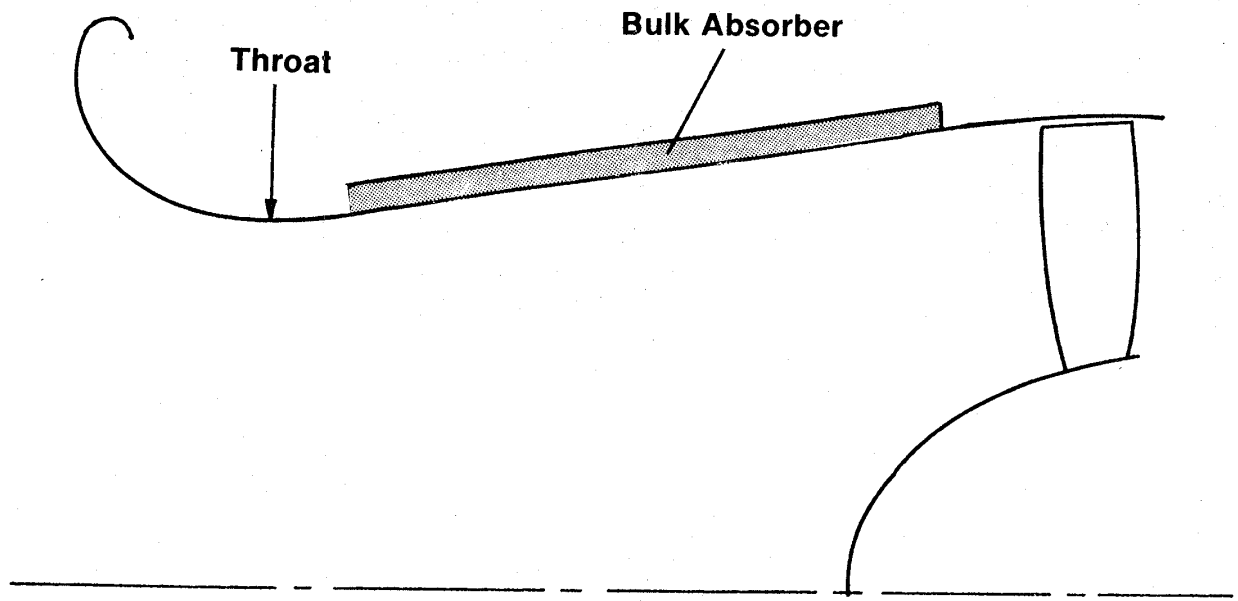

PNL Suppression Predicted

Takeoff	**13.5 PNdB**
Approach	**10.4 PNdB**

Figure 178. OTW Inlet Configuration.

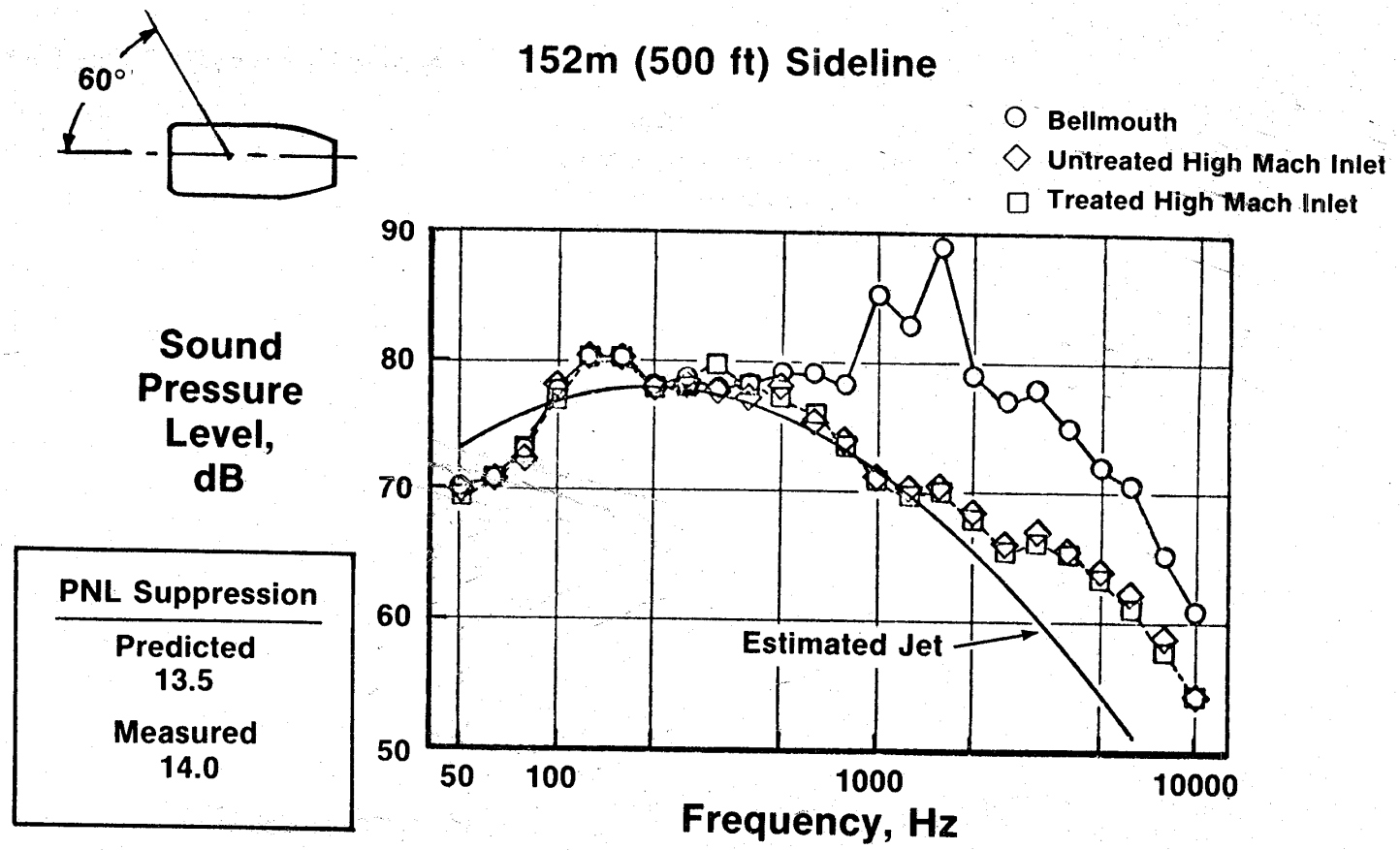

Figure 179. OTW Inlet-Radiated Noise at Takeoff.

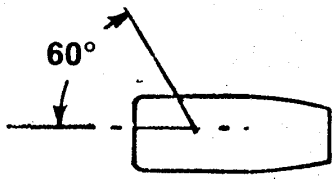

PNL Suppression	
Predicted	Measured
10.4	7.5

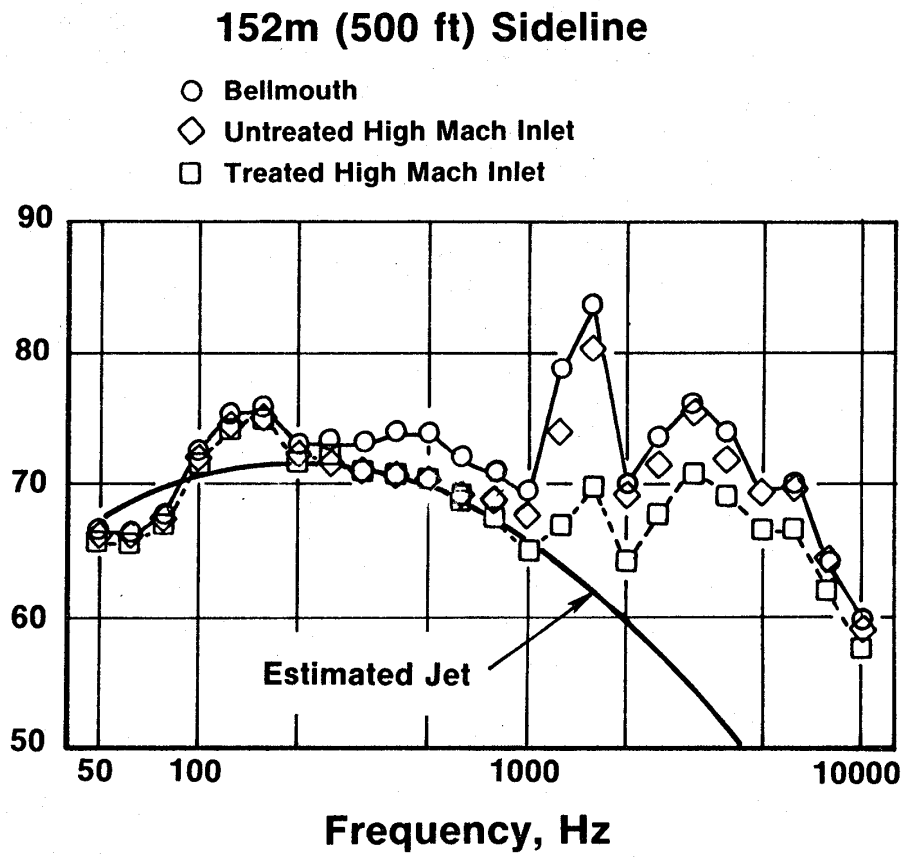

Figure 180. OTW Inlet-Radiated Noise at Approach.

in this design is not the performance of the bulk absorber as a treatment but that the requirement for a high-porosity, perforated face sheet in the presence of high subsonic wall Mach numbers tends to generate high-frequency broadband noise that reduces the effective suppression bandwidth. In spite of this, 7.5 PNdB of inlet suppression with only wall treatment is good suppression performance.

The measured system exhaust suppression is shown in Figure 181 by comparing the baseline and the fully suppressed configurations. The suppressed spectrum, which will be shown later, is controlled by jet noise - making the measurement of aft suppression very difficult. Less than 5 PNdB of system suppression is shown here, and it increases to only 6 PNdB when the calculated jet noise is removed. The four shaded symbols are reduced by removing the calculated jet noise. In Figure 182 the plot of the suppressed and unsuppressed spectra shows two reasons for the low measured suppression. First, the second-harmonic source level being lower than predicted leaves very little tone suppression available. Second, the suppression above 2500 Hz is effectively zero, and this is the apparent result of a "floor-noise source" which prevents the suppression from being detected in the far-field measurements. This floor source is apparently boundary-layer noise generated in the exhaust duct and common nozzle from the high-velocity airflow over perforated surfaces. Although the wall Mach numbers were kept as low as possible, the calculated levels from flow noise are very close to the measured spectrum levels above 2500 Hz. The lack of high-frequency suppression is evident in Figure 183, a comparison of the measured and predicted suppression spectra at takeoff. The "missing second harmonic" in the source spectra produces the discrepancy at 3150 Hz.

The OTW reverse-thrust test was conducted with the exhaust deflected downward and forward, with impingement on the concrete pad, as shown in Figure 184. Scale-model testing prior to the engine test indicated that the flow-over-the-ground-plane source would not be a major factor in the engine reverse-thrust noise measurements. Of greater importance were parameters such as lip angle, lip length, and distance of blocker from nozzle exit plane. The full-scale engine design incorporated these scale-model results to the fullest extent possible consistent with thrust-reverser performance and mechanical design. But it was expected, based on the scale-model program, that the engine levels would exceed the noise goal by about 6 PNdB. This prediction was confirmed by the engine data shown in Figure 185. Based on the scale-model tests, lower noise levels could have been achieved with larger nozzle-to-blocker spacing and increased reverser lip length, but these "noise improvements" could not be incorporated in the current engine design because of mechanical-design requirements for deployment and stowage.

In summary, the calculated system levels shown in Table XXXI for the OTW were within 2.2 EPNdB of meeting the system noise goal at takeoff and were lower by 0.4 EPNdB than the noise goal at approach.

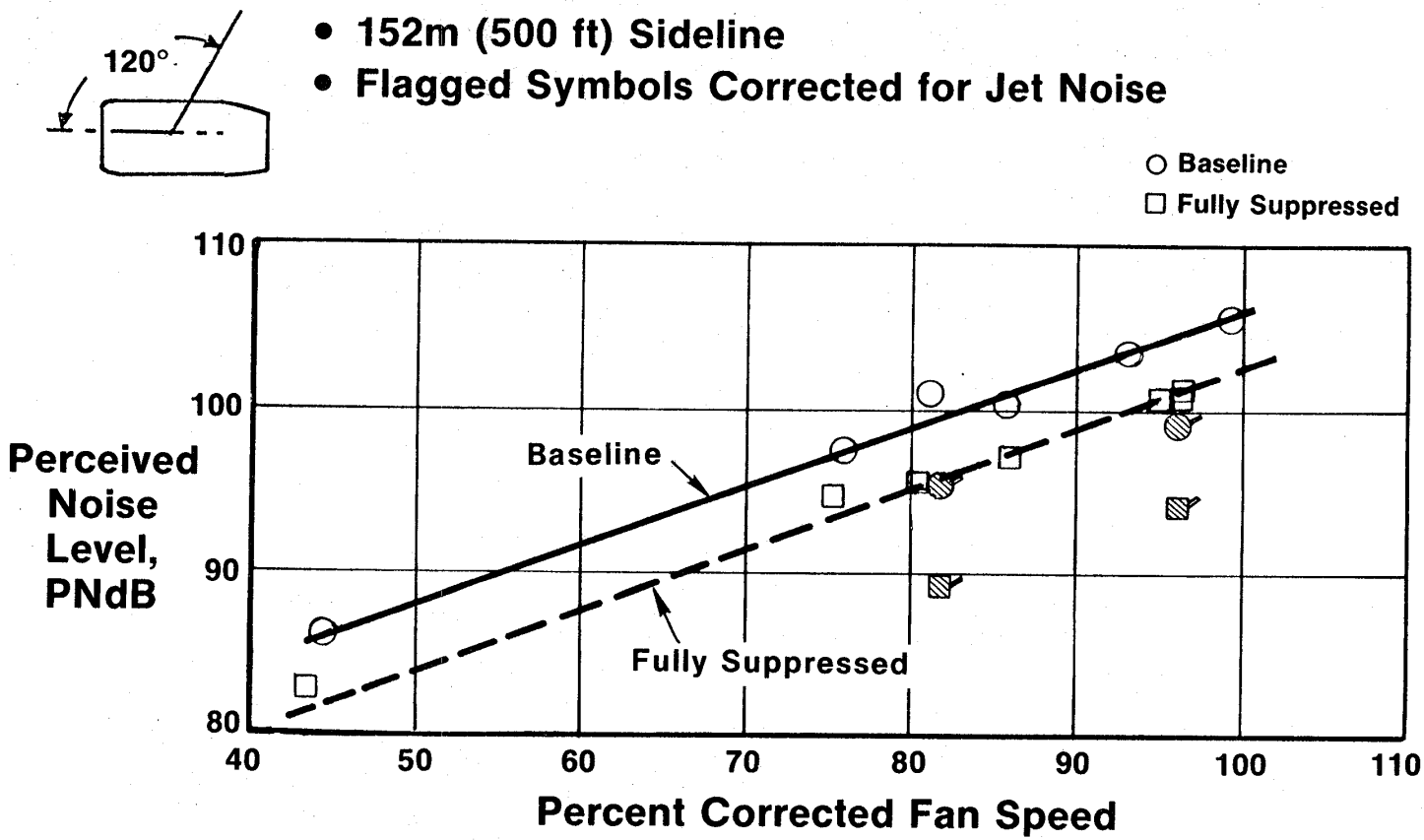

Figure 181. Measured Exhaust PNL.

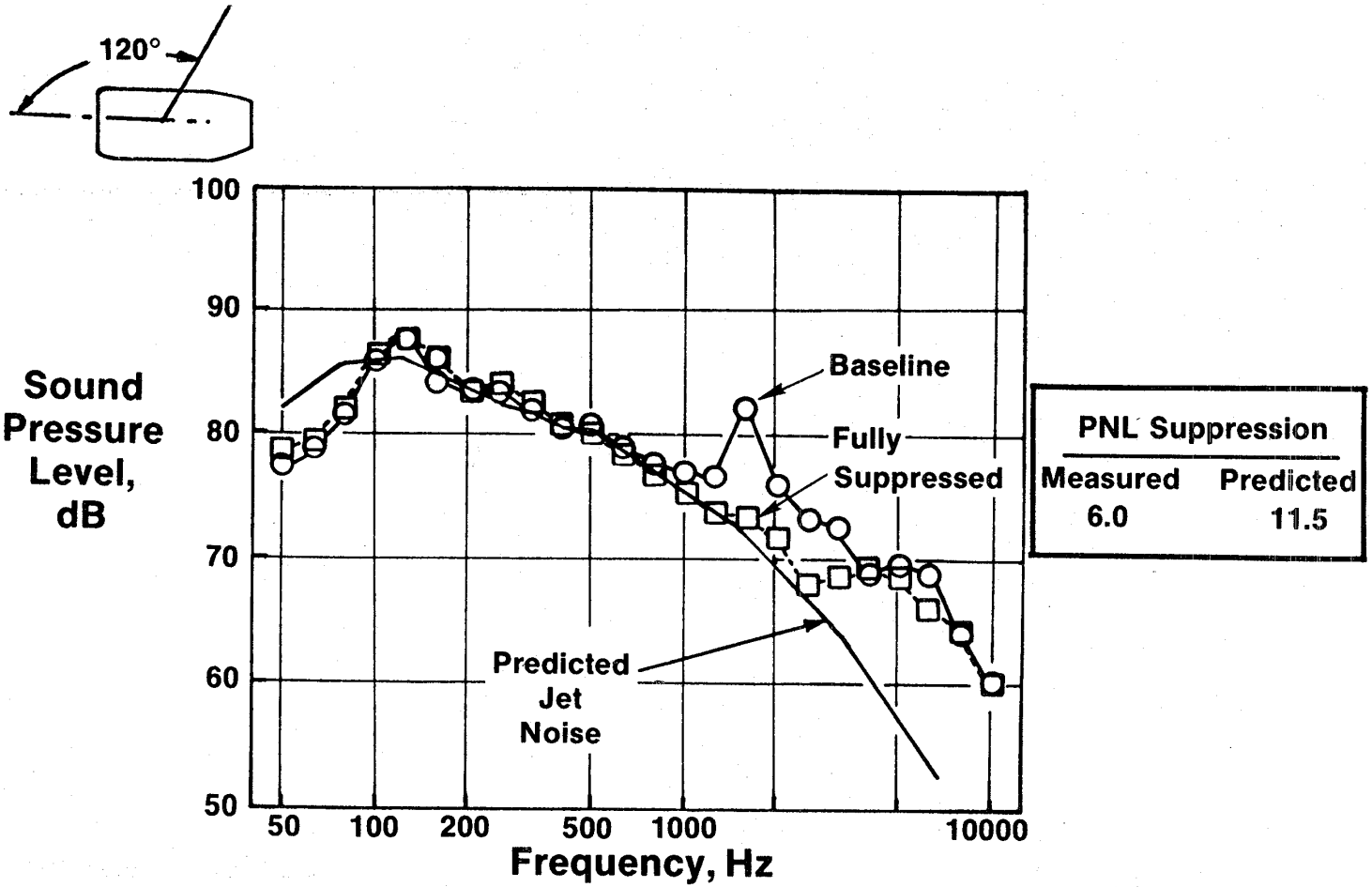

Figure 182. OTW Exhaust-Radiated Noise at Takeoff.

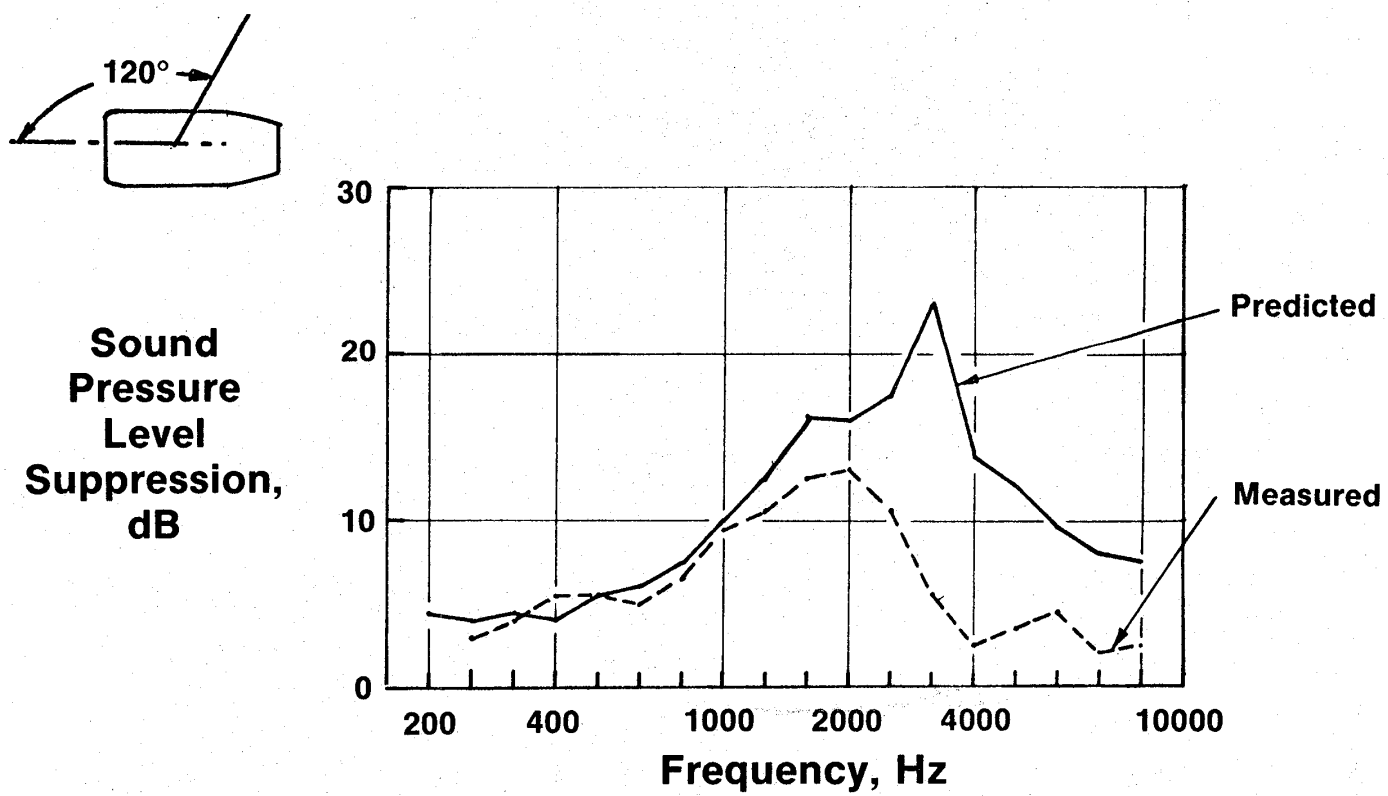

Figure 183. OTW Exhaust Suppression at Takeoff.

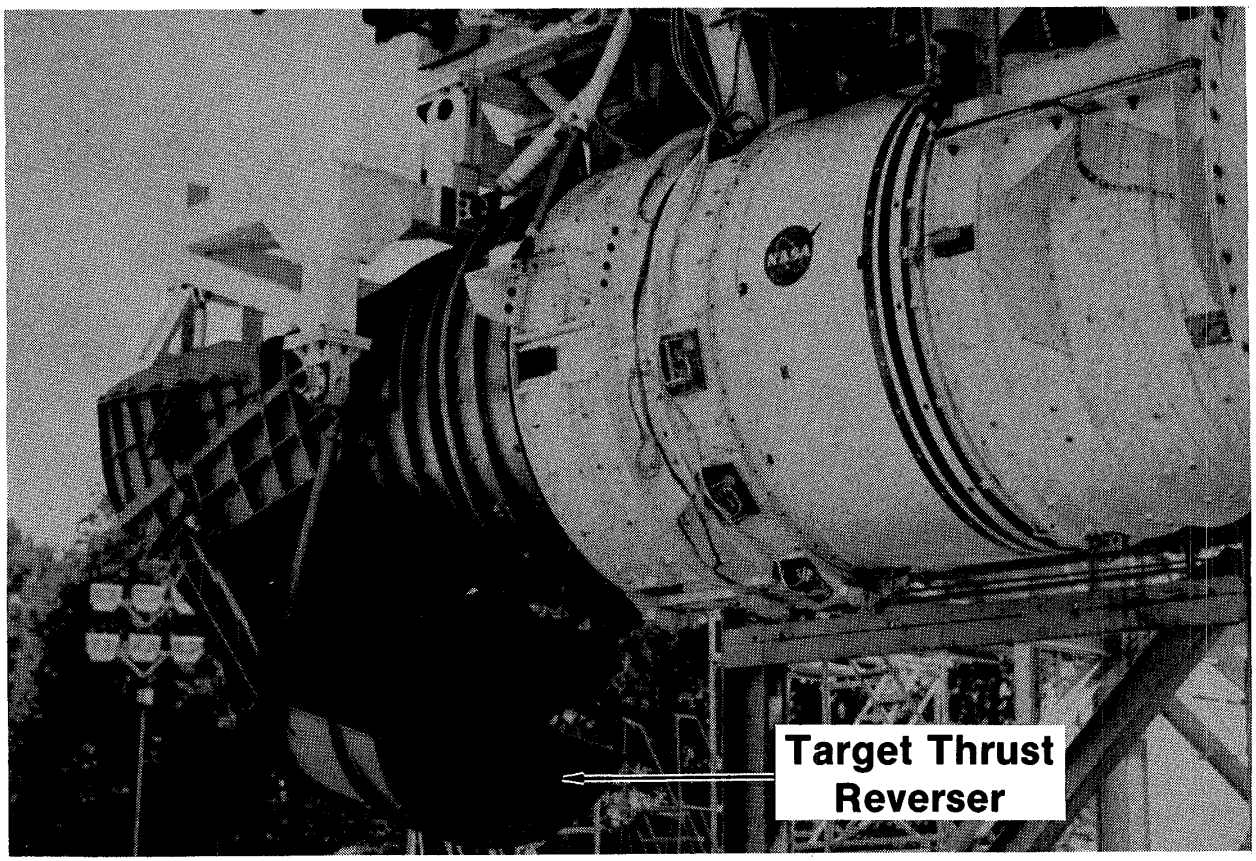

Figure 184. OTW QCSEE with Thrust Reverser Deployed.

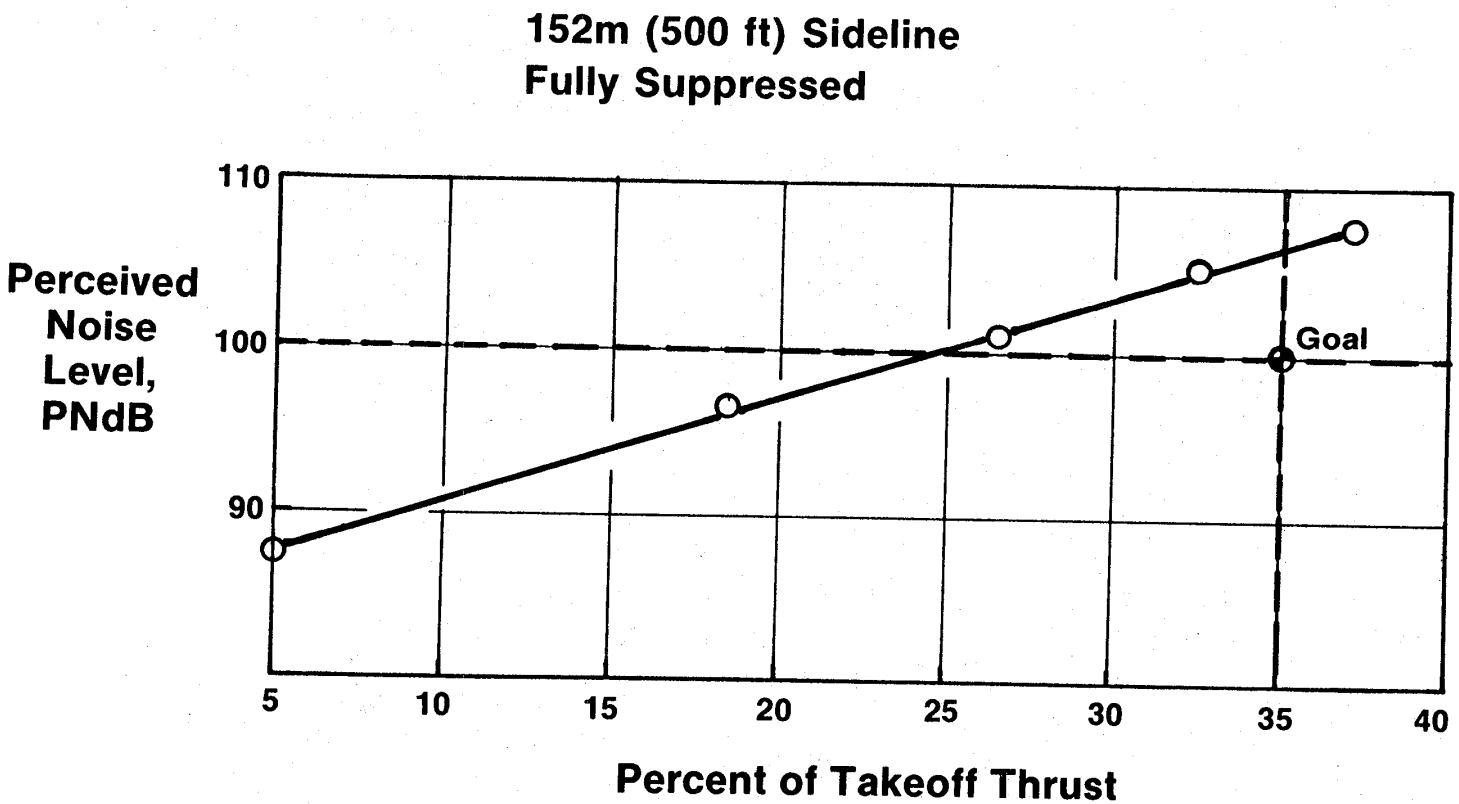

Figure 185. OTW Reverse-Thrust System Noise.

Table XXXI. OTW Boilerplate Nacelle System Noise.

	Forward Quadrant		Aft Quadrant	
	Engine	Jet/Flap	Engine	Jet/Flap
Takeoff				
PNL	94.8	95.8	96.8	93.2
Quadrant Total PNL	99.0		99.1	
System EPNL	97.2			
Approach				
PNL	95.4	89.9	90.8	87.2
Quadrant Total PNL	97.1		93.1	
System EPNL	94.6			

4.5.4 Summary

Using the measured engine-noise levels from the program and calculated flap noise, contours have been calculated both for UTW- and for OTW-powered aircraft. The takeoff and approach flight paths are shown in Figure 186 for a 66,700-kg (147,000-lb) TOGW aircraft, along with 90, 95, and 100 EPNdB contours. To provide some perspective of how small these noise contours are, the 95 EPNdB contour areas are listed in Table XXXII and compared to similar areas of two typical narrowbody jets and a widebody aircraft. The contour area for the widebody is one-fouth to one-tenth of the narrowbody contour while the QCSEE-powered aircraft give another step reduction of one-tenth, producing 95 EPNdB contours of less than 1.295 km^2 (1/2 mi^2).

In summary, the noise goals for the QCSEE progam were very challenging, representing a noise-reduction-technology step of about 10 EPNdB. Although many of the low-noise characteristics of the engines resulted from the basic cycle design, several unique noise-reduction concepts have been demonstrated which are applicable to many engines, and these represent an improvement in low-noise technology. The most difficult aspect of the QCSEE noise goal was to achieve simultaneous success with the prediction and suppression of several major noise-source components. Simultaneous success was necessary since all of these sources were contributors to the suppressed-engine perceived noise levels; therefore, missing even one of the component levels jeopardized achievement of the noise goals. As a result of this aspect of the program, the following list of accomplishments can be placed in perspective.

- Takeoff and approach system levels for both engines were within 2 EPNdB of the 152-m (500-ft) sideline goal of 95 EPNdB.

- The baseline system noise measurements met or were lower than the predictions on the OTW engine. Baseline levels on the UTW engine were higher than anticipated, but the program has provided a large data base for understanding and predicting variable-pitch-fan noise.

- The hybrid inlet was successful at takeoff power settings, achieving 14 to 15 PNdB suppression at the maximum forward angle. This represents three times the suppression achieved in the past without the use of splitters or variable inlet geometry. Up to 7.5 PNdB suppression was measured at approach power; this is an improvement over previous designs.

- Aft fan suppression of 2 dB was demonstrated for treated vanes. This is a significant suppression for a very modest amount of treated area.

- Aft fan-duct suppression was as predicted where flanking noise-transmission paths and/or "floor noise sources" didn't prevent accurate measurement.

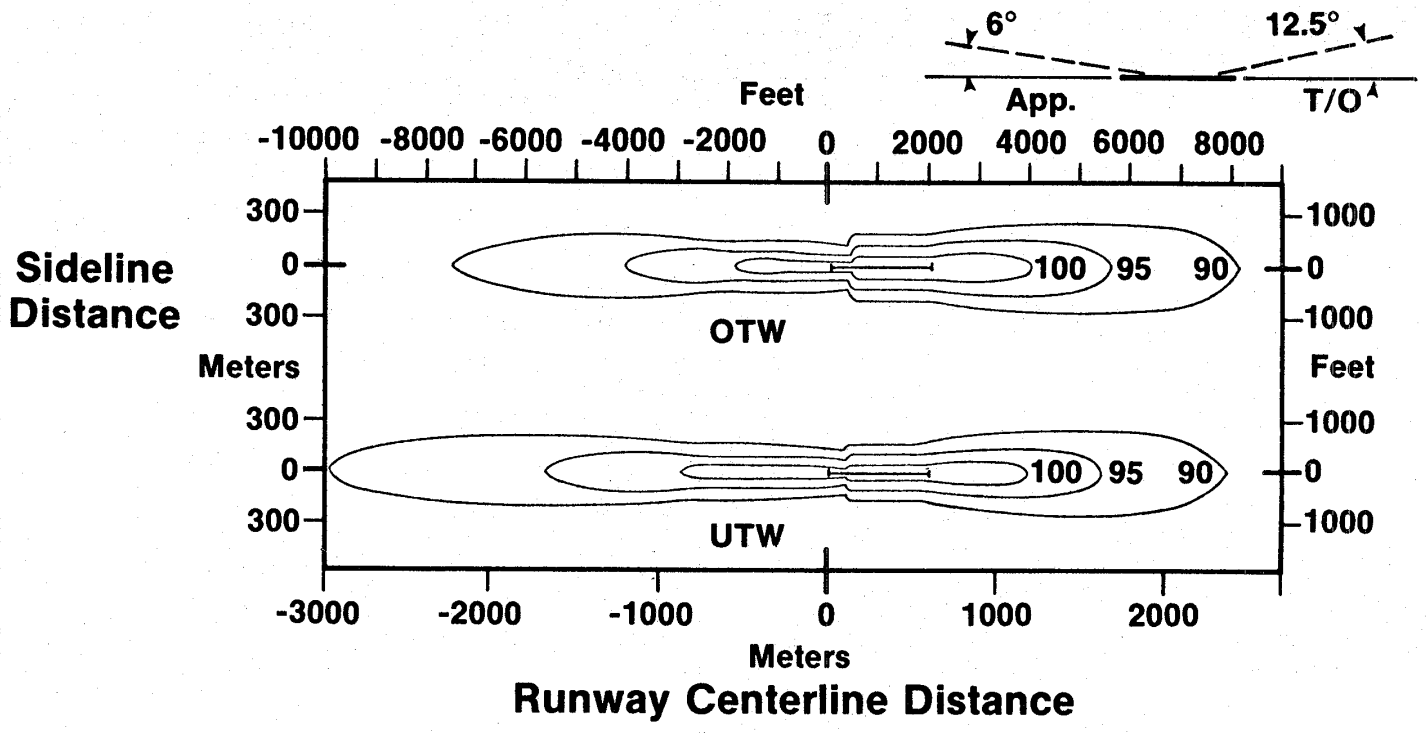

Figure 186. QCSEE Approach and Takeoff EPNdB Contours.

Table XXXII. Comparison of Footprint Areas: QCSEE to Typical Current Aircraft.

Aircraft	TOGW		95 EPNL Contour Area	
	kg	(lb)	Sq km	Sq mi
707 (Jet)	146,000	(322,000)	66.5	25.66
DC-9 (Fanjet)	44,500	(98,000)	31.8	12.25
DC-10-30 (Fanjet)	252,000	(555,000)	9.4	3.57
QCSEE — UTW	66,700	(147,000)	1.0	0.38
QCSEE — OTW	66,700	(147,000)	0.8	0.32

- The suppression of the unique core-nozzle suppressor, designed to attenuate both high-frequency turbine noise and low-frequency combustor noise, was not completely measured due to the masking effects of jet noise and duct-flow noise.

- The reverse-thrust noise produced by both the UTW reverse-pitch fan and the OTW reverser was higher than predicted, but again the data available from engine and scale-model programs provide the basis for more accurate prediction models.

Finally, from the acoustic technology standpoint, in almost every case where component acoustic objectives were not completely met the data and understanding of the limiting problems are available and will ensure the improvement of similar designs in the future.

4.6 MEASURED PROPULSION SYSTEM WEIGHT

The weight of each of the advanced components was measured during assembly of the engines. However, the UTW and OTW experimental engines contained a number of differences, from ultimate flight configurations, that affected system weight. These included the following items.

In the interest of reducing program cost, a number of material substitutions and fabrication shortcuts were made in the experimental hardware. An example is the use of titanium blades in place of composites in the OTW fan.

Boilerplate nacelle components were built to allow the use of interchangeable acoustic treatment and hard-wall panels. The nacelle hardware was designed for use on both engines, with some compromise in flowpath and length for the OTW engine.

Both engines were heavily instrumented for experimental testing. A photograph of the UTW engine nearing completion of assembly is shown in Figure 187. The weight of wires, tubes, connectors, rake mounting pads, and slip-ring supporting structure totaled several hundred pounds in each engine.

Finally, the engines were designed to meet noise objectives with a 610-m (2000-ft) runway. As a result of the airline operational scenario and the aircraft company design studies, it was determined that a 915-m (3000-ft) runway would be a better compromise between aircraft economics and ability to operate from small airports. This would be reflected in a reduced takeoff power setting for the flight engines, reducing noise and allowing the acoustic splitter and core exhaust nozzle treatment to be eliminated with significant weight savings.

Because of these differences between the experimental and flight-engine configurations, it was necessary to modify the actual hardware weight results to reflect the equivalent weight of flight engines.

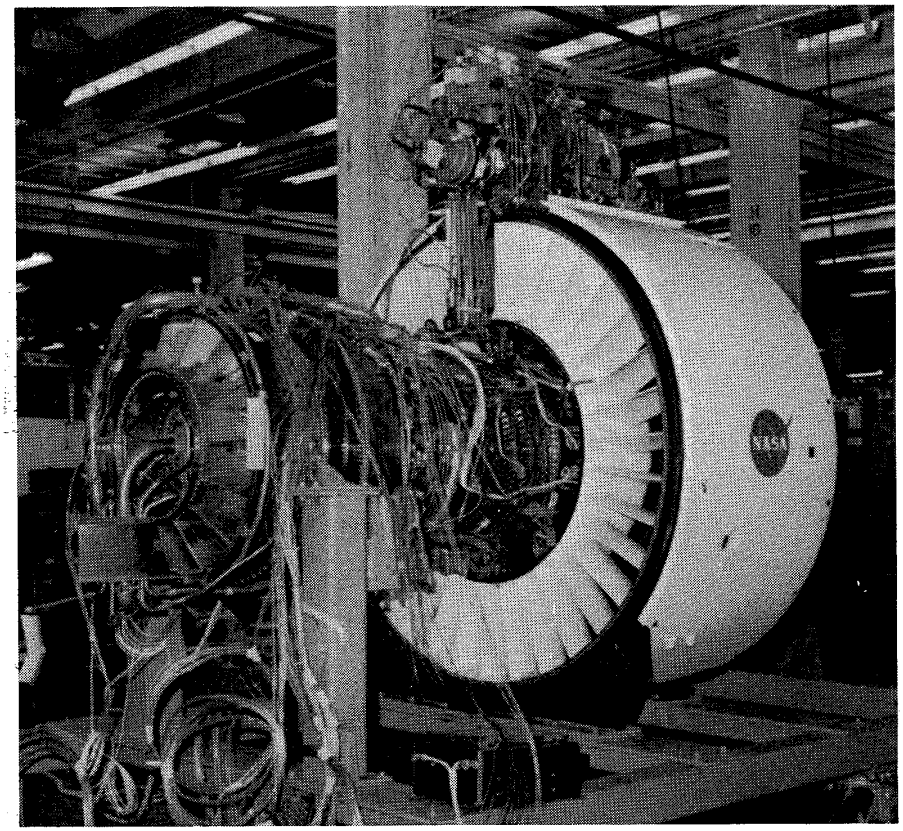

Figure 187. UTW Engine Assembly.

4.6.1 UTW System

Table XXXIII shows the weight breakdown of the UTW experimental engine and the projected weight of a UTW flight configuration. Some of the significant differences are as follows:

The F101 core was designed for a supersonic flight envelope and provided excess inlet-temperature capability. The use of more titanium in the compressor and freedom to redesign the turbine frame would save weight as shown.

The fan rotor utilized a steel shaft, and the reduction gear a steel star carrier, for cost saving. Substitution of titanium would save weight.

The composite fan frame included many shortcuts in fabrication technique, material thicknesses, potting and sealing compounds, additional instrumentation, and service lines. A detailed analysis of the measured frame weight showed that a substantial weight saving from the experimental hardware is possible, even after adding a metal sump liner to the flight frame.

Differences in the smaller components are primarily a result of using special-purpose parts in place of off-the-shelf components.

Total projected weight of the flight engine is 1436 kg (3166 lb) compared to the actual 1693 kg (3732 lb) weight of the experimental engine.

Table XXXIV shows a similar comparison of the nacelle components. The major differences here are results of eliminating the acoustic splitter and core nozzle treatment. In addition a number of metal inserts for instrumentation rakes and struts could be eliminated. The core cowl could be made in two pieces instead of four if a larger autoclave were available. The equivalent flight weight of the composite nacelle is 466 kg (1028 lb) which, added to the engine weight, results in a total propulsion system weight of 1902 kg (4194 lb).

4.6.2 OTW System

Table XXXV shows the OTW engine weight breakdown. Differences between the experimental and flight-weight numbers are much like those of the UTW engine with one major exception: the titanium fan blades and resulting heavier disk are reflected in a much greater saving in fan-rotor weight in the flight configuration.

The OTW nacelle weight is shown on Table XXXVI for the flight engine since only boilerplate components were built for this engine. The projected flight propulsion system weight is 1980 kg (4364 lb).

Table XXXIII. UTW Engine Weight.

	Experimental		Flight	
	(kg)	(lb)	(kg)	(lb)
Modified F101 Core & LPT Turbine	663	1461	622	1372
Fan Rotor	217	478	192	423
Reduction Gear	93	204	86	190
Composite Fan Frame	318	702	215	474
Brgs., Drives & Lube Components	275	607	201	444
Fuel System	32	70	20	45
Electrical System	26	58	15	33
VP Mechanism (Ball Spline)	69	152	62	137
Piping, Wiring and Misc.	36	80	22	48
Total Engine	1693	3732	1436	3166

Table XXXIV. UTW Nacelle Weight.

	Experimental (kg)	Experimental (lb)	Flight (kg)	Flight (lb)
Composite Inlet	242	533	150	330
Composite Fan Duct	125	275	91	201
Composite Flare Nozzle	41	90	30	67
Composite Core Cowl	69	153	41	91
Core Exhaust Nozzle	93	206	64	142
Lube & Hydraulic System	161	354	78	172
Instrumentation (Approximately)	227	500	11	25
Total Nacelle	958	2111	466	1028
Engine			1436	3166
Propulsion System			1902	4194

Table XXXV. OTW Engine Weight.

	Experimental		Flight	
	(kg)	(lb)	(kg)	(lb)
Modified F101 Core & LP Turbine	663	1461	622	1372
Fan Rotor	364	802	173	382
Reduction Gear	90	198	83	184
Composite Fan Frame	312	687	208	459
Brgs., Drives & Lube Components	275	607	189	417
Fuel System	34	74	20	44
Electrical System	26	58	15	33
Piping, Wiring and Misc.	36	80	20	43
Total Engine	1799	3967	1331	2934

Table XXXVI. OTW Nacelle Weight.

	Experimental	Flight (kg)	Flight (lb)
Composite Inlet	Boilerplate	150	330
Composite Fan Duct	Boilerplate	117	259
Composite Core Cowl	Boilerplate	40	88
Core Exhaust Nozzle	Boilerplate	38	84
Aft Nacelle	Boilerplate	113	250
"D" Nozzle/Thrust Reverser	Boilerplate	121	266
Lube & Hydraulic System	Boilerplate	64	140
Instrumentation	Boilerplate	6	13
Total Nacelle		649	1430
Engine		1331	2934
Propulsion System		1980	4364

4.7 THRUST-TO-WEIGHT RATIO ASSESSMENT

Thrust-to-weight ratio was evaluated on both an uninstalled and an installed basis. Table XXXVII shows both goal and projected values. The goals were set on the basis of conceptual design studies at the outset of the program. The projected numbers have been adjusted to take into account the results of actual design and testing experience. This experience has caused a small reduction in our expectations, but the absolute levels are still relatively high, and the reductions are within the scatter range of such predictions.

To place these installed values in their proper context, the experimental engine cycles were selected for acoustic and other considerations rather than to optimize weight. Large, high-bypass engines generally suffer heavy installation penalties. These penalties have been largely offset by the lightweight integrated QCSEE nacelle components, with the result that both propulsion systems exhibit attractive installed thrust-to-weight characteristics that are comparable with the best current CTOL propulsion systems.

Table XXXVII. Thrust-to-Weight Assessment.

	UTW		OTW	
	N/kg	lb/lb	N/kg	lb/lb
Uninstalled				
• Goal	60.8	(6.2)	72.6	(7.4)
• Projected	56.7	(5.78)	70.2	(7.16)
Installed				
• Goal	42.2	(4.3)	46.1	(4.7)
• Projected	40.7	(4.15)	45.6	(4.65)

5.0 CONCLUSIONS

A number of significant conclusions can be drawn from the results of the QCSEE design and development effort. Some of these conclusions apply only to short-haul engines, but many are of a general nature applicable to other types of advanced propulsion systems.

5.1 ENGINE PERFORMANCE

Since both engines met the forward-performance goals, there should be no reluctance to apply very high bypass cycles in cases where the aircraft thrust requirements can be matched. Since these cycles have very low fan pressure ratio and high thrust lapse, they are most applicable to powered-lift aircraft.

Because of the use of the F101 core engine without boost stages, both engines exhibited low cycle pressure ratios. As a result, cruise sfc was not as attractive as it could be if an advanced-design, higher-pressure-ratio core were used. Therefore, particularly in view of the current energy situation and rising fuel cost, product versions of the engines should incorporate higher-pressure-ratio cores.

Although the UTW engine failed to meet the 35% reverse-thrust goal, it did produce 27% reverse thrust; this might be sufficient to stop an aircraft on a 915-m (3000-ft) runway. Furthermore, additional development testing could result in higher levels of reverse thrust. It may be concluded that the variable-pitch fan concept can be developed to provide effective thrust reversal.

While the OTW engine exceeded the 35% reverse-thrust goal, it did so with higher than expected pressure losses. Reverse-thrust noise could be reduced by redesigning the aft nacelle flowpath.

5.2 FAN PERFORMANCE

The OTW and UTW fans both performed satisfactorily during sea level static engine tests, and most of the fan aeroperformance goals established for the experimental engine programs were met. Some futher development of the UTW fan is required to meet altitude-cruise performance goals, and the reduced pumping of this fan during engine reverse-mode tests needs to be understood and improved. Important advances in fan aerodynamic technology were demonstrated during the QCSEE program, and these advanced fan features can be used with confidence in future turbofan engines for short-haul aircraft.

5.3 COMPOSITE FAN BLADES

It was concluded that some form of lightweight blade must be developed to make variable-pitch fans practical. Because of lack of FOD resistance during bird ingestion, the QCSEE composite blade is acceptable only for experimental ground test. Subsequent developments of other programs have identified candidate materials that could possibly solve this problem; however, none of this work has been completed to date. Some of these material candidates are:

- Stitched or multidirectional-weave polymerics
- Superhybrid
- Boron aluminum
- Hollow titanium

5.4 VARIABLE-PITCH SYSTEMS

Both variable-pitch systems, the harmonic drive and the ball spline, demonstrated concept feasibility during whirl-rig and engine testing. Either system could be developed for operational use.

Actual blade-turning moments exceeded the anticipated (calculated) values; therefore, either system must be sized for somewhat higher torque capacity than originally specified.

5.5 MAIN REDUCTION GEAR

The QCSEE main reduction gear transmitted up to 12.7 MW (17,000 hp) for many hours without incident - a significant accomplishment for a lightweight gear system.

Total time on the UTW gear is approximately 202 hours: test rig, 49 hours; engine, 153 hours.

Total time on the OTW gear is approximately 135 hours: test rig, 36 hours; engine (GE), 58 hours; engine (NASA), 41 hours.

Although this is hardly sufficient operating experience on which to ensure the achievement of the 36,000 hours life and 6,000 hours time before overhaul (TBO) objectives, the feasibility of a geared fan drive has been satisfactorily demonstrated; with the benefit of further development effort, acceptable reduction-gear performance and life for operational engines can be expected.

5.6 COMPOSITE FRAME

Based on the information generated by the QCSEE program, the following conclusions have been reached concerning the use of graphite/epoxy for engine frames.

- Composite construction shows promise for application to major frames. It has been shown that these frames can take advantage of the unique characteristics of composites.
- The static tests of the frame verified the analysis, and engine tests were in reasonable agreement.
- As the frame was actually built, it was difficult to fabricate. The need for better part tooling and better assembly tooling was apparent. In the future it should be more efficient to use fewer individual pieces by more piece integration in the as-molded condition.
- The sump area was difficult to seal against oil leakage. The use of a metal sump liner would help.

5.7 COMPOSITE NACELLE

The following conclusions have been reached concerning the use of advanced composite materials in engine nacelle hardware.

- The program demonstrated the ability to design stiff, light, thin, nacelle structures utilizing composite materials.
- Basic, low-temperature, nacelle structures can be easily fabricated using state-of-the-art techniques.
- The PMR/graphite inner cowl provided a successful demonstration of a new, high-temperature, composite system.

5.8 DIGITAL CONTROL

During the NASA/GE QCSEE program, two engine-mounted digital controls were designed, fabricated, and tested on the two experimental engines. Throughout the engine-test program, approximately 200 hours of operation, the digital controls scheduled the engine variables and maintained engine operation within all safety limits. Several experiments were performed during the engine-test program to evaluate the control system capability with respect to control-system requirement. Nearly all requirements were met satisfactorily. Table XXXVIII compares primary control system requirements with engine-test

results. As a result of this successful development program, the digital control technology base has been expanded and will hasten the application of digital controls on future propulsion systems.

5.9 LOW-EMISSION COMBUSTOR

The double-annular combustor was successfully developed to meet the EPA 1979 emissions standards for class T2 engines within the very limited space available in the F101 combustor envelope. The principles used are directly applicable to other engines and should be considered depending upon the specific emissions requirements.

5.10 ACOUSTICS

Although the 95 EPNdB sideline-noise goal was not reached by either engine, both demonstrated within about 2 dB of the goal. This is considered to be an outstanding accomplishment in light of the severity of the goal. Both engines demonstrated 95 EPNdB contour areas of less than 1.295 km^2 (1/2 mi^2). This would confine the noise nuisance to the airport proper and alleviate the community noise problems.

Some of the noise-reduction features (such as the low-tip-speed, low-pressure-ratio fans) are most applicable to short-haul engines. However, if community noise becomes a sufficiently powerful driver, these features could be used in CTOL aircraft by oversizing the engines and accepting a weight penalty.

5.11 WEIGHT

The projected thrust-to-weight ratio of UTW and OTW flight engines are comparable on an installed basis with the best current CTOL propulsion systems. Therefore, it can be concluded that it is feasible to produce economically competitive, powered-lift aircraft systems meeting demanding noise and pollution requirements.

Table XXXVIII. Control System Summary and Conclusions.

Requirements	Results	
	UTW	OTW
• Set Percent Rated Thrust	✓	✓
• Maintain Engine Safety Limits	✓	✓
• Reduce Pilot Workload	✓	✓
• Control Inlet Mach Number	✓	N/A
• Rapid Thrust Response	Partial	✓
• Failure Detection and Corrective Action	N/A	Partial
• Engine Condition Monitoring	✓	✓
• Interface with Aircraft Digital Computer	✓	✓

6.0 RECOMMENDATIONS

The following recommendations for future development action are made considering those items excluded from, or not completed under, the QCSEE program. The intent of each is to bring the new technology elements a step closer to utilization. A number of these recommendations are included in the test program being conducted at the NASA Lewis Research Center. However, all are included below for completness.

Overall Engines

- Conduct additional UTW reverse-thrust testing with instrumentation to determine the cause of lower-than-predicted reverse thrust.
- Conduct transient UTW thrust-reversal testing.

Composite Fan Blades

- Pursue the development of alternate lightweight blade approaches to provide a flightworthy design. This is essential to the operational use of a variable-pitch fan and applicable to many other fixed-pitch fan engines.

Variable-Pitch Actuation Systems - If interest in variable-pitch fans remains high enough to warrant further development of the UTW fan, the following modifications in the variable-pitch actuation systems are suggested:

- The cam/harmonic system could be modified to increase torque capacity by 40% to ensure moving the blades at all fan speeds. This would entail increasing the size of the hydraulic motor in the beta regulator, modifying the core cowl to accept the longer regulator, and procuring a higher-torque-rated flexible cable. The stronger cable would also be stiffer and might present an installation problem.
- The running hysteresis of the ball spline system could probably be improved by rebuilding the ball spline and ball screw using larger diameter balls to reduce clearance.

Main Reduction Gear

- Conduct extended reduction gear endurance testing using the available back-to-back rig and QCSEE hardware. Early testing should include further optimization of the lube supply and scavenge system to attempt to reduce churning and further improve gear efficiency.

Composite Frame and Nacelle

- Static load test the OTW composite fan frame to destruction to determine if it meets design load objectives.

- The composite core cowl was cooled by shop air and an insulation blanket throughout UTW engine testing. Full verification of this design would include the design and testing of a flight-type heat shield and the use of fan-discharge air for cooling.

Digital Control

- Conduct UTW transient testing with electrical gain adjustment of the pitch-control system.

- Reprogram and test the OTW FICA system.

Low-Emissions Combustor

- Conduct engine testing of a double-annular combustor to develop pattern factor and profile.

Acoustics

- Verify wing/flap interaction-noise assumptions.

- Evaluate boundary-layer noise effect as a noise floor for aft fan-duct suppression.

- Evaluate "D" nozzle acoustic characteristics more fully by using acoustic probes correlated with far-field microphones. Include hard-wall core nozzle testing. Alternately, test with conical nozzles to separate core- and fan-noise sources.

- Conduct additional UTW acoustic tests to:

  a. Verify wing/flap interaction-noise assumptions.

  b. Utilizing acoustic probes, determine precise causes of higher than predicted fan source noise for both forward and reverse thrust.

  c. Evaluate suppression of the core nozzle by use of probes and/or coherence measurements.

7.0 RELATED REPORTS

1. Main Reduction Gears Test Program Final Report, 3/77, CR134669.
2. QCSEE Preliminary Analysis and Design Report, Vol. I, 10/74, CR134838.
3. QCSEE Preliminary Analysis and Design Report, Vol. II, 10/74, CR134839.
4. UTW Engine Composite Fan Blade Design, 5/75, CR134840.
5. Aerodynamic and Preliminary Mechanical Design of the QCSEE OTW Fan, 9/75, CR134841.
6. UTW Fan Preliminary Design, 2/75, CR134842.
7. UTW Engine Composite Fan Blade Preliminary Design Test Report, 9/75, CR134846.
8. Under the Wing (UTW) Final Design Report, 6/77, CR134847.
9. Over the Wing (OTW) Final Design Report, 6/77, CR134848.
10. Demonstration of Short Haul Aircraft Aft Noise Reduction Techniques on a 20 inch (50.8 cm) Diameter Fan, Vol. I, 4/75, CR134849.
11. Demonstration of Short Haul Aircraft Aft Noise Reduction Techniques on a 20 inch (50.8 cm) Diameter Fan, Vol. II, 4/75, CR134850.
12. Demonstration of Short Haul Aircraft Noise Reduction Techniques on a 20 inch (50.8 cm) Diameter Fan, Vol. III, 4/75, CR134851.
13. Hamilton Standard Cam/Harmonic Variable Pitch Fan Actuation System Detailed Design Report, 3/76, CR134852.
14. Aerodynamic Characteristics of 30.5 cm Diameter Inlets, 8/75, CR134866.
15. Test Results From a 14 cm Inlet for a Variable Pitch Fan Thrust Reverser, 12/75, CR134867.
16. Preliminary UTW Flight Propulsion System Analysis Report, 2/76, CR134868.
17. Main Reduction Gears Detailed Design Final Report, 3/75, CR134872.
18. Ball Spline Pitch Change Mechanism Design Report, 3/77, CR134873.
19. Main Reduction Gears Bearing Development Program, 4/76, CR134890.

20. Acoustic Analysis of Aft Noise Reduction Techniques Measured on a Subsonic Tip Speed 50.8 cm (20 inch) Diameter Fan, 1/77, CR134891.

21. UTW Engine Simulation Results, 8/77, CR134914.

22. Aerodynamic and Mechanical Design of the QCSEE Over the Wing Fan, 4/76, CR134915.

23. Clean Combustor Test Report, 10/75, CR134916.

24. UTW Digital Control System Design Report, 1/78, CR134920.

25. UTW Boilerplate Nacelle and Core Exhaust Nozzle Design Report, 10/76, CR135008.

26. Aerodynamic and Mechanical Design of the QCSEE Under the Wing Fan, 3/77, CR135009.

27. Composite Fan Frame Subsystem Test Report, 9/77, CR135010.

28. Aerodynamic and Aeromechanical Performance of a 50.8 cm (20 inch) Diameter 1.34 Pressure Ratio Variable Pitch Fan with Core Flow, 8/77, CR135017.

29. UTW Engine Composite Fan Blade Final Design Test Report, 2/77, CR135046.

30. OTW Engine Simulation Results, 10/78, CR135049.

31. UTW Composite Nacelle Subsystem Test Report, 7/77, CR135075.

32. Acoustic Performance of a 50.8 cm (20 inch) Variable Pitch Fan and Inlet, Vol. I, 11/78, CR135117.

33. Acoustic Performance of a 50.8 cm (20 inch) Variable Pitch Fan and Inlet, Vol. II, 11/78, CR135118.

34. Whirl Test of Cam/Harmonic Pitch Change Actuation System, 10/78, CR135140.

35. Core Engine Noise Measurements, 12/77, CR135160.

36. OTW Boilerplate Nacelle Design Report, 5/77, CR135168.

37. UTW Engine Boilerplate Nacelle Test Report, Vol. I Summary, 12/77, CR135249.

38. UTW Engine Boilerplate Nacelle Test Report, Vol. II Aerodynamic Performance, 12/77, CR135250.

39. UTW Engine Boilerplate Nacelle Test Report, Vol. III Mechanical Performance, 12/77, CR135251.

40. Acoustic and Aerodynamic Tests on a Scale Model OTW Thrust Reverser and Forward Thrust Nozzle, 1/78, CR135254.

41. Acoustic Treatment Design and Development, 11/78, CR135266.

42. Under the Wing (UTW) Engine Acoustic Design, 1/78, CR135267.

43. Over the Wing (OTW) Engine Acoustic Design, 6/78, CR135268.

44. Composite Frame Design, 9/78, CR135278.

45. PMR Core Cowl Design Report, 7/78, CR135279.

46. Preliminary OTW Flight Propulsion System Analysis Report, 6/77, CR135296.

47. OTW Propulsion System Test Report, Vol. I Summary, 1/78, CR135323.

48. OTW Propulsion System Test Report, Vol. II Aerodynamics and Performance, 7/78, CR135324.

49. OTW Propulsion System Test Report, Vol. III Mechanical Performance, 2/78, CR135325.

50. OTW Propulsion System Test Report, Vol. IV Acoustic Performance, 5/79, CR135326.

51. OTW Digital Control System Design Report, 11/78, CR135337.

52. UTW Composite Nacelle Design Report, 8/78, CR135352.

53. Ball Spline Pitch Change Mechanism Whirligig Test Report, 10/78, CR135354.

54. UTW Engine Composite Nacelle Test Report, Vol. I Summary, Mechanical and Aerodynamic Performance, 5/79, CR159471.

55. UTW Engine Composite Nacelle Test Report, Vol. II Acoustic Performance, Pending, CR159472.

56. Clean Combustor Development Report, Pending, CR159483.

DISTRIBUTION LIST

AiResearch Division
Garret Corporation
F.B. Wallace
P.O. Box 5217
Phoenix, Arizona 85010

American Airlines
Maintenance and Engineering Center
K. Grayson
Tulsa, Oklahoma 74151

Andrews Air Force Base
Lt. Col. G. Strand
AFSC Headquarters
Washington, D.C. 20334

AVCO/Lycoming
S. Deckert
550 S. Main Street
Stratford, Connecticut 06497

The Boeing Company
H. Higgins
P.O. Box 3999
Seattle, Washington 98124

The Boeing Company
Wichita Division
D. Torkelson
Wichita, Kansas 67210

Bolt, Beranek and Newman, Inc.
R. Hayden
50 Moulton Street
Cambridge, Massachusetts 02138

Curtiss-Wright Corporation
Power Systems Division
W. Johnson
One Passaic Street
Wood Ridge, New Jersey 07075

Department of Transportation
NASA/DOT Joint Office of Noise Abatement
C. Foster
Office of Secretary
Washington, D. C. 20590

Detroit Diesel Allison Division
of General Motors
F. Walters
Suite 312
333 West First Street
Dayton, Ohio 45402

Douglas Aircraft Company
L. Malthan
3855 Lakewood Boulevard
Long Beach, California 90801

Environment Protection Agency
J. Schettino
1835 "K" Street, NW
Washington, D.C. 20460

Federal Aviation Administration
Noise Abatement Division
J. Woodall
Washington, D.C. 20590

General Dynamics Convair Division
G. Nicoloff
San Diego, California 92112

Grumman Aerospace Corporation
C. Hoeltzer
South Oyster Bay Road
Bethpage, New York 11714

Hamilton Standard
Division of United Aircraft
A. Jackson
Windsor Locks, Connecticut 06096

Lockheed Aircraft Corporation
T. Higgins
Burbank, California 91503

Lockheed Georgia Company
H.S. Sweet
Marietta, Georgia 30060

NASA Installations

NASA Headquarters
N.F. Rekos
Washington, D.C. 20546

NASA-Ames Research Center
L. Roberts
Moffett Field, California 94035

NASA-Flight Research Center
D.R. Scott
Edwards, California 93523

NASA-Langley Research Center
R. Kuhn
Hampton, Virginia 23665

NASA-Lewis Research Center
21000 Brookpark Road
Cleveland, Ohio 44135

M.A. Beheim
D.N. Bowditch
L.J. Chelko
C.C. Ciepluch
E.W. Conrad
A. Ginsburg
M.J. Hartmann
R.H. Kemp
Lewis Library
R.W. Luidens
D.L. Nored
Report Control Office
L.W. Schopen
R.W. Schroeder
M.F. Valerino

NASA/Air Force Liaison
Wright-Patterson Air Force Base
Dayton, Ohio 45433

L. Obery
C. Simpson
Col. C.E. Painter
G.K. Richey
G.P. Peterson

Pratt & Whitney Aircraft
Division of United Aircraft Corp.
J. Chew
20800 Center Ridge Road
Rocky River, Ohio 44116

Rohr Corporation
F. Hom
Box 878
Foot and H Street
Chula Vista, California 92012

Wyle Laboratories
L. Sutherland
128 Maryland Street
El Segundo, California 90245

Rockwell International
Los Angeles Division
Attn: D. Schlundt
International Airport
Los Angeles, California 90009

End of Document